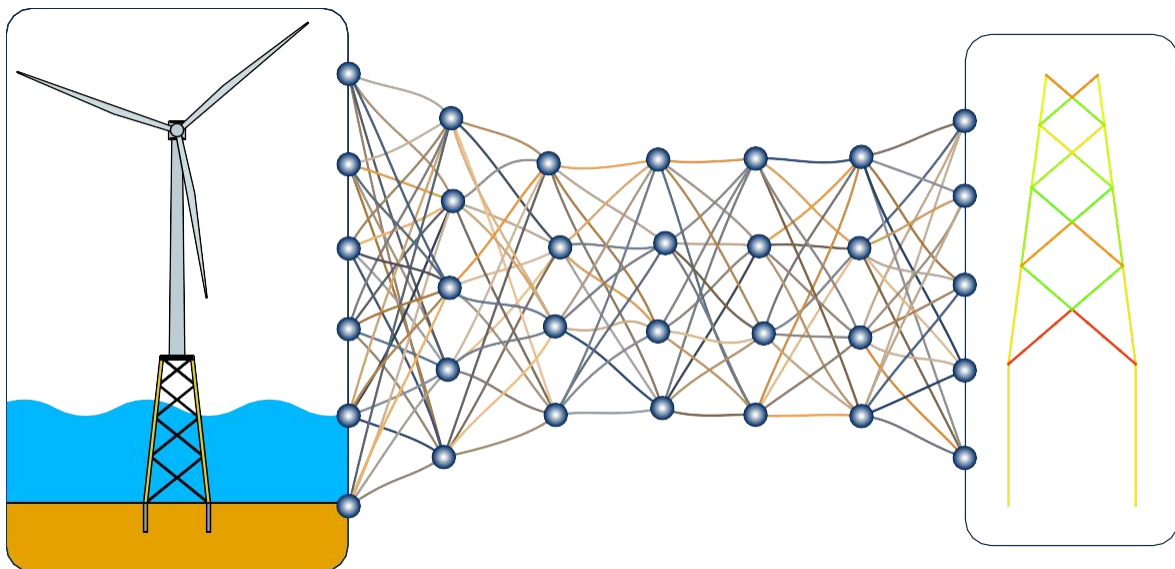


DOCTORAL DISSERTATION

Implementation of ANN-based models to assist in the analysis and design of jacket foundations structures for offshore wind turbines



Román Quevedo Reina

Continuum Mechanics and Structures Division

Las Palmas de Gran Canaria • June 2024



Programa de Doctorado: Tecnologías de Telecomunicación e Ingeniería Computacional



Implementation of ANN-based models to assist in the analysis and design of jacket foundations structures for offshore wind turbines

Román Quevedo Reina

Universidad de Las Palmas de Gran Canaria
Escuela de doctorado

Programa de doctorado
Tecnologías de Telecomunicación e Ingeniería Computacional

Directores:

Dr. Juan José Aznárez González Dr. Guillermo M. Álamo Meneses

Las Palmas de Gran Canaria, June 2024

Acknowledgements

I want to express my thanks to my supervisors, Juan José Aznárez and Guillermo Álamo, for giving me the opportunity to develop this work. Many years have passed since you gave me the opportunity to work in this field for my final degree project, so, to begin with, I thank you for the trust you have placed in me. Over the years, your guidance and advice, both professionally and personally, have been very valuable. Despite the professionalism that you demonstrate at work, your closeness and the humour with which you face adversity are characteristics that I sincerely admire about you.

Also, I want to extend this thanks to the entire Continuum Mechanics and Structures Division for helping me and making my daily routine pleasant. You have been very patient with me despite how annoying I am, so I take advantage of this acknowledgment to apologize for so many debates. I would like to highlight the role of Orlando Maeso, Luis A. Padrón, and Fidel García for serving as directors behind the scenes, not only in terms of research but also for my professional career.

I am also grateful to the Structural Mechanics Section of KU Leuven for their warm welcoming. Specially to Prof. Geert Lombaert and Prof. Sting François for their attention and dedication. Your suggestions and contributions have enriched the final work.

Finally, I want to thank the support of my entire family. All my gratitude to my parents for their patience and positive tips; to Juanqui and Elvira for showing me the positive side of things; and Patricia for all.

The author was recipient of a predoctoral fellowship (TESIS2020010095) by the Agencia Canaria de Investigación, Innovación y Sociedad de la Información de la Consejería de Economía, Industria, Comercio y Conocimiento and by the European Social Fund (ESF) from July until October 2020, and he is currently recipient of the predoctoral fellowship (FPU19/04170) by the Ministerio de Universidades (MIU) of Spain, which also provided financial support for two short-term research stays at KU Leuven (EST22/00507 and EST23/00392).

This work was supported by the Ministerio de Ciencia e Innovación and the Agencia Estatal de Investigación of Spain (MCIN /AEI / 10.13039/501100011033) through Research Projects BIA2017-88770-R and PID2020-120102RB-I00.

Las Palmas de Gran Canaria, June 2024
Román Quevedo Reina



CONTENTS





Contents	i
List of Figures	vii
List of Tables	xi
1 Introduction and background	3
1.1 Introduction	3
1.2 Aims and objectives	4
1.3 Research group framework	4
1.3.1 Research Project BIA2017-88770-R	5
1.3.2 Research Project PID2020-120102RB-I00	6
1.4 Published works derived from the Ph. D. Thesis	6
1.4.1 Contributions in JCR journals	6
1.4.2 Conference contributions	7
1.5 Structure of the dissertation	7
2 Structural model	13
2.1 Introduction and general hypothesis	13
2.2 Design loads	16
2.2.1 Permanent loads	16
2.2.2 Environmental load scenarios	16
2.2.3 Wind loads	17
2.2.4 Sea load	19
2.3 Numerical model for structural analysis	21
2.3.1 Jacket substructure response	21
2.3.2 Soil-structure interaction	22
2.3.3 Water-structure interaction	23
2.3.4 Damping	23
2.3.5 Dynamic characterization	24
2.3.6 Equivalent static analysis	25
2.4 Design principles	25
2.4.1 Geometric requirements	26
2.4.2 Ultimate limit states (ULS)	29
2.4.3 Serviceability limit states (SLS)	30
2.4.4 Fatigue limit states (FLS)	30
3 Jacket optimization	35
3.1 Introduction	35
3.2 Case study	36
3.3 Methodology	37
3.4 Jacket design	40
3.5 Influence of the soil-structure interaction	42
3.6 Conclusions	45



CONTENTS

4	Surrogate models based on artificial neural networks	49
4.1	Introduction	49
4.2	Artificial Neural Networks: basic concepts	49
4.2.1	Numerical approach	49
4.2.2	Architectures	51
4.2.3	Nature of model's output	52
4.2.4	Learning process	52
4.3	Ensemble model	55
4.4	Surrogate model for pile stiffness estimation	55
4.4.1	Problem statement	55
4.4.2	Methodology	58
4.4.3	Architecture selection	59
4.4.4	Ensemble model performance	61
4.4.5	Application examples	64
4.5	Surrogate model for dynamic characterization of offshore wind turbine on jacket structure	66
4.5.1	Problem statement	66
4.5.2	Ranges of variables established for analysis	68
4.5.3	Methodology	70
4.5.4	Architecture selection	71
4.5.5	Ensemble model performance	75
4.5.6	Application example	76
4.6	Conclusions	78
5	Surrogate models for jacket evaluation	83
5.1	Introduction	83
5.2	Problem statement	83
5.2.1	Wind turbine	84
5.2.2	Site conditions	84
5.2.3	Jacket substructure	84
5.2.4	Structural feasibility	85
5.3	Synthetic dataset	85
5.3.1	Wind turbine	86
5.3.2	Site conditions	87
5.3.3	Jacket substructure	89
5.3.4	Structural feasibility	90
5.4	Classification model	91
5.4.1	Architecture	91
5.4.2	Training process	92
5.4.3	Model prediction	92
5.4.4	Model performance	95
5.5	Regression model	99
5.5.1	Architecture	99
5.5.2	Training process	100



5.5.3	Model prediction	100
5.5.4	Model performance	100
5.6	Classification and regression models comparison	103
5.7	Conclusions	104
6	Metamodel-assisted optimization	109
6.1	Introduction	109
6.2	Case study	109
6.3	Methodology	110
6.4	Jacket design	112
6.5	Conclusions	115
7	Summary, conclusions, and future research directions	119
7.1	Summary and conclusions	119
7.2	Future research directions	120
A	Nonlinear Winkler springs model	127
A.1	Introduction and general hypotheses	127
A.2	Model description	127
A.3	Validation results	128
B	Resumen en castellano	133
B.1	Objetivos	133
B.2	Modelo estructural	133
B.3	Optimización del jacket	135
B.4	Modelos subrogados basados en redes neuronales artificiales	136
B.5	Modelo subrogado para la evaluación del jacket	137
B.6	Optimización asistida por el modelo subrogado	137
B.7	Conclusiones	138
	Bibliography	143
	Nomenclature	153



List of Figures

2.1	Representation of an OWT on a jacket support structure with four legs and four levels of bracing, all with the same inclination.	13
2.2	Flow diagram of the calculation process implemented in the structural model. Arrows connect the input variables or intermediate results with the processes that require that information. The numbers in brackets indicate the sections of this chapter in which each process is detailed.	15
2.3	Representation of the extrapolation of the aeroelastic damping produced in the rotor of the wind turbine considered on a fixed base in the system with the wind turbine on the jacket foundation.	24
2.4	Representation of the air gap needed between the jacket platform and the maximum wave crest.	27
2.5	Geometric variables considered in the joints. Adapted from DNVGL-RP-C203 [1].	27
2.6	Allowable regions for the natural frequencies of the OWT.	31
3.1	Representation of three examples of jacket designs indicating the variables included (blue) or fixed (black) in the optimization process.	38
3.2	Mass of jackets obtained in the design process, differentiated by the numbers of legs (markers) and bracing levels.	40
3.3	Diagram of the overall process of SSI relevance analysis. Designs obtained under each hypothesis are evaluated using both.	43
3.4	Utilization factors of jackets obtained in the design processes assuming soil-structure interaction effects (left) or a rigid base (right).	44
3.5	Utilization factors of jackets obtained in the design processes evaluated considering the soil-structure interaction (SSI) or a fixed base (FB).	45
4.1	Schematic representation of a simple fully connected neural network.	50
4.2	Most common activation functions used in ANNs.	51
4.3	Single hollow pile embedded in non-homogenous halfspace	56
4.4	Conceptual diagram of the fully connected neural network used for the surrogate model for pile stiffness. Input and output variables included are properly defined in Section 4.4.1	59
4.5	The 50th, 90th, 95th and 99th percentiles of the relative errors obtained by trained neural networks evaluated over test dataset.	61
4.6	Complementary cumulative distribution function (CCDF) of the error in the predictions for the individuals ANNs and the ensemble model for pile stiffness prediction.	62
4.7	Complementary cumulative distribution function (CCDF) of the error in the predictions for the ensemble model for pile stiffness prediction.	63



LIST OF FIGURES

4.8	Heatmap of the number of observations of the relative error and the coefficient of variation of the surrogate model.	63
4.9	Pile head stiffness for the lateral behaviour of a single pile depending on the pile-soil relative stiffness. Comparison of the ensemble model against fitted expressions.	64
4.10	Influence of pile length on the head stiffness for large diameter monopiles embedded in several soil profiles with the same average stiffness. Results comparing the ensemble model and the continuum model.	65
4.11	Representation of an ANN with 22 neurons in the input layer, 10 neurons in each of the two hidden layers, and 1 neuron in the output layer.	71
4.12	ANN's error cumulative distribution function for training, validation, and test data. One selected network with 4 hidden layers and 125 neurons per hidden layer, trained with a 100 000 dataset.	72
4.13	Error percentiles of different ANN with 4 hidden layers and 125 neurons per hidden layer, trained with a 100 000 samples.	73
4.14	Mean of the error percentiles of the different configurations against the number of parameters, differentiating by the dataset size.	74
4.15	Training duration of the different configurations against the number of parameters, differentiating by the dataset size.	75
4.16	Comparison of error percentiles between individual ANNs and ensemble model (EM).	76
4.17	Fundamental frequency (f_n) of the three cases described in Table 4.4 with respect to soil's shear wave velocity (c_s). Comparison between the structural model and the ANN-based surrogate model.	78
5.1	Values of the scale and shape parameters of Weibull distribution estimated for different nautic zones by Appendix B of DNVGL-RP-C205 [2]. Limits considered in this section for generating the dataset.	88
5.2	Boxplots of the classification metrics of all classification models, considering all the partial predictions aggregations and ensemble strategies.	96
5.3	Boxplots of the classification metrics of all classification models.	97
5.4	Boxplots of the classification metrics of all classification models. Different sizes of the ANNs are marked by colours.	97
5.5	Boxplots of the classification metrics of all classification models. Different partial checks aggregation strategies are marked by colours.	98
5.6	Boxplots of the classification metrics of all classification models. Different ensemble strategies are marked by colours.	99
5.7	Boxplots of the classification metrics of all regression models, considering all the partial predictions aggregation and ensemble strategies.	101
5.8	Boxplots of the classification metrics of all regression models.	101
5.9	Boxplots of the classification metrics of all regression models. Different sizes of the ANNs are marked by colours.	102
5.10	Boxplots of the classification metrics of all regression models. Different partial checks aggregation strategies are marked by colours.	103



5.11	Boxplots of utilization factors of global feasibility of the jacket in test dataset, grouped by the probability of feasibility predicted by the surrogate model. Blue boxplots are for predictions made by the maximum MCC classification model, and red boxplots are for predictions made by the maximum MCC regression model.	104
6.1	Diagram of the metamodel-assisted optimization process.	111
6.2	Mass of jackets obtained in the metamodel-assisted optimization process, differentiated by number of legs (markers) and bracing levels.	113
6.3	Angle of the bracings of the jackets obtained in the metamodel-assisted optimization process, differentiated by number of legs (markers) and bracing levels. Black dashed lines mark the lower and upper limits imposed to bracings angle in the synthetic dataset generation for training the surrogate model.	114
6.4	Evolution of the mass of the jacket designs obtained through the metamodel-assisted optimization process in each iteration. Green curve fragments show feasible jacket designs, and a transition from yellow to red indicates non-feasible jackets with utilization factors from lowest to highest. Black dashed lines represent the mass of the jacket designs obtained in Chapter 3.	114
7.1	Mass (up) and capital expenses (down) of jackets obtained in the design process addressed in Chapter 3, differentiated by the numbers of legs (markers) and bracing levels.	123
A.1	Representation of static Winkler model used for the evaluation of lateral foundation capacity.	128
A.2	Lateral head load against the lateral head displacement of the embedded pile. Rows represent different lengths of the pile, and columns represent different eccentricities of the lateral load.	129
B.1	Representación del sistema estructural. Aerogenerador soportado por una estructura jacket cimentada sobre el lecho marino.	134
B.2	Representación de tres ejemplos de diseño del jacket, indicando las variables incluidas (azul) o fijas (negro) en el proceso de optimización.	136
B.3	Diagrama del proceso de optimización asistido por el metamodelo.	138



List of Tables

2.1	Load states considered in the presented model, proposed by Arany et al. [3].	17
2.2	Load factors [4].	26
3.1	Wind turbine properties (adapted from [5]).	37
3.2	Ranges of the expressions considered in the design process. The jacket design variables are obtained from these expressions.	39
3.3	Values of the design variables of the five selected jackets.	42
4.1	Limits established for the dimensionless variables that define the problem.	57
4.2	Definition of architectures used for the architecture selection of the surrogate model for pile stiffness.	60
4.3	Search space for wind turbine, site, and jacket structure variables.	68
4.4	Parametric study cases of OWTs supported on jackets adapted from bibliography.	77
5.1	Search space of the wind turbine variables.	86
5.2	Search space of the site conditions variables.	87
5.3	Search space of the jacket substructure variables.	89
5.4	Input variables of the surrogate model for jacket feasibility evaluation.	91
5.5	Metrics of the classification and regression models with the highest MCC.	104

A vertical solid black line runs down the page. To its left, several dashed grey lines curve across the page, some entering from the top and others from the bottom. A dark blue rectangular box is positioned on the left side, containing the main title.

1. Introduction and background

- 1.1 Introduction
- 1.2 Aims and objectives
- 1.3 Research group framework
- 1.4 Published works derived from the Ph. D. Thesis
- 1.5 Structure of the dissertation





1.1 Introduction

Wind power technology has experienced significant growth in recent years, and an increasing prevalence of offshore wind farms has been observed owing to better offshore wind conditions and fewer space limitations for their installation [6]. According to the Offshore Wind Market Report, which analysed more than 200 global operating offshore wind energy projects up to 2020 [7], monopile foundations are the most frequent choice for these devices, representing 74.8% of the total, followed by jacket substructures at 10.8%. However, this trend is different for announced projects [7], where monopiles and jackets account for 51.6% and 21.5%, respectively. This change is mainly due to the increase in manufacturing options and depths at which wind turbines are installed.

To support this demand and assist in the expansion of offshore wind turbines (OWT), greater efficiency in the design and manufacturing of jacket structures should be pursued. Nevertheless, the design of complex structural systems, such as jacket structures, is a task that consumes relevant computational resources, because several load cases are considered and many structural elements must be evaluated and verified. This becomes more significant the more rigorous the calculation models implemented are. In this sense, a consideration that has not been sufficiently studied is the relevance of the soil–structure interaction (SSI), which is usually not included in optimization processes.

The main objective of this dissertation is to explore the implementation of models based on artificial neural networks (ANNs) to assist in the analysis and design of jacket structures for OWTs, taking into account the SSI effects. For this purpose, a structural numerical model is developed to obtain the jacket response to several load cases. Then, an ANN-based surrogate model is generated from the structural model to enhance the design process.

The structural model considers the expected external loads acting on the structure and the interaction among the wind turbine, the jacket elements, the foundation, and the seabed, taking into account the SSI. Then, the technical requirements imposed for these support structures are checked. Therefore, this model is used to evaluate jacket structures and guide the design process through feasible structures, that is, jacket structures that verify the imposed requirements.

In order to study the importance of SSI in the design process of jacket structures, an initial analysis is performed. For this purpose, the influence of the SSI on the structural feasibility of relevant jacket designs, obtained through an optimization process, is evaluated.

An ANN-based surrogate model is trained from a synthetic dataset previously evaluated through the structural model. This surrogate model may replace the structural model during the design process, reducing the consumption of computational resources. To analyse the usefulness of this surrogate model, a metamodel-assisted optimization process is performed. The designs obtained through this strategy highlight the advantages of using specific-developed surrogate models.

1.2 Aims and objectives

The aim of this Ph. D. Thesis is to explore the implementation of ANN-models to assist in the analysis and design of jacket structures for OWTs, taking into account the SSI effects. To address this objective, two partial objectives are established:

1. The development of a structural numerical model for studying the response of OWTs, incorporating the SSI effects. Therefore, it can be used in the development of strategies for the design of the support structure of the wind turbine. In order to evaluate the feasibility of the jacket as the support structure for the OWT, this model must take into account:
 - All the relevant elements of the system and their mutual interactions: the seabed, the foundation, the jacket substructure, the tower, and the nacelle-rotor-blade assembly.
 - The expected loads acting to the wind turbine and the jacket structure, which are the weight of the wind turbine and the structural elements, and the drag forces produced by the wind and the sea.
 - The technical requirements imposed by guidelines and recommended practices to support structures for OWTs.
2. Explore the usefulness of implementing ANN-based models to assist in the design process of support jacket structures for OWTs. These models should be able to replace the structural model in some stages of the design process. An enhancement in the jacket designs process is expected by taking advantage of the lower computational cost of the surrogate models.

1.3 Research group framework

The research group where this Ph. D. Thesis is developed works on the formulation and implementation of numerical models for solving problems of structural dynamics and elastic wave propagation. The models created have provided numerical solutions to several problems. Some of them are:

1. Soil–water–structure interaction problems. Seismic response of vault dams [8].
2. SSI problems. Dynamic response of pile foundations [9, 10] or buried structures [11, 12].
3. Dynamic behaviour of poroelastic media [13, 14].
4. Outdoor acoustic propagation. Study and optimization of the effectiveness of anti-noise screens [15].



All of them addresses the presence of unbounded media. For this reason, the basic numerical methodology used in the development of all these models is the Boundary Element Method. This methodology naturally takes into account the energy radiation, which offers advantages in the numerical treatment of problems that involve unbounded regions. Furthermore, based on these models, optimization strategies applied to some of these problems have recently been addressed [12, 15].

In this context, the research group has taken advantage of the experience in the infinite media problems to address another task: the design and analysis of the support structures of OWTs. This is a relevant problem, where the influence of SSI on these devices should be taken into account. The present Ph. D. Thesis belongs to this framework, being part of two research projects.

1.3.1 Research Project BIA2017-88770-R¹

The Research Project BIA2017-88770-R, which has already concluded, was supported by the Subdirección General de Proyectos de Investigación of the Ministerio de Economía, Industria y Competitividad (MINECO) and Agencia Estatal de Investigación (AEI) of Spain and FEDER. This project was entitled “Influence of soil–structure interaction phenomena in the seismic response of offshore wind turbines”, and was focused on two main objectives:

1. The development, implementation and validation of numerical models for the evaluation of the wind turbine and the support structure response. These models aimed to analyse the system constituted by the seabed, the foundation, the substructure, and the tower of the wind turbine as a coupled system, incorporating their mutual interactions, to obtain the structural dynamic response.

Several foundation typologies were considered, including gravity foundations, suction caissons, and embedded piles. Also, mono or multi-element substructures were assumed as the support structure. Coupled harmonic formulations of finite element method (substructure, tower, foundation) and boundary element methods (soil–foundation interaction) were implemented.

2. The model developed for first objective was applied to relevant problems to study the response of wind turbines and the effects of seismic excitation. The influence of the foundation typology, the soil, and the excitation characteristics were analysed, focusing on the relevance of SSI phenomena.

This Ph. D. Thesis contributed to the development of the first objective of the research project by developing a model for evaluating the structural response of the jacket structure for OWTs.

¹Adapted from the Scientific Report for the application of the Research Project. Supported by the Subdirección General de Proyectos de Investigación of the Ministerio de Economía, Industria y Competitividad (MINECO) and Agencia Estatal de Investigación (AEI) of Spain and FEDER. Project duration: 3 years (January 2018 – December 2020).

1.3.2 Research Project PID2020-120102RB-I00²

The Research Project PID2020-120102RB-I00, on which work continues, is supported by the Ministerio de Ciencia e Innovación (MCI) and the Agencia Estatal de Investigación (AEI) of Spain. The project is entitled “ANN-based design of the support structures of offshore wind turbines including advanced models of soil-structure interaction and seismic actions”, and is focused on two main objectives:

1. The development of a methodology, based on artificial neural networks, for the design of the support structures for offshore wind turbines founded on the seabed, including its foundation. The requirements that these structures must verify, the environmental loads, the geotechnical conditions, and aspects such as water depth must be taken into account. The search for solutions with lower economic cost and material consumption are also included as a design criterion. The structural analysis is carried out using the computational models developed by the group in previous research projects, and the design methodology will be based fundamentally on artificial neural networks under a supervised learning paradigm.
2. The application of the models, already developed by the research group, to expand the studies included in the previous Research Project BIA2017-88770-R. The identification of main factors that determine the seismic response of offshore wind turbines is intended.

The first objective of the research project is mainly developed in the present Ph. D. Thesis. The evaluation of technical requirements imposed for jacket support structures by international standards, the development of ANNs-based surrogate models for jacket evaluation, and the metamodel-assisted optimization of jacket design establish the bases for completing this objective.

1.4 Published works derived from the Ph. D. Thesis

The publications and communications derived from the results obtained during the development of the objectives established for the present Ph. D. Thesis are listed in this section.

1.4.1 Contributions in JCR journals

- C. Medina, G. M. Álamo and R. Quevedo-Reina. Evolution of the seismic response of monopile-supported offshore wind turbines of increasing size from 5 to 15 MW including dynamic soil-structure interaction. *Journal of Marine Science and Engineering*, 9(11), 2021

²Adapted from the Scientific Report for the application of the Research Project. Supported by the Ministerio de Ciencia e Innovación (MCI) and the Agencia Estatal de Investigación (AEI) of Spain. Project duration: 3 years (July 2021 – June 2024).



- R. Quevedo-Reina, G. M. Álamo, L. A. Padrón and J. J. Aznárez. Surrogate model based on ANN for the evaluation of the fundamental frequency of offshore wind turbines supported on jackets. *Computers & Structures*, 274:106917, 2023
- R. Quevedo-Reina, G. M. Álamo, S. François, G. Lombaert and J. J. Aznárez. Importance of the soil–structure interaction in the optimisation of the jacket designs of offshore wind turbines. *Ocean Engineering*, 303:117802, 2024
- R. Quevedo-Reina, G. M. Álamo and J. J. Aznárez. Estimation of pile stiffness in non-homogeneous soils through artificial neural networks. *Engineering Structures*, 308:117999, 2024
- B. Benítez-Suárez, R. Quevedo-Reina, G. M. Álamo and L. A. Padrón. PSO-based design and optimization of jacket substructures for offshore wind turbines. *Marine Structures*, (under review), 2024

1.4.2 Conference contributions

- R. Quevedo-Reina, G. M. Álamo, L. A. Padrón and J. J. Aznárez. Dynamic characterization of offshore wind turbines supported on a jacket using artificial neural networks. *World Congress in Computational Mechanics and ECCOMAS Congress*, Oslo, Norway, 5–9 June 2022
- R. Quevedo-Reina, G. M. Alamo, L. A. Padrón, J. J. Aznárez and O. Maeso. Characterization of pile stiffness using artificial neural networks. *Congress on Numerical Methods in Engineering*, Las Palmas de Gran Canaria, Spain, 12–14 September 2022
- R. Quevedo-Reina, G. M. Alamo, L. A. Padrón, J. J. Aznárez and O. Maeso. Structural evaluation of offshore wind turbines supported on a jacket using artificial neural networks. *Congress on Numerical Methods in Engineering*, Las Palmas de Gran Canaria, Spain, 12–14 September 2022
- C. Medina, G. M. Alamo and R. Quevedo-Reina. Respuesta sísmica de aerogeneradores marinos monopilotados de gran tamaño considerando la interacción dinámica suelo-estructura. *Congress on Numerical Methods in Engineering*, Las Palmas de Gran Canaria, Spain, 12–14 September 2022

1.5 Structure of the dissertation

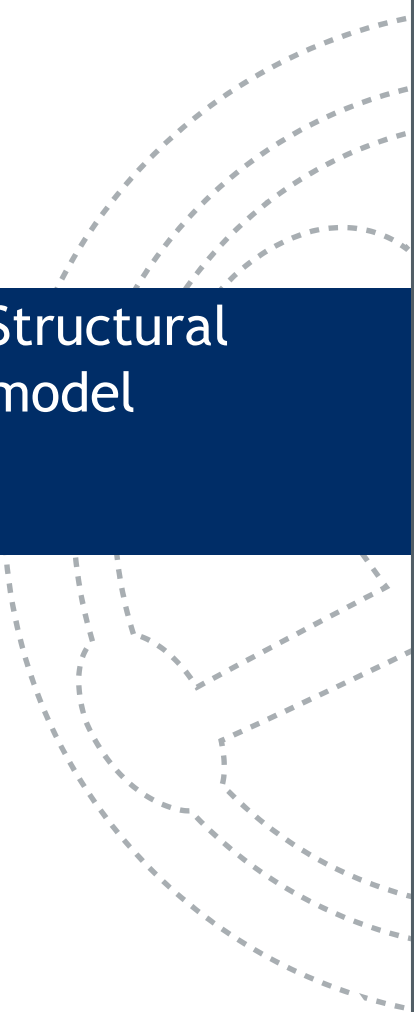
The work developed during the Ph. D. Thesis is structured in this document. The contents are divided in seven chapters and two appendices that organize the partial objectives addressed. Instead of a single state-of-the-art review at the beginning of the document, specific introductions are included in every chapter. In addition, every chapter collects the specific conclusions extracted on it. The contents included in the chapters and appendices are the following:



- Chapter 1: Introduction and background.
It is the present chapter. A brief introduction of the motivation of this dissertation and its main objectives are detailed.
- Chapter 2: Structural model.
This chapter presents the structural model for jacket assessment developed. This model incorporates the loads acting on the structure, the evaluation of the jacket response, taking into account the SSI, and the verification of the technical requirements imposed.
- Chapter 3: Jacket optimization.
In this chapter, an initial approach of an optimization procedure to obtain jacket designs is performed. To ensure the feasibility of the jackets designs, the structural model presented in Chapter 2 is used. Additionally, the importance of SSI in the optimization process of these structures is analysed.
- Chapter 4: Surrogate models based on artificial neural networks.
A brief introduction of the surrogate models based on ANNs is presented. In order to explore the capabilities of this methodology, two surrogate models for related problems are developed: first, a surrogate model for pile stiffness estimation, and later, a surrogate model for dynamic characterization of OWT on a jacket structure, including SSI effects.
- Chapter 5: Surrogate models for jacket evaluation.
In this chapter, ANN-based surrogate models for jacket evaluation are developed, following the methodology presented in Chapter 4. To train these models, the structural behaviour of the jacket as the support structure for the OWT is extracted from the structural model described in Chapter 2.
- Chapter 6: Metamodel-assisted optimization.
This chapter performs a metamodel-assisted optimization process to obtain jacket designs. The surrogate model developed in Chapter 5 is used. Optimization results are compared to those obtained in Chapter 3.
- Chapter 7: Summary, conclusions, and future research directions.
As the chapter title indicates, the main aspects of the developed tasks and their conclusions are summarized. In addition, some future research directions are proposed.
- Appendix A: Nonlinear Winkler springs model.
This appendix present the nonlinear Winkler spring model developed to evaluate the lateral pile capacity in the model described in Chapter 2.
- Appendix B: Resumen en castellano.
This appendix contains a summary in Spanish of the present Ph. D. Thesis.

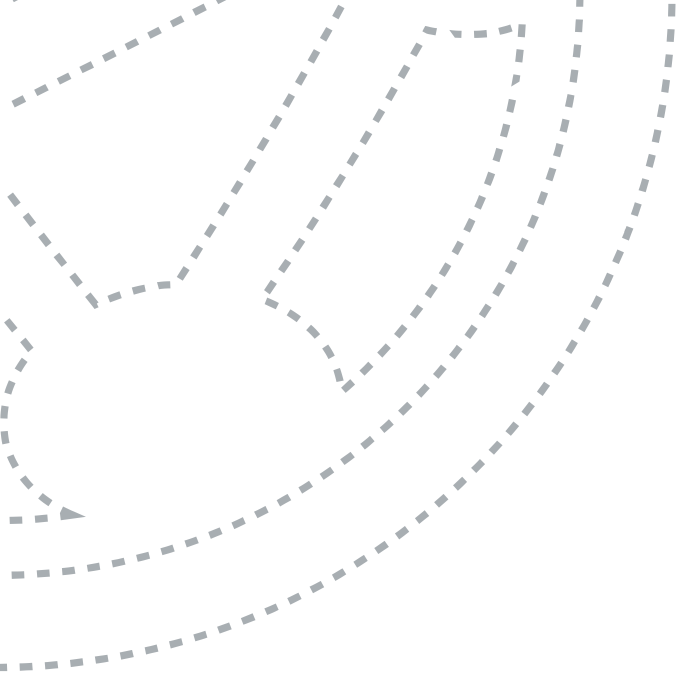


After the contents of the document, the complete list of the bibliographical references is included. Also, the nomenclature with the acronyms utilized in the document, and the Greek and Roman symbols used as variables are detailed.



2. Structural model

- 1.1 Introduction and general hypothesis
- 2.2 Design loads
- 2.3 Numerical model for structural analysis
- 2.4 Design principles



2.1 Introduction and general hypothesis

This chapter presents the structural model used to evaluate the response and feasibility of the jacket as support structure of OWT. This model is a fundamental element for the Ph. D. Thesis, because it will be used as an auxiliary tool to develop the specific objectives of the other chapters of the document.

A jacket foundation is a three-dimensional structure composed of tubular elements welded as a frame structure, as shown in Figure 2.1. The geometry of this structure is typically reduced to three or four legs joined by different levels of bracing, which provide stability.

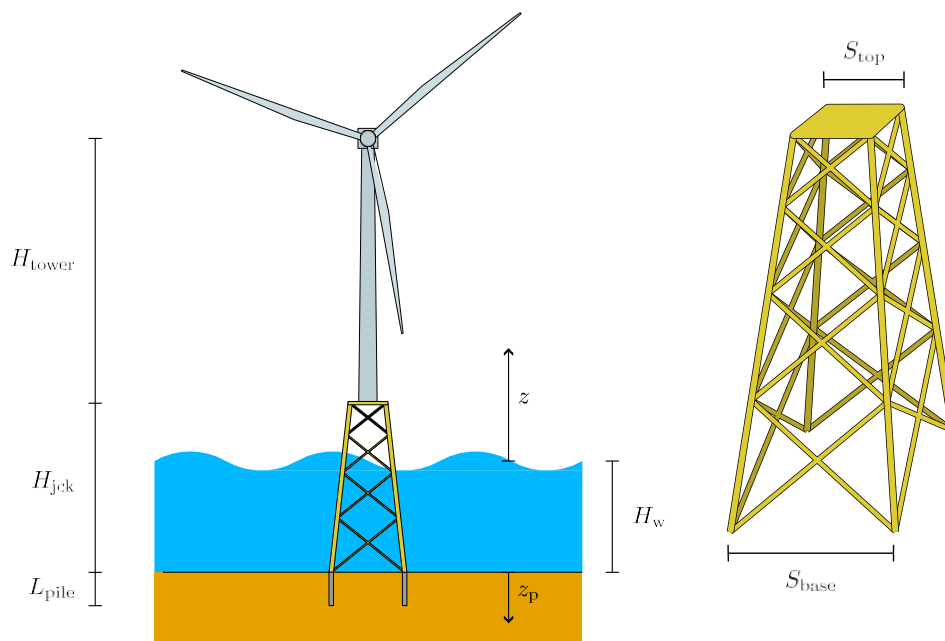


Figure 2.1. Representation of an OWT on a jacket support structure with four legs and four levels of bracing, all with the same inclination.

From a general perspective, the system topology can be defined by the following set of hyperparameters: the height of the structure (H_{jck}), number of legs (n_{leg}), number of bracings (n_{br}) and their spacing, and separation of the legs at the base (S_{base}) and top (S_{top}). Regarding cross-sections, note that the geometries of several elements must coincide to provide radial symmetry to the structure. The structural assembly is fixed to the seabed using foundation elements connected to the bottom of the legs of the structure. A pile foundation is assumed in this Ph. D. Thesis.

Three different modules can be found within the presented model. First, the evaluation of the design loads that are considered to act on the support structure, detailed in Section 2.2. Gravitational loads derived from the wind turbine and the structural elements, as well as their buoyancy, are included. In addition, a set of load cases of the environmental loads produced by the drag forces of the wind and the sea, proposed by

Arany et al. [3], are taken into account. Also, IEC [25] and DNV [2, 4] standards are also consulted for the loads definition.

Second, the numerical model used to obtain the structural response is described in Section 2.3. An equivalent static analysis through a linear finite element model is performed to obtain the displacements and internal forces produced by the external loads. SSI is considered by pile-heads impedance functions computed by a previously developed model [10].

Third, the technical requirements listed in Section 2.4 are checked. Some geometric restrictions are imposed to ensure the feasibility of the structure. Also, most relevant failure criteria from DNV [4, 26] and API [27] codes are taken into account.

Figure 2.2 shows a flow diagram of all the processes implemented in the model and the information flow. This information flow is represented by arrows that start with the corresponding input variables or outputs of the intermediate processes, and end with the process that requires this information.

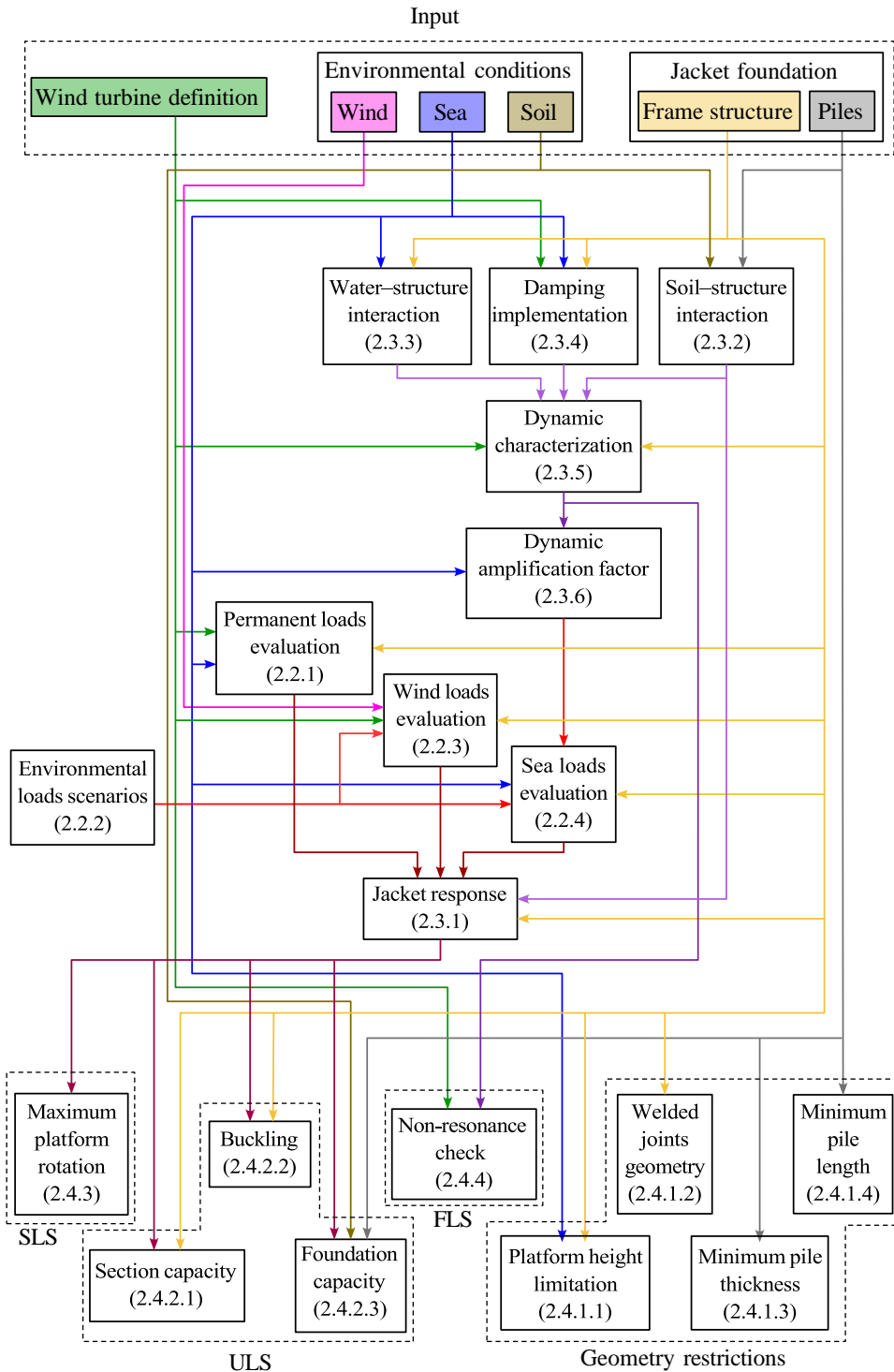


Figure 2.2. Flow diagram of the calculation process implemented in the structural model. Arrows connect the input variables or intermediate results with the processes that require that information. The numbers in brackets indicate the sections of this chapter in which each process is detailed.

2.2 Design loads

The jacket structure must support permanent loads derived from gravitational action, and variable loads caused mainly by the action of meteorological and hydrological phenomena. International standards include all loads that must be considered in the design. However, this model includes the most relevant loads for determining the design of this type of foundation, as described in this section.

2.2.1 Permanent loads

The permanent loads considered in this Ph. D. Thesis are limited to gravitational loads. First, the self-weight is considered as a distributed vertical load for all the tubular members of the jacket structure. The platform and wind turbine weights are considered as punctual vertical loads applied to the centre of the jacket top platform.

The other contribution is the hydrostatic pressure on the submerged elements, which produces buoyancy forces. Considering the hydrostatic pressure produced by water, punctual loads at the nodes owing to the pressure on the free faces of the section and a normal sectional load distributed along the element owing to the pressure gradient in the section are considered.

2.2.2 Environmental load scenarios

DNV codes [4] contain numerous load combinations that must be verified in OWT designs. Evaluating all of them in an approximate procedure such as the one proposed herein would increase the computational cost of the process and reduce the advantages of its use. Therefore, the environmental loads implemented in this model are reduced to those derived from the action of wind and sea, which are known to be the most frequent and significant in this type of offshore structure. The five load hypotheses proposed by Arany et al. [3] are adopted as the most significant hypotheses for the proposed evaluation model. The load states listed in Table 2.1 are based on different combinations of wind and waves. The wind conditions are as follows.

- U1 - Normal turbulence scenario: The average wind speed is equal to the rated wind speed (U_R) under a normal turbulence model (NTM).
- U2 - Extreme turbulence scenario: The average wind speed is equal to the rated wind speed (U_R) under an extreme turbulence model (ETM).
- U3 - Extreme gust at rated wind speed scenario: The average wind speed is equal to the rated wind speed (U_R) under the 50-y extreme operating gust (EOG).
- U4 - Extreme gust at cut-out scenario: The average wind speed is equal to the cut-out wind speed (U_{out}) under the 50-y extreme operating gust (EOG).

Conversely, the conditions related to waves are

Table 2.1. Load states considered in the presented model, proposed by Arany et al. [3].

Scenario	Wind model	Wave model	Alignment	Limit state
E1	NTM at U_R (U1)	1-y ESS (W1)	Collinear	ULS and SLS
E2	ETM at U_R (U2)	50-y EWH (W4)	Collinear	ULS and SLS
E3	EOG at U_R (U3)	1-y EWH (W2)	Collinear	ULS and SLS
E4	EOG at U_{out} (U4)	50-y EWH (W4)	Collinear	ULS and SLS
E5	ETM at U_R (U2)	50-y EWH (W4)	Misaligned 90°	ULS and SLS

W1 - 1-y extreme sea state: A stationary wave scenario with a 1-y significant wave height.

W2 - 1-y extreme wave height: A stationary wave scenario with a 1-y maximum wave height.

W3 - 50-y extreme sea state: A stationary wave scenario with a 50-y significant wave height.

W4 - 50-y extreme wave height: A stationary wave scenario with a 50-y maximum wave height.

The expressions needed to evaluate these scenarios are summarized in subsequent sections.

2.2.3 Wind loads

The main component of wind action is the load on the wind turbine rotor. This can be simplified as

$$F_{TH} = \frac{1}{2} \rho_a A_R C_T (u_m + u_{tb})^2 \quad (2.1)$$

where A_R represents the wind turbine rotor area, u_m and u_{tb} are the mean and turbulent components of the wind speed, respectively, and C_T is the thrust coefficient used by Arany et al. [3].

$$C_T = \begin{cases} \frac{3.5(2u_m + 3.5)}{u_m^2} & u_m \leq U_R \\ \frac{3.5U_R(2U_R + 3.5)}{u_m^3} & U_R < u_m \leq U_{out} \end{cases} ; \text{ being } C_T \leq 1 \quad (2.2)$$

where U_R and U_{out} are the rated and cut-out wind speeds of the wind turbine, respectively.

In addition, the wind load acting on the structural elements located above sea level is considered. In this case, a distributed load is implemented along the element according to DNVGL-RP-C205 [2].

$$f_{th} = \frac{1}{2} C_D D_{Qa} \sin(\alpha_w) u_{wind}(z)^2 \quad (2.3)$$

where C_D represents the drag coefficient (defined in Equation (2.14)), α_w the angle between the wind direction and the element axis, and u_{wind} is the wind velocity, which depends on the height (z):

$$u_{wind}(z) = u_{wind}(z_{ref}) \left(\frac{z}{z_{ref}} \right)^{0.12} \quad (2.4)$$

To evaluate this load in the different load cases, the mean speed (u_m) is considered to be the one that characterizes the load state (Table 2.1), whereas the turbulent speed (u_{tb}) is estimated from the associated wind model (defined by IEC-61400-1 [25]).

- Normal turbulence model (NTM)

The standard deviation presented by the wind turbulence under this model is defined as

$$\sigma_{NTM} = I_{ref} (0.75 u_m + 5.6) \quad (2.5)$$

where I_{ref} is the expected value of the turbulence intensity at 15 m/s, which depends on the class of the wind turbine. In this Ph. D. Thesis, a value of 0.16 is taken as it is the most critical case. In a real wind turbine, it must be understood that the pitch control will modify the blade orientation, and with it, the drag coefficient. Therefore, turbulence with a sufficiently low frequency of variation should not be included in this calculation because there would be a different load hypothesis at another wind speed. It is assumed that the frequency limit that the pitch control could not correct is the maximum rotor speed ($f_{r,max}$) [3]. The Kaimal spectrum [28] is used to recalculate the standard deviation of turbulence:

$$\sigma_{NTM, f_{KS} \geq f_{r,max}} = \sigma_{NTM} \int_{f_{r,max}}^{\infty} \frac{4.84 \Lambda_1}{1 + \frac{6.8 \cdot 1 \Lambda_1}{u_m} f_{KS}}^{\frac{5}{3}} df = \sigma_{NTM} \int_{f_{r,max}}^{\infty} \frac{1}{1 + \frac{6.8 \cdot 1 \Lambda_1}{u_m} f_{r,max}}^{\frac{2}{3}} df \quad (2.6)$$

where Λ_1 is the scalar parameter of longitudinal turbulence,

$$\Lambda_1 = \begin{cases} 0.7z & z \leq 60 \text{ m} \\ 42 & z \geq 60 \text{ m} \end{cases} \quad (2.7)$$

Given that the IEC-61400-1 [25] standard establishes the 90% percentile as a representative value for this turbulence model, the turbulent component of speed would be

$$u_{tb} = 1.282 \sigma_{NTM, f_{KS} \geq f_{r,max}} \quad (2.8)$$

- Extreme turbulence model (ETM)

The procedure for obtaining the turbulent component of the velocity in the extreme turbulence model is similar to that of the normal turbulence model. In this case, the standard deviation also depends on the annual average wind velocity at the hub level (u_{avg}), as indicated by the following expression:

$$\sigma_{ETM} = 2 I_{ref} \left(0.072 \frac{u_{avg}}{2} + 3 \frac{u_m}{2} - 4 \right) + 10 \quad (2.9)$$

The same procedure as in Equation (2.6) is applied, and the representative value for turbulence is established at the 95th percentile.

$$u_{tb} = 1.645 \sigma_{ETM, f_{KS} \geq f_{r,max}} \quad (2.10)$$

- Extreme operating gust (EOG)

In the case of the extreme operating gust, the turbulent component of wind velocity is defined by the following expression:

$$u_{tb} = \min \left(1.35 (0.8 u_{e50} - u_m); \frac{3.3 \sigma_{NTM}}{1 + \frac{D_{rotor}}{10 \Lambda_1}} \right) \quad (2.11)$$

where σ_{NTM} is defined by Equation (2.5), Λ_1 by Equation (2.7), D_{rotor} is the rotor diameter, and u_{e50} is the reference wind speed, which is established by the class of the wind turbine and is defined as the mean value of 10 min of the extreme wind speed at the height of the hub, with a recurrence period of 50 y. Because this reference data is generally not available, following DNVGL-RP-C205 [2], its value is estimated from the characterization of the wind in the area:

$$u_{e50} = \lambda_{wind} \left(-\ln \left(1 - \frac{1}{5256} \right) \right)^{\frac{1}{k_{wind}}} \quad (2.12)$$

where λ_{wind} and k_{wind} are the scale and shape parameters of the Weibull distribution of wind velocity, respectively.

2.2.4 Sea load

A drag force perpendicular to the element is considered for the submerged elements of the jacket. The tangential component is neglected. According to DNVGL-RP-C205 [2], the force received by the structural element can be evaluated as follows:

$$f_{wn} = Q_w C_M \frac{\pi D^2}{4} v_n^2 + \frac{1}{2} Q_w C_D D |v_n| v_n \quad (2.13)$$

where v_n and \dot{v}_n are the normal components of the water particle velocity and acceleration, respectively, C_M is the mass coefficient (taken as 2 for safety reason), and C_D is the drag coefficient, which is obtained via

$$C_D = \begin{cases} 0.65 & \Delta \leq 10^{-4} \\ \frac{(29 + 4 \log(\Delta))/20}{1.05} & 10^{-4} < \Delta \leq 10^{-2} \\ 1.05 & \Delta > 10^{-2} \end{cases} \quad \text{being } \Delta = 5 \cdot 10^{-6}/D \quad (2.14)$$

The water particle velocity and acceleration fields are defined through the superposition of the wave and current models. Both models are extracted from DNVGL-RP-C205 [2].

- Current model:

The implemented current model assumes constant velocities; therefore, its contribution to the acceleration field is neglected. The velocity of the water particles is obtained from the superposition of the wind-generated and circulatory currents:

- Wind-generated current: This is modelled by a linear profile from the water surface to a depth of 50 m. The induced speed on the surface corresponded to 3% of the wind speed at a height of 10 m.

$$v_{c,wind}(z) = v_{c,wind}(0) \frac{(z + 50)}{50} \quad \text{for } -50 \text{ m} \leq z \leq 0 \quad (2.15)$$

- Circulatory currents: The tidal current velocity profile along water depth (H_w) is considered. The particle velocity on the surface is assumed to represent current environmental data.

$$v_{c,circ}(z) = v_{c,circ}(0) \frac{(z + H_w)}{H_w} \quad \text{for } z \leq 0 \quad (2.16)$$

- Wave model

To define the water particle velocity and acceleration fields completely, it is necessary to determine the wave period. According to DNVGL-ST-0437 [4], the wave period in deep water can be assumed to be within the following range:

$$11.1 \frac{\overline{h_{wave}}}{g} \leq T_{wave} \leq 14.3 \frac{\overline{h_{wave}}}{g} \quad (2.17)$$

From this interval, the lower limit can be assumed to be the period of the wave in the calculation, because it is the worst-case scenario. The velocity and acceleration fields can then be defined according to the Airy wave theory.

$$v_{w,x} = \frac{\pi h_{\text{wave}} \cosh(k_{\text{wave}}(z + H_w))}{T_{\text{wave}} \sinh(k_{\text{wave}} H_w)} \cos \left(k_{\text{wave}} x - \frac{2\pi}{T_{\text{wave}}} t \right) \quad (2.18a)$$

$$v_{w,z} = \frac{\pi h_{\text{wave}} \sinh(k_{\text{wave}}(z + H_w))}{T_{\text{wave}} \sinh(k_{\text{wave}} H_w)} \sin \left(k_{\text{wave}} x - \frac{2\pi}{T_{\text{wave}}} t \right) \quad (2.18b)$$

$$\dot{v}_{w,x} = \frac{2\pi^2 h_{\text{wave}} \cosh(k_{\text{wave}}(z + H_w))}{T_{\text{wave}}^2 \sinh(k_{\text{wave}} H_w)} \sin \left(k_{\text{wave}} x - \frac{2\pi}{T_{\text{wave}}} t \right) \quad (2.18c)$$

$$\dot{v}_{w,z} = -\frac{2\pi^2 h_{\text{wave}} \sinh(k_{\text{wave}}(z + H_w))}{T_{\text{wave}}^2 \sinh(k_{\text{wave}} H_w)} \cos \left(k_{\text{wave}} x - \frac{2\pi}{T_{\text{wave}}} t \right) \quad (2.18d)$$

where k_{wave} is the wave number obtained by solving the following implicit equation:

$$\frac{2\pi}{k_{\text{wave}} T_{\text{wave}}} = \sqrt{\frac{g}{k_{\text{wave}} \tanh(k_{\text{wave}} H_w)}} \quad (2.19)$$

2.3 Numerical model for structural analysis

The proposed model performs an equivalent static analysis of the jacket response under external forces. However, the dynamic characterization of the system is a fundamental aspect for the feasibility evaluation of the structure. Therefore, the dynamic effects of the water–structure interaction, damping, and SSI are introduced for this calculation.

2.3.1 Jacket substructure response

To analyse the static response of the jacket foundation, the wind turbine and its loads are replaced by the loads transferred to the jacket. This is mechanically allowed because the wind turbine forms an isostatic subsystem, and the efforts at the tower base depend only on the loads and not on the displacements. Nevertheless, this element must be included in the dynamic characterization described in Section 2.3.5. A linear finite element model is implemented to obtain the response of the jacket structure under the loads described in Section 2.2. For each load case, the following system of equations is solved:

$$\mathbf{K} \cdot \mathbf{u} = \mathbf{F}_{\text{ext}} \quad (2.20)$$

Where \mathbf{F}_{ext} represents the vector of the external forces acting on the structure, \mathbf{K} is the stiffness matrix of the system, and \mathbf{u} is the nodal displacement.

The structural elements are modelled using Timoshenko beam theory [29], considering a rigid connection between the elements in the welded joints. The platform is considered to be rigid, linking the nodes of the upper legs.

All the external forces applied to the wind turbine and the weight of the platform are transformed into an equivalent system of forces applied on the central node located at the top of the jacket structure, whereas the external forces on the jacket are considered as trapezoid-distributed loads. Non-trapezoidal distributed loads, such as wave loads from sea states, are discretized into sufficient trapezoidal intervals to approximate the variability of the loads along the elements, and each interval is computed as an independent trapezoidal load.

2.3.2 Soil-structure interaction

SSI is considered by including the foundation stiffness in the stiffness matrix of the structure,

$$\mathbf{K} = \begin{bmatrix} \mathbf{K}_{j,j} & \mathbf{K}_{j,f} \\ \mathbf{K}_{f,j} & \mathbf{K}_{f,f} + \mathbf{K}_{SSI} \end{bmatrix} \quad (2.21)$$

where $\mathbf{K}_{a,b}$ represent the stiffness sub-matrices related to the jacket (\square_j) or foundation link (\square_f) nodes, and \mathbf{K}_{SSI} is the impedance matrix of the foundation (which can include all the effects related to stiffness, damping, and inertia relevant for the natural frequencies calculation in Section 2.3.5). In general, the impedance matrix of the foundation contains all the terms corresponding to the lateral, torsional, and axial modes of the piles, as well as the coupled terms representing the pile–soil–pile interaction.

This model allows the implementation of different impedance functions to reproduce the SSI. In this Ph. D. Thesis, the stiffness of the pile foundation is obtained from a previously developed continuum numerical model [10] that has been verified and successfully employed in the analysis of several SSI problems (see, for example, [30, 31]). This model is based on the integral expression of the reciprocity theorem in elastodynamics and the use of advanced fundamental solutions for reproducing the behaviour of the layered soil. These fundamental solutions already satisfy the free-field and inter-layer boundary conditions, which avoid any meshing of the soil surfaces. Piles are treated as load lines in the soil formulation and their stiffness and inertial contribution are considered through their definition as finite elements beams. Pile–soil coupling is made by imposing compatibility and equilibrium conditions in terms of displacements and soil–pile interaction forces, respectively. This model reproduces the three-dimensional linear elastic response of a group of piles embedded in soil. The impedance matrix obtained through this model contains all terms corresponding to the individual pile response and pile–soil–pile interaction of the lateral (horizontal, rocking, and swaying) and axial (vertical) modes. No torsional interaction is considered between the individual piles and the surrounding soil.

Despite it is a model generally oriented to the analysis of dynamic problems in the frequency domain, it is implemented in such a way that it can reproduce the corresponding static problem assuming sufficiently low frequencies. In the case of a static analysis (such as that described in Section 2.3.1), results are obtained considering a wavelength of the shear wave of the soil at reference depth 100 times greater than the pile diameter. These assumptions result in a very efficient but accurate model.

However, the proposed structural model can also neglect any SSI effect by considering the bottom of the legs to be completely fixed (that is, the rigid base assumption).

2.3.3 Water-structure interaction

To consider the water–structure interaction phenomena, the distributed mass of the submerged elements is increased for the transverse displacements by the following term:

$$m_w = \rho_w \frac{\pi (D - 2T)^2}{4} + C_A \rho_w \frac{\pi D^2}{4} \quad (2.22)$$

where C_A is the added mass coefficient, which is typically considered to be 1. Equation (2.22) shows two different terms. The first is attributed to the mass contained inside the structural element (in case it is filled with water), and the second is associated with the interaction with the surrounding water, which is established according to DNV-RP-C205 [2].

2.3.4 Damping

Four sources of damping of the dynamic system are included in the proposed model.

- Frequency-independent material damping is considered, and the hysteretic damping coefficient is used to define a complex-valued Young's modulus.
- Energy dissipation by the water–structure interaction is simplified as an increase in the damping of the material of the submerged tubular elements.
- Energy dissipation by the SSI is introduced by the imaginary component of the impedance matrix added to the system.
- Aeroelastic damping is incorporated as a local hysteric frequency-independent damper into the rotor shaft. The damping coefficient is obtained as $C^a = 2 \xi_{ae} K^{eq}$ from the considered aeroelastic damping ratio for the device (ξ_{ae}) and the equivalent stiffness corresponding to the fundamental mode of the wind turbine founded on a rigid base (K^{eq}). Owing to the particular dynamic characteristics of this system, the equivalent stiffness value could be approximated using the static stiffness at the rotor height. Once the local damping is determined, it is applied to the rotor node of the complete system, where the wind turbine is supported by the jacket structure. A representation of this is shown in Figure 2.3.

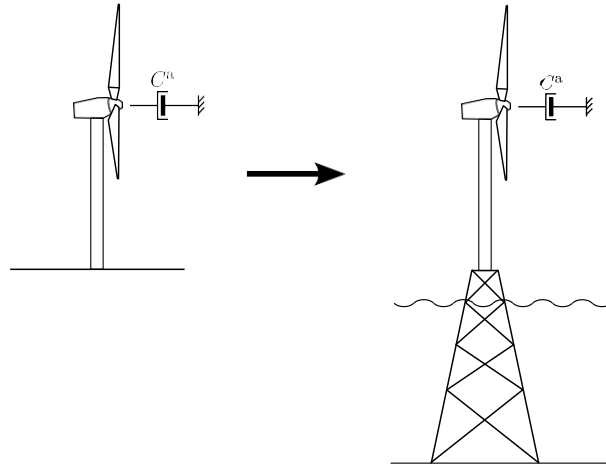


Figure 2.3. Representation of the extrapolation of the aeroelastic damping produced in the rotor of the wind turbine considered on a fixed base in the system with the wind turbine on the jacket foundation.

2.3.5 Dynamic characterization

To obtain a dynamic characterization of the structural system, it is necessary to incorporate the wind turbine into the finite element model. For this purpose, the tower is discretized into a sufficient number of elements with a uniform section so that it is capable of reproducing its tapered geometry, and it is linked to the upper central node of the jacket structure. With respect to the mass of the system, a mass matrix is constructed to collect the inertial behaviour of the tubular elements of the jacket and the water–structure interaction (Section 2.3.3). In addition, the mass and inertias of the rotor-nacelle assembly (RNA) and the mass of the platform are introduced as punctual masses and inertias.

The natural frequencies of the system are obtained by solving the eigenvalue problem $\mathbf{K} \omega^2 \mathbf{M} = 10$. When the SSI interaction model is frequency-dependent, this procedure must be solved iteratively while updating the impedance values.

Because damping is introduced into the system through complex terms in the stiffness matrix, the natural frequencies obtained are complex valued. Therefore, the values of the real natural frequency and damping of the system are obtained through an analogy with a system of one degree of freedom using the following expressions:

$$f_n = |\tilde{f}| \tag{2.23a}$$

$$\xi_n = \frac{\text{Im}(\tilde{f})}{|\tilde{f}|} \tag{2.23b}$$

where \tilde{f} represents the complex frequency obtained by the eigenvalue, f_n is the natural frequency of the system, and ξ_n is the equivalent viscous damping of the vibration mode.

2.3.6 Equivalent static analysis

The structural response is evaluated using an equivalent static analysis, as indicated by Equation (2.20). However, the considered environmental loads exhibits time dependence, which has to be adequately addressed. Wind loads are assumed to vary over long periods of time; therefore, they can be directly considered as static loads.

However, the wave load presents a significant oscillation over short periods of time, which can induce dynamic effects on the structure that increase the stresses to which it is subjected. Therefore, following the recommendation of Arany et al. [3], the contribution of the waves to the sea load is increased by the following dynamic amplification factor (DAF):

$$DAF = \frac{1}{\sqrt{\left(1 - \frac{1}{T_{wave} f_n}\right)^2 + \left(\frac{\xi_n}{T_{wave} f_n}\right)^2}} \quad (2.24)$$

where T_{wave} represents the period of the wave excitation, f_n is the natural frequency of the system, and ξ_n is the mode damping. For the conservative approach, the highest amplification factor among the different vibration modes is selected. Because the sea load is obtained from the nonlinear superposition of the wave (periodic) and current (static) velocity fields, the DAF value is only applied to the dynamic component of the sea load, that is, the difference between the total sea load and the load obtained only because of the current velocity field:

$$f_{wn}^{eq} = f_{wn}^{current} + DAF (f_{wn} - f_{wn}^{current}) \quad (2.25)$$

In addition to the dynamic amplification effects, wave oscillation induces a significant variation in the magnitude and direction of sea loads (Equation (2.18)). To account for this variation and ensure that the jacket structure is evaluated at a critical instant in the wave cycle, different phases of the wave cycle must be considered and verified. To collect the load variability accurately, 15 independent load states are included for each sea state, with their phases homogeneously distributed throughout the wave cycle.

2.4 Design principles

The requirements that jacket foundations should fulfil, established by international standards, are detailed in this section. According to their characteristics, the restrictions can be geometric, with some limitations imposed on the dimensions of the structural elements or the assembly according to technical criteria, or failure, which are the criteria that determine the integrity and functionality of the structural assembly. This last group is divided into ULS, SLS, and FLS. Structural analysis is required to determine the forces, displacements, and dynamic characterization of the jacket foundation.

To easily measure the feasibility of the structure, a utilization factor (η) is introduced for each check. This factor is used to transform the generic expressions of the

inequality constraints into dimensionless and uniform inequalities by dividing the two terms of the inequality; thus, the requirement is fulfilled if its value is equal to or less than 1. This new indicator allows a clear comparison of the closeness of the evaluated design to the restrictions imposed on each check.

To determine the effects of external loads on the structure, a partial safety factor method is used to obtain the target safety level. For the material factor (γ_M), DNVGL-ST-0126 [32] recommends taking a value of 1.1 for tubular structures, whereas the load factor can be found in DNVGL-ST-0437 [4]. Table 2.2 lists the values considered for each load type depending on the required check. To reduce the calculation, and assuming that it is sufficiently secure, a value of 1.1 is considered for the different ULS checks in permanent loads.

Table 2.2. Load factors [4].

	ULS (Favourable)	ULS (Unfavourable)	SLS
Permanent loads	0.90	1.10	1.00
Environmental loads	1.35	1.35	1.00

2.4.1 Geometric requirements

2.4.1.1 Platform height

Jacket platforms for offshore support structures do not need to be designed to resist direct wave impacts. Therefore, the height of the platform should be set to be sufficient to overcome the largest expected waves, including an air gap (represented in Figure 2.4). This air gap (g_a) must be at least 20% of the wave height, but with a minimum value of 1 m, according to DNVGL-ST-0126 [32].

$$H_{\text{jek}} \geq H_w + \frac{H_{\text{EWH},50}}{2} + \max\{0.2 H_{\text{ESS},50}, 1\} \quad (2.26)$$

where H_w represents the maximum expected depth of water, $H_{\text{EWH},50}$ is the 50-y extreme wave height, and $H_{\text{ESS},50}$ is the 50-y extreme sea state.

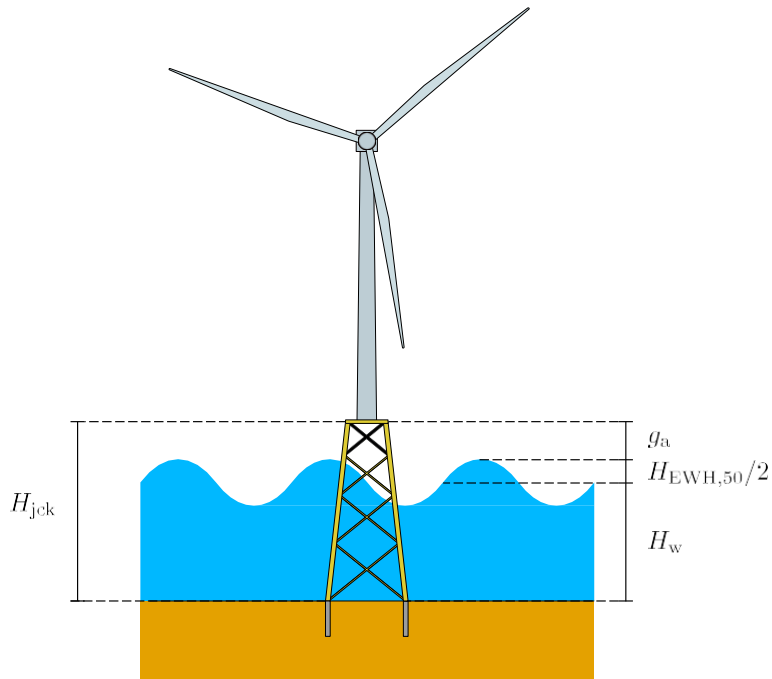


Figure 2.4. Representation of the air gap needed between the jacket platform and the maximum wave crest.

2.4.1.2 Welded joints

Geometric restrictions are imposed on the joints to achieve viable structures from a constructive perspective. These limits are taken from Appendix B of DNVGL-RP-C203 [1]. Based on the variables defined in Figure 2.5, the dimensionless parameters are defined, as shown in Equation (2.27). The adopted intervals are indicated in Equation (2.28).

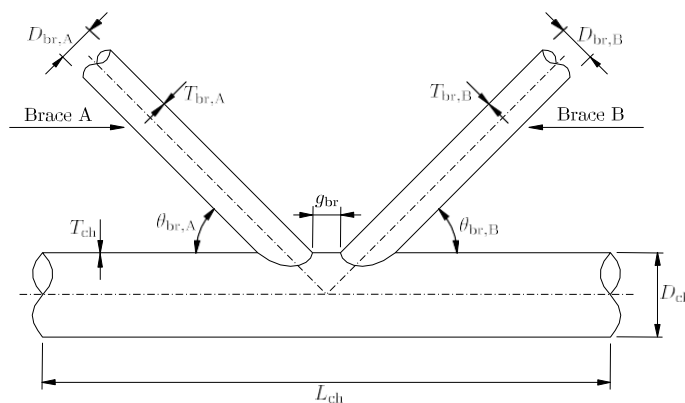


Figure 2.5. Geometric variables considered in the joints. Adapted from DNVGL-RP-C203 [1].

$$\beta_{br,AVB} = D_{br,AVB}/D_{ch} \tag{2.27a}$$

$$\alpha_{ch} = 2L_{ch}/D_{ch} \quad (2.27b)$$

$$\tau_{br,AVB} = T_{br,AVB}/T_{ch} \quad (2.27c)$$

$$\zeta_{br} = g_{br}/D_{ch} \quad (2.27d)$$

$$\gamma_{ch} = D_{ch}/(2T_{ch}) \quad (2.27e)$$

$$0.2 \leq \beta_{br,AVB} \leq 1 \quad (2.28a)$$

$$4 \leq \alpha_{ch} \quad (2.28b)$$

$$0.2 \leq \tau_{br,AVB} \leq 1 \quad (2.28c)$$

$$0.6\beta_{br,AVB}/\sin(\theta_{br,AVB}) \leq \zeta_{br} \leq 1 \quad (2.28d)$$

$$8 \leq \gamma_{ch} \leq 32 \quad (2.28e)$$

$$20^\circ \leq \theta_{br,AVB} \leq 90^\circ \quad (2.28f)$$

2.4.1.3 Minimum pile thickness

To ensure that the pile foundation resists the loads derived from the installation process, API Recommended Practice 2A-WSD [27] indicates that the thickness of the pile should be:

$$T_{pile} \geq \frac{6.35}{1000} + \frac{D_{pile}}{100} \quad (2.29)$$

2.4.1.4 Embedded length of pile

Following the recommendation of Arany et al. [3], a lower limit is included for the length of the pile, such that its critical length is reached. For this purpose, the expression proposed by Randolph [33] is used:

$$L_{pile} \geq D_{pile} \left[\frac{E_{pile}}{G_s} \left(\frac{64I_{pile}}{\pi D_{pile}^4} \right)^{\frac{2}{7}} \left(1 + \frac{3}{4} \nu_s \right) \right]^{\frac{7}{2}} \quad (2.30)$$

where I_{pile} and E_{pile} are the moment of inertia of the pile cross-section and Young's modulus of its material, respectively, and G_s and ν_s are the shear modulus and Poisson's ratio of the soil, respectively.

2.4.2 Ultimate limit states (ULS)

2.4.2.1 Section capacity

Given that it is an elastic material, the von Mises yield criterion is used for evaluating the resistance capacity of the section. This equivalent stress (σ_v) must be less than or equal to the elastic strength of the material (f_y) reduced by the material factor (γ_M).

$$\sigma_v \leq \frac{f_y}{\gamma_M} \quad (2.31)$$

2.4.2.2 Buckling

Buckling-failure modes must be verified. For this purpose, the column buckling strength is assessed for each beam element between the two welded joints, according to Section 3.8 of DNVGL-RP-C202 [26]. To avoid the evaluation of joint stiffness and assuming that it is safer, the effective length factor is taken to be equal to 1, as if all joints are pinned connections. The stability requirement for a shell column subjected to axial compression and bending is given by

$$\frac{\sigma_{a0,Sd}}{f_{kcd}} + \frac{1}{f_{akd}} \left[\frac{\sigma_{m1,Sd}}{1 - \frac{\sigma_{a0,Sd}}{f_{E1}}} + \frac{\sigma_{m2,Sd}}{1 - \frac{\sigma_{a0,Sd}}{f_{E2}}} \right]^2 \leq 1 \quad (2.32)$$

where $\sigma_{a0,Sd}$ is the design axial compression stress, $\sigma_{mi,Sd}$ is the maximum design bending stress about a given axis, f_{akd} is the design local buckling strength, f_{kcd} is the design column buckling strength, and f_{Ei} is the Euler buckling strength. Moreover, an analysis of the global buckling modes by a linear buckling analysis is conducted to ensure structural stability.

Also, the shell buckling stability for unstiffened circular cylinders is checked according to Section 3.4 of DNVGL-RP-C202 [26].

2.4.2.3 Foundation capacity

To evaluate the capacity of the pile foundation, API Recommended Practice 2A-WSD [27] is followed. Two criteria are considered: lateral capacity and bearing capacity.

Lateral capacity

To evaluate the lateral capacity, an auxiliary model based on nonlinear Winkler springs is used to reproduce the lateral pile–soil interaction according to the standard. This model is detailed in Appendix A.

Independent of the SSI model used in the structural analysis (Section 2.3.2), the loads that equilibrate the jacket structure at the bottom node of the legs are considered and used as the head loads of each pile ($F_{H,L}$, M_H). To evaluate the pile, two planes

of the forces that are assumed to be most relevant are considered: the plane with the highest lateral force and the corresponding bending moment, and the plane with the highest bending moment and the corresponding lateral force.

Two failure criteria are established to verify the lateral capacity of the foundation: the pile yield and soil resistance. The first implies that the tensile stress produced by the maximum bending moment along the pile cannot exceed the yield stress limit. The latter ensures that the soil can resist the loads induced by the pile without becoming unstable. This condition is checked by defining different amplification-reduction factors of the lateral load and bending moment at the pile head and determining the case in which the displacement of the pile head tends to infinity, which would indicate the maximum lateral force the soil can support.

Bearing capacity

The axial bearing capacity of the piles is also evaluated by comparing the axial forces at each pile head against the ultimate bearing capacity of the piles, computed as

$$Q_u = Q_s + Q_p = f_s A_s + q_p A_p \quad (2.33)$$

where Q_s is the skin friction resistance obtained by multiplying the unit skin friction capacity (f_s) by the side surface area of the pile (A_s), and Q_p is the total end-bearing resistance, evaluated as the unit end-bearing capacity (q_p) multiplied by the gross end area of the pile A_p . The values of these areas depend on whether the pile is assumed to be plugged or unplugged. For plugged piles, the side surface area of the pile is limited to the external area, whereas the entire bottom cross-section is considered for the gross end area. However, for unplugged piles, only the pile annular area acts on the end-bearing capacity, and the inner wall surface is also incorporated to compute the frictional resistance. Once the values for both hypotheses are computed, the smallest value is considered as the pile's ultimate axial bearing capacity. Finally, for the pull-out bearing capacity, the foundation resistance is provided by the total skin friction, together with the effective weight of the pile and the assumed soil plug.

2.4.3 Serviceability limit states (SLS)

To ensure correct operation of the wind turbine, DNVGL-ST-0126 [32] recommends a maximum limit rotation at the bottom of the tower. In this case, a limit of 0.25° is applied to the jacket platform.

2.4.4 Fatigue limit states (FLS)

To reduce the risk of long-term material fatigue failure, DNVGL-ST-0126 [32] states that the natural frequencies of a structural assembly cannot coincide with the rotor speed or blade frequency to avoid resonance. The following conditions should be fulfilled:

$$\frac{f_{RO}}{f_n} \leq 0.95 \quad \text{or} \quad \frac{f_{RO}}{f_n} \geq 1.05 \quad (2.34)$$

where f_{RO} represents the frequencies to avoid (all bandwidths of the rotor speed and blade transition frequency), and f_n are the different natural frequencies of the structure. Figure 2.6 shows the allowable regions for the natural frequencies. This code also indicates that, to verify this condition, all natural frequencies at least 20% higher than the blade transition frequency must be obtained.

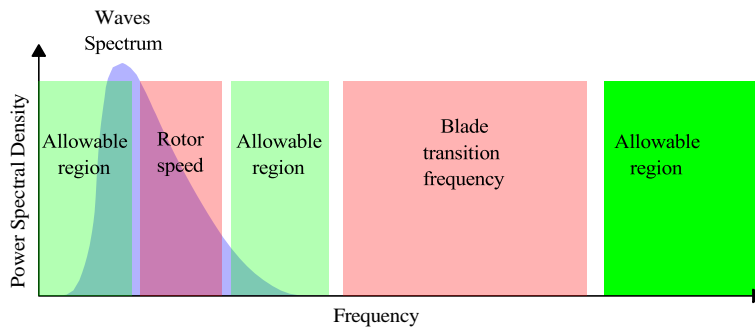


Figure 2.6. Allowable regions for the natural frequencies of the OWT.



3. Jacket optimization

- 3.1 Introduction
- 3.2 Case study
- 3.3 Methodology
- 3.4 Jacket design
- 3.5 Influence of the soil-structure interaction
- 3.6 Conclusions





3.1 Introduction

The correct design of jacket structures that support offshore wind turbines (OWTs) is very important for the expansion of this technology and, therefore, for the achievement of renewable energy objectives. However, this calculation is complex because it requires the evaluation of numerous load cases and the verification of many structural elements. Some authors have developed optimization procedures to obtain efficient jacket designs. Oest et al. [34] optimized a jacket based on a previous design using sequential linear programming. Chew et al. [35] optimized a jacket structure using a sequential quadratic programming approach. Stolpe et al. [36] addressed the optimization of a jacket structure as a support for a larger wind turbine (10 MW) through a mixed optimization strategy that defined the main topological aspects of the structure using pattern search optimization, while sizing the sections using gradient-based methods. In addition, using sequential linear programming, Couceiro et al. [37] optimized a jacket by considering different levels of bracing and compared the results. Ju et al. [38] used Powell's method to optimize the jacket support structure of 10-MW and 15-MW wind turbines with three and four legs at water depths of 35, 50, and 80 m and performed a preliminary analysis of the influence of these variables on the total mass of the foundation. All the above studies used structural simulations in the time domain, except for Oest et al. [34], who performed a static analysis for different time steps. These models usually involve high computational costs, which make it difficult for them to optimize many systems or to conduct parametric analyses. To avoid this drawback, Jalbi and Battacharya [39] proposed a simplified methodology for estimating the axial forces in tubular members, assuming a truss structure. This procedure is useful for obtaining the first approximation of a design, without verifying the feasibility of the structure.

The influence of the soil–structure interaction (SSI) on the response of specific jacket structures for OWTs has been studied recently. Abdullahi et al. [40] analysed the variations in the natural frequencies of an OWT on monopile and jacket structures while considering the flexibility of the pile foundation. Sharmin et al. [41] compared the seismic response of a jacket-supported OWT in different soils and on a rigid base, where the SSI was found to be of great relevance. Shi et al. [42] investigated the effect of the lateral flexibility of a pile foundation on the internal forces in certain elements of a predefined jacket structure under design loads. They used a Winkler spring model to incorporate the SSI, although the vertical component was not considered. However, few authors have incorporated the effects of foundation flexibility in the optimization of jacket structures. One example is the work of Ju et al. [38], who implemented nonlinear springs along a buried pile to incorporate foundation flexibility. However, the relevance of including SSI effects in jacket structure analysis models to obtain more efficient and less expensive designs has not been studied in depth.

In this chapter, the optimization procedure of the jacket structure of a case study is conducted. To evaluate the feasibility of the support structure, the structural model described in Chapter 2 is used. The intention of the work presented in this chapter is to obtain an initial approach to the design of a jacket. Taking advantage of this pro-

cedure, an analysis of the influence of soil–structure interaction in relevant structures is performed. First, the case study is defined in Section 3.2. Then the methodology followed for the optimization is described in Section 3.3. Results of the optimization process are shown in Section 3.4. Finally, the influence of SSI is analysed in Section 3.5, followed by the main conclusions in Section 3.5.

3.2 Case study

To obtain the jacket design, it is necessary to define the case study. First, the characteristics of the wind turbine must be specified, including both the physical properties, such as the mass and geometry of the tower, and the operating conditions of the device. Then, the environmental conditions of the site where the system is located, which include the depth of the sea, wave and wind conditions, and geotechnical characteristics, are also needed because they affect the requirements that the jacket structure must verify.

The selected wind turbine is the DTU 10-MW reference wind turbine [5]. According to the characteristics of the proposed model, the properties of the device necessary to evaluate the structure are those that define the geometry of the tower (tower height, bottom and top diameters, and bottom and top thicknesses), inertia provided by the RNA (mass and moments of inertia about the roll and yaw axes), aeroelastic damping of the rotor (in the fore-aft and side-side directions), rotor diameter, and operation conditions (rated wind speed and rotor velocities). Table 3.1 lists the properties and their values, adapted from Bak et al. [5]. The values of aeroelastic damping are assumed from the intervals proposed by Chen et al. [43]. It is assumed that the tower and tubular elements of the jacket are composed of steel and had the following properties: density of $7\,850\text{ kg/m}^3$, Young's modulus of 210 GPa, Poisson's ratio of 0.3, hysteretic damping coefficient of 0.5%, and yield stress of 350 MPa.

The environmental conditions at the site where the wind turbine is located must be also specified. Wind conditions are defined by a Weibull distribution with an average speed of 10 m/s and a shape parameter of 1.8. For the metocean data, those described by Jalbi et al. [39] are taken, where the variables are a water depth of 50 m, a 1-y significant wave height of 6.6 m, a 1-y maximum wave height of 12.42 m, a 50-y significant wave height of 8.27 m, and a 50-y maximum wave height of 15.33 m; the circulatory current is neglected. In addition, it is assumed that in the submerged structural elements of the jacket, the damping of the material increased by one percentage point.

Finally, the jacket structure is assumed to be founded on sand, defined as a homogeneous soil with a Young's modulus of 25 MPa, a Poisson's ratio of 0.49, a density of $2\,000\text{ kg/m}^3$, a hysterical damping ratio of 2.5%, and an angle of internal friction of 30° .

Table 3.1. Wind turbine properties (adapted from [5]).

Variable	Value
Tower height (H_{tower})	119 m
Rotor diameter (D_{rotor})	178.3 m
Bottom diameter (D_{bottom})	8.3 m
Bottom thickness (T_{bottom})	0.038 m
Top diameter (D_{top})	5.5 m
Top thickness (T_{top})	0.020 m
Mass (M_{RNA})	$674 \cdot 10^3$ kg
Inertia about roll axis ($I_{\text{RNA,roll}}$)	$156 \cdot 10^6$ kg·m ²
Inertia about yaw axis ($I_{\text{RNA,yaw}}$)	$974 \cdot 10^5$ kg·m ²
Fore-aft direction damping ($\xi_{\text{ae,FA}}$)	6.00%
Side-side direction damping ($\xi_{\text{ae,SS}}$)	0.75%
Rated wind speed (U_{R})	11.4 m/s
Minimum rotor speed ($f_{\text{r,min}}$)	6.0 rpm
Maximum rotor speed ($f_{\text{r,max}}$)	9.6 rpm

3.3 Methodology

Some assumptions are made to simplify the process and reduce the dimensions of the optimization problem. First, the height of the jacket is fixed at 59.3 m, which is the minimum value allowed according to Equation (2.26). All bracing elements are assumed to have the same inclination. Regarding the grouping of the geometry of the different tubular elements, all the elements of each bracing level have the same cross-section, all the legs are uniform through their lengths and equal, and all the piles have the same dimensions. Finally, the design of the jacket platform is neglected. It is directly considered as a punctual mass equivalent to a 20-cm-thick steel plate that would fill the polygon defined by the upper extremes of the legs.

In this way, the design variables of this problem are as follows: the number of legs (n_{leg}), the number of bracing levels (n_{br}), the separation of the legs at the base (S_{base}) and top (S_{top}), the diameter (D_{leg}) and thickness (T_{leg}) of the legs, the diameter (D_{br_i}) and thickness (T_{br_i}) of the elements of each bracing level (i), and the diameter (D_{pile}), thickness (T_{pile}), and length (L_{pile}) of the piles. However, the number of legs and bracing levels are excluded from the optimization process because they are discrete variables, resulting in a different design for each combination. Figure 3.1 shows a schematic representation of the optimization variables. To limit the solution search space, many

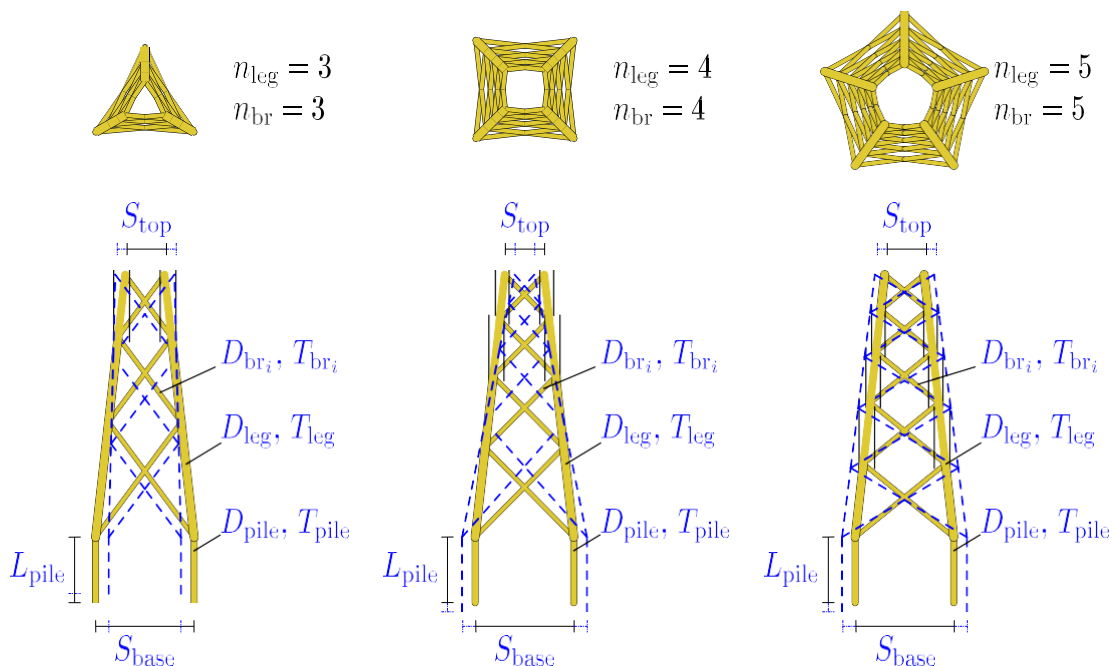


Figure 3.1. Representation of three examples of jacket designs indicating the variables included (blue) or fixed (black) in the optimization process.

of the design variables are not directly used but are defined from dimensionless ratios. The relationships between the design variables and their ranges are presented in Table 3.2.

The objective of the optimization process is to obtain a feasible jacket design that minimizes the amount of material used, which is a significant economic cost. Therefore, the total mass of the structure is established as a cost function. In addition, some restrictions are imposed to avoid the failure of the structure or structural elements against external loads (ULS), ensure the correct functionality of the system (SLS), avoid the collapse of the structure owing to cyclic loads (FLS), and limit the geometry of certain elements under technical criteria. Therefore, if the lower and upper limits are considered to limit the search space, the following optimization problem under inequality constraints can be established:

$$\begin{aligned}
 &\text{Minimize } M_{\text{jck}}(X) \\
 &\text{subject to } X \geq \text{lower limit} \\
 &\quad \quad \quad X \leq \text{upper limit} \\
 &\quad \quad \quad \eta_j(X) \leq 1, j = 1, \dots, n
 \end{aligned} \tag{3.1}$$

where M_{jck} is the mass of the jacket foundation, X represents the variables modified in the optimization process, and η is the utilization factor of the constraint j .

Owing to the large number of optimization processes conducted in this study, a surrogate model is used to reduce the total number of evaluations of the structural

Table 3.2. Ranges of the expressions considered in the design process. The jacket design variables are obtained from these expressions.

Expression	Lower limit	Upper limit
n_{leg}	3	5
n_{br}	2	10
S_{base}	15 m	35 m
$\frac{S_{top} - D_{bottom} \cdot \tan\left(\frac{\pi}{n_{leg}}\right)}{S_{bottom} - D_{bottom} \cdot \tan\left(\frac{\pi}{n_{leg}}\right)}$	0	1
D_{leg}	0.6 m	2.5 m
T_{leg}/D_{leg}	1/64	1/16
D_{pile}	0.8 m	4 m
T_{pile}/D_{pile}	1/80	1/4
L_{pile}/D_{pile}	8	18
D_{br_i}/D_{leg}	0.2	1
T_{br_i}/D_{br_i}	1/64	1/16

model and the total computational cost [44]. The optimization procedure based on the “surrogateopt” function already implemented in MATLAB [45] is used, which creates an internal surrogate model adapted from model evaluations and speeds up the process. This surrogate model is based on interpolation using radial basis functions, which consists of a linear combination of radially symmetric functions centred at defined points.

$$L_{RBF}(X) = \sum_{i=1}^n w_i \varphi(X, X_{c_i}) \tag{3.2}$$

where φ is the radial basis function, X_{c_i} are the centres of the function, and w_i are the weights of the functions. Setting the already evaluated points as centres, the weight values are obtained using least squares to construct the interpolation function. First, the optimization process generates random points and evaluates them to build the initial surrogate models for both the objective function and nonlinear constraints. These interpolation functions are used for evaluating numerous random points. From these, a new point to be evaluated by the structural model is selected by considering the expected performance given by the surrogate model and the distance from previously known points. The surrogate model is then updated, and the process is repeated until the stopping criterion is met.

To achieve a balance between obtaining an acceptable design and a fast procedure, the number of model evaluations in each execution of the MATLAB function is limited to 100. Next, the “surrogateopt” function is applied iteratively, introducing the

accumulated evaluations as previously evaluated points until the mass of the obtained solution do not reduce the previous one by more than 1%. This procedure is followed for each of the established combinations of the numbers of legs and bracing levels, performing five repetitions of each to estimate the convergence of the process.

3.4 Jacket design

Once the optimization process is concluded, five jacket designs per each combination of number of legs and bracing levels are obtained. Figure 3.2 shows the masses of the obtained designs grouped by the numbers of legs and bracing levels. To do this, the cases are separated on the x-axis according to the number of bracing levels; red crosses are used for three-legged jackets, blue squares for four-legged jackets, and green diamonds for five-legged jackets. These results show that there are significant differences in the global mass among the five designs obtained for each combination of the numbers of legs and bracing levels. This indicates that the design process does not guarantee the global optimal design of the jacket structure; however, the implementation of more rigorous optimization procedures would significantly increase the computational cost and is outside the scope of this Ph. D. Thesis. However, general trends can be observed from Figure 3.2. First, the mass of the structure tends to decrease as the number of bracing levels increase, until six bracing levels are reached. From that point onwards, a slight increase in the mass of the assembly is observed, which is more sensitive when the structure has fewer legs. The structures obtained with four or more bracing levels become lighter as the number of legs increased.

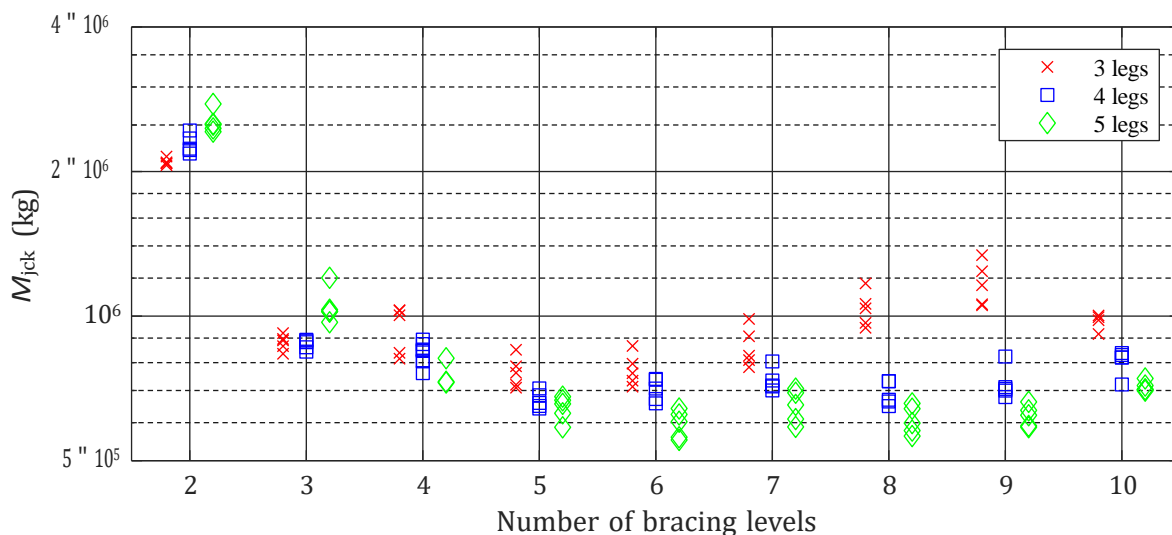


Figure 3.2. Mass of jackets obtained in the design process, differentiated by the numbers of legs (markers) and bracing levels.

To determine the optimal jacket design, it is necessary to select the design that verifies all imposed requirements and imposes a lower economic cost. However, many

researchers use the global mass of the jacket as a function to minimize in the optimization process of these structures (see, for example, [34, 35, 37, 38]). This is mainly owing to the complexity and variability of estimating the cost of such structural systems, which have a high number of joints. For this reason, the process is usually simplified by considering the mass of the assembly, because the amount of material required is a main factor affecting the final cost. Considering these criteria, and according to the results shown in Figure 3.2, the selected range of jacket designs in this problem can be limited to four-legged cases that have from four to six bracing levels, because lower values in these variables imply a significant growth in the global mass of the structure, and higher values imply an increase in costs owing to the increase in the number of welded joints. Table 3.3 lists the dimensions of five lighter jackets obtained within this range.

Table 3.3. Values of the design variables of the five selected jackets.

	Design 1	Design 2	Design 3	Design 4	Design 5
n_{leg}	4	4	4	4	4
n_{br}	5	5	6	5	6
S_{base} (m)	27.96	28.61	25.33	30.85	27.45
S_{top} (m)	14.63	12.94	15.28	12.63	12.77
D_{leg} (m)	0.984	1.015	1.071	0.971	1.077
T_{leg} (mm)	42.88	48.15	43.29	47.33	45.49
D_{pile} (m)	2.552	2.398	2.393	2.644	2.540
T_{pile} (mm)	31.9	30.3	30.3	33.1	31.8
L_{pile} (m)	30.9	31.6	34.1	28.0	28.5
D_{br_1} (m)	0.484	0.406	0.430	0.504	0.362
T_{br_1} (mm)	10.1	16.0	9.3	11.4	12.9
D_{br_2} (m)	0.404	0.416	0.522	0.509	0.327
T_{br_2} (mm)	12.0	10.4	12.0	9.9	14.4
D_{br_3} (m)	0.344	0.391	0.358	0.664	0.336
T_{br_3} (mm)	13.5	12.4	10.6	12.0	18.8
D_{br_4} (m)	0.746	0.557	0.342	0.415	0.667
T_{br_4} (mm)	13.2	17.4	9.1	21.9	17.2
D_{br_5} (m)	0.614	0.546	0.433	0.658	0.336
T_{br_5} (mm)	21.4	18.9	14.6	13.8	14.5
D_{br_6} (m)	-	-	0.653	-	0.509
T_{br_6} (mm)	-	-	23.4	-	23.4
M_{jck} (kg)	$642 \cdot 10^3$	$650 \cdot 10^3$	$658 \cdot 10^3$	$659 \cdot 10^3$	$672 \cdot 10^3$

3.5 Influence of the soil-structure interaction

To study the relevance of the SSI in this type of structure, it is necessary to analyse whether significant differences appear in the response of the structure when considering this interaction compared to the rigid base assumption. However, the large number of variables defining the structure makes it unviable to conduct a parametric study that exhaustively considers all possible configurations. For this reason, this brief study proposes to test the relevance of SSI phenomena in feasible jacket designs obtained

from an optimization process, in order to obtain relevant conclusions.

As expected, the results of the optimization process should also be affected by the hypothesis considered in the connection of the base of the leg with the soil. This study aims to show the direction and its relevance. The strategy consists in performing the optimization process imposing the bottom legs on a fixed base (FB). Once the new jacket designs are obtained, together with obtained in Section 3.4 considering SSI, the structural model is used for evaluating the utilization factors of the imposed requirements on the jacket under the same hypothesis with which it is obtained and the other. Figure 3.3 shows the combination of designs and hypotheses used to compare the results.

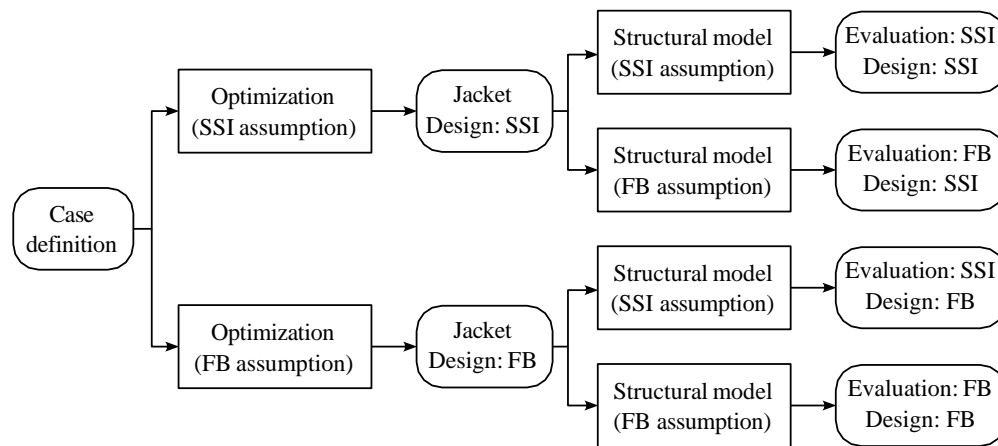


Figure 3.3. Diagram of the overall process of SSI relevance analysis. Designs obtained under each hypothesis are evaluated using both.

To prevent unrealistic designs from modifying the conclusions drawn from this study, designs with four legs and four, five, and six levels of bracing are selected, as they are considered more efficient according to the results of Section 3.3. Then, the same design procedure is followed, but considering the bottom legs are on a fixed base (FB), and all the designs are evaluated with the structural model.

Figure 3.4 shows a boxplot of the utilization factors (defined in Section 4.4.1), which reflect the safety level with different restrictions imposed on each of the designs obtained. First, the results show that all the values obtained are less than one because they are obtained from a design process that verifies all the restrictions. Thus, the criteria in which the indicators presented values close to 1 are those that limited the final dimensions of the jacket. In the case of designs considering the SSI, the ULS in the bracings and the limitation of the rotation of the tower base of the wind turbine are the most restrictive requirements, whereas when the legs are considered on a fixed base, the ULS in the bracings and load capacity of the foundation are the most relevant restrictions.

To evaluate the influence of the SSI model on the utilization factors, the designs obtained considering the SSI are evaluated assuming a rigid base and vice versa. Figure

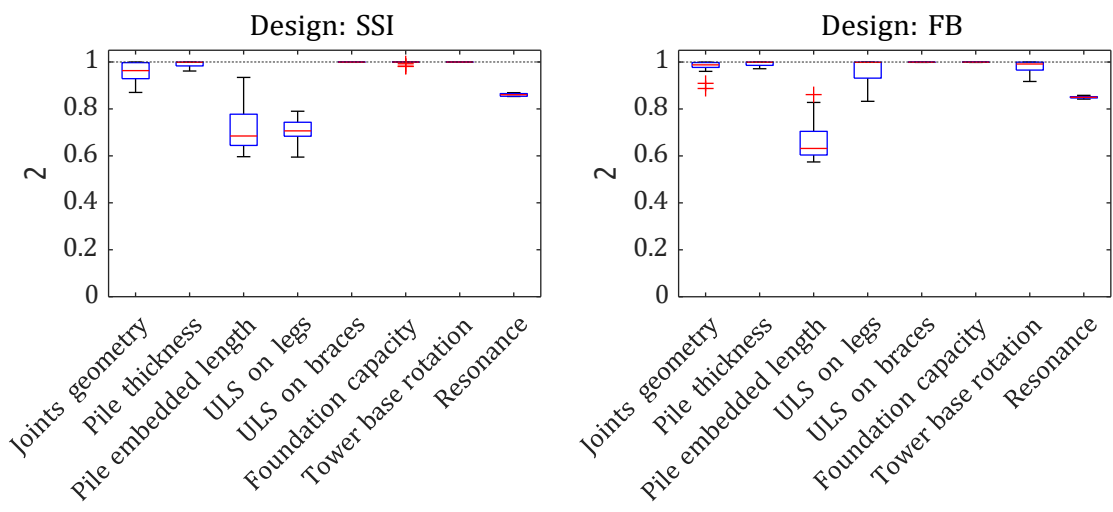


Figure 3.4. Utilization factors of jackets obtained in the design processes assuming soil–structure interaction effects (left) or a rigid base (right).

3.5 shows boxplots of the utilization factors, where the top left and bottom right subplots are the same as those in Figure 3.4. Restrictions associated with the geometry of the welded joints, the thickness of the pile, and the critical length of the pile are omitted because they are purely geometric restrictions that are not affected by the numerical model used to evaluate the structure. The failure criterion that is most affected by the foundation assumption is the rotation at the base of the tower because considering the SSI made the structure more flexible and increases the displacements. However, this criterion is not relevant, because it is a recommendation of the DNV [32] and is not mandatory. Finally, when the designs obtained assuming a fixed base are evaluated considering the SSI, the ULS requirements for the legs and bracings of the jacket are not satisfied. This implies that the redistribution of efforts by considering foundation flexibility has significant relevance in the failure criteria of these structures, and therefore, should not be neglected.

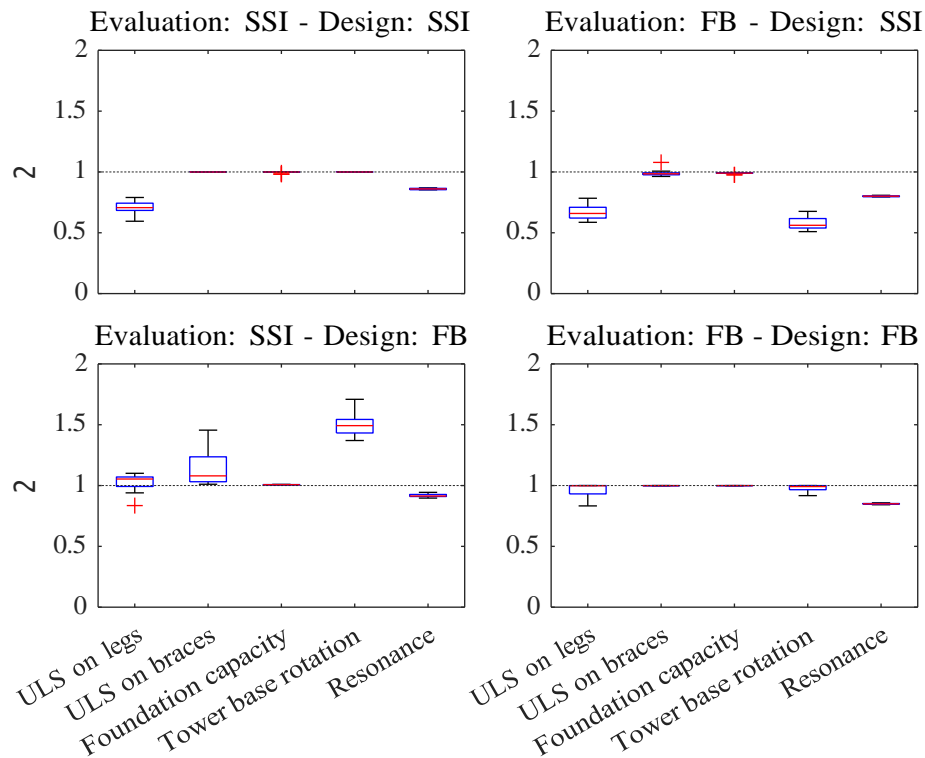



Figure 3.5. Utilization factors of jackets obtained in the design processes evaluated considering the soil–structure interaction (SSI) or a fixed base (FB).

3.6 Conclusions

This chapter presents an initial approach to the optimization process of a jacket design for a specific location and wind turbine. The structural model presented in Chapter 2 is used for evaluating requirements imposed to the structure during the optimization. Owing to the complexity of the system and the high number of variables that define it, a global optimum during the optimization process is not guaranteed. More exhaustive optimization procedures could be implemented in future stages, but this is outside the scope of this Ph. D. Thesis. However, general trends are observed in the designs obtained in this study case. Jacket designs trend to be more efficient, in terms of global mass, when the number of bracing levels increase up to six bracing levels. In addition, for jackets with more than 3 bracing levels, they become more efficient when the number of legs increase. Taking this into account, and considering that a greater number of welded joints increase the economic cost, the 4-legged jackets with four, five, and six bracing levels are considering the most rational cases to be considered for the jacket design in this study case.

An analysis of the influence of the SSI on feasible jacket designs obtained through an optimization process is also performed. The influence of the SSI is measured via the utilization factors of the design requirements of the jackets evaluated considering the SSI but obtained assuming that the bottom legs are fixed and those evaluated

considering the bottom legs to be fixed but obtained assuming the SSI. ULS verifications in the legs and bracing elements are not satisfied when considering the SSI in designs obtained assuming a fixed base, whereas this does not occur significantly when evaluating as fixed-base the designs obtained assuming SSI. It is concluded that the redistribution of internal forces produced by considering the flexibility of the foundation increases the stress on some structural elements, highlighting the need to incorporate this characteristic into structural models of OWT jacket support structures.



4. Surrogate models based on artificial neural networks

- 4.1 Introduction
- 4.2 Artificial Neural Networks: basic concepts
- 4.3 Ensemble model
- 4.4 Surrogate model for pile stiffness estimation
- 4.5 Surrogate model for dynamic characterization of offshore wind turbine on jacket structure
- 4.6 Conclusions





4.1 Introduction

In recent years, the research community is given more attention to Deep learning methodologies [46]. Some examples of the application of ANNs to solve civil engineering problems, among many others, are the following. Asteris et al. [47] used an ANN to predict the fundamental frequency of a complex RC framed structure. Thaler et al. [48] developed an ANN to predict the nonlinear response of a structure under earthquakes. Li et al. [49] implemented an ANN to predict the long term fatigue damage of floating OWTs. Regarding pile foundations: Franza et al. [50] trained an ANN to evaluate the impedance functions of 2x2 inclined pile groups in homogeneous soils, Kummar et al. [51] used hybrid ANNs to determine the bearing capacity of pile foundations, and Kennedy et al. [52] implemented ANNs to solve the inverse problem of determining the pile length from measurements of ground vibrations.

This chapter introduces the concept and behaviour of ANNs, the machine learning technique implemented in this Ph. D. Thesis. Section 4.2 classifies the main typologies of ANNs and describes basic concepts. Section 4.3 introduces the methodology of ensemble learning. Then, two surrogate models developed for structural problems related to the main topic of this Ph. D. Thesis are presented. First, in Section 4.4, a surrogate model for prediction of pile stiffness is developed. Second, in Section 4.5, a surrogate model capable of estimate the fundamental frequency of a jacket-supported OWT is described. Finally, Section 4.6 summarizes the main conclusions drawn from them.

4.2 Artificial Neural Networks: basic concepts

Artificial neural networks (ANNs) are computational models inspired by the human brain's neural network, which have shown a promising ability to perform a wide range of tasks, such as image and speech recognition, natural language processing, and even driving autonomous vehicles. They are particularly specialized at identifying patterns in large datasets, making them valuable tools for big data analysis and predictive modelling. A deep introduction to this topic can be found in many specialized references (see, for example, [53, 54]).

4.2.1 Numerical approach

An ANN is a computational technique based in the interconnection of many simple processing units called neurons. In general terms, ANNs are constituted by an input layer where the information is introduced, one (shallow neural network) or more (deep neural network) hidden layers where the information is processed, and an output layer where the expected result is obtained. A schematic representation is shown in Figure 4.1.

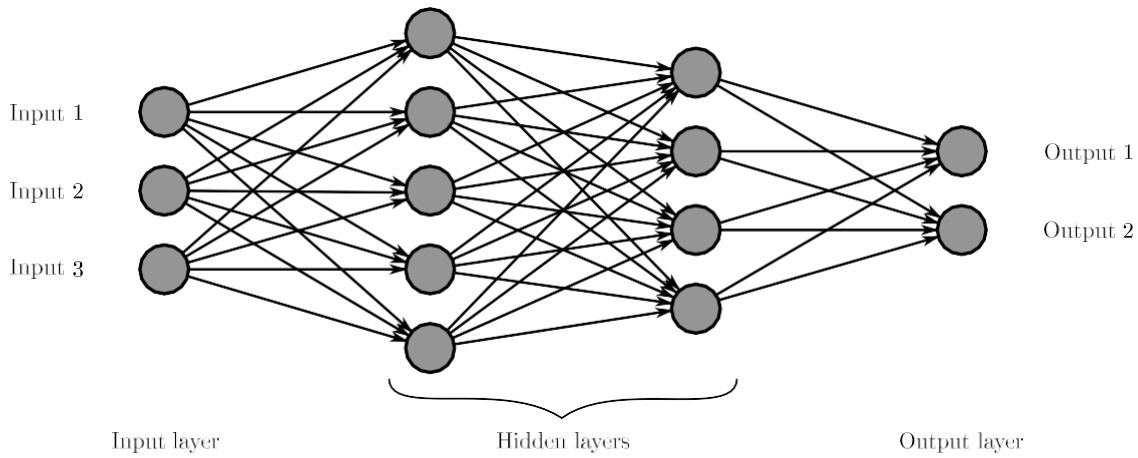


Figure 4.1. Schematic representation of a simple fully connected neural network.

4.2.1.1 The neuron

The minimal processing unit of the ANN is the neuron. It can be mathematically understood as the linear combination of neuron's inputs. This is often followed by an activation function to introduce non-linearity into the model. Then, the neuron's output would be the following:

$$a_j^{ly} = h \left(B_j^{ly} + \sum_{i=1}^n W_{i,j}^{ly} a_i^{ly-1} \right) \quad (4.1)$$

where a_j^{ly} is the output of the neuron j of the layer ly , h is the activation function, B_j^{ly} is the bias of the neuron, and $W_{i,j}^{ly}$ are weights of the different inputs of the neuron. The values of the bias and the weights are the learnable parameters that allow the system to conduct the desired task.

As can be demonstrated, in an ANN composed by neurons without activation function, the output can be reduced to a linear combination of the input. In this case, the model would not be able to fit any nonlinear function. However, the activation function introduces nonlinearities in the numerical model, allowing for more complex behaviour of the network. The most common activation functions used in ANNs, represented in Figure 4.2, are the following:

- Rectified linear unit (ReLU): $h(\tilde{a}) = \max \{0, \tilde{a}\}$.
- Leaky rectified linear unit (Leaky ReLU): $h(\tilde{a}) = \max \{0.1 \tilde{a}, \tilde{a}\}$.
- Exponential linear unit (ELU): $h(\tilde{a}) = \begin{cases} \tilde{a} & \tilde{a} \geq 0 \\ e^{-1} & \tilde{a} < 0 \end{cases}$.
- Sigmoid function: $h(\tilde{a}) = \frac{1}{1 + e^{-\tilde{a}}}$.

- Hyperbolic tangent function (Tanh): $h(\tilde{a}) = \frac{e^{\tilde{a}} - e^{-\tilde{a}}}{e^{\tilde{a}} + e^{-\tilde{a}}}$.
- Softsign function: $h(\tilde{a}) = \frac{\tilde{a}}{1 + |\tilde{a}|}$.

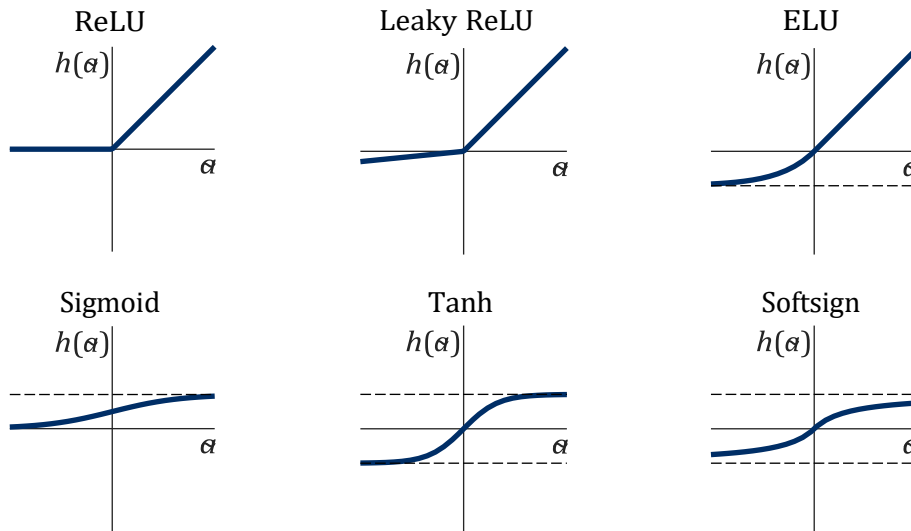


Figure 4.2. Most common activation functions used in ANNs.

Taking into account the behaviour of the neuron, the ANN can be understood as a sequence of linear combinations of nonlinear functions.

4.2.1.2 Universal approximation theorem

Despite the simple behaviour of the neuron, ANNs reach higher capacities through the aggregation of many of them, each processing part of the information. The universal approximation theorem [55, 56] states that any measurable continuous function from one finite-dimensional space to another can be approximated with any desired nonzero error by an ANN with only one hidden layer. However, the number of neurons that this hidden layer must contain is not established and may be arbitrarily large to achieve the desired error.

4.2.2 Architectures

One of the multiple research fields in deep learning is focused on developing more efficient architectures for the network. Thus, the first element to consider is to manipulate the number of hidden layers (NoHL) and the number of neurons per hidden layer (NoNpHL). Both variables affect the number of neurons in the network, which modify the number of parameters (NoP) and the ability of the network to fit the desired function. Intuitively, the NoNpHL indicate the number of internal variables set

in the layer, while the NoHL is the number of transformations that are made over the internal variables.

However, different categories of ANNs can be established attending to the interconnections between the neurons of the different layers:

- Fully connected neural networks: all the neurons from one layer are connected to all the neuron of the previous layer. This architecture is used for unstructured data, where the different inputs variables have no dependencies.
- Convolutional neural Networks: the neurons of one layer are only connected to a sub-set of the neurons of the previous layer. This architecture is used for grid-like data, such as images.
- Recurrent neural networks: the neurons of layer have loops that allow information to persist across different time steps. This architecture is used for sequential data, such as time series.

4.2.3 Nature of model's output

Attending to the nature of the model's output, the machine learning models can be divided into regression models and classification models. Regression models predict a continuous output. This means the model's output can take any value, representing the magnitude or quantity of the output variable prediction. In this case, the output layer of the ANN must have the same number of neurons as output variables, and these neurons do not require an activation function to work.

On the other hand, classification models predict discrete outputs, typically in the form of classes or categories. Depending on the number of outputs and labels, there are different classification models:

- Binary classification model: the model has one output that can be assigned to one of two possible classes. In this case, the ANN should have one neuron in the output layer with an activation function, typically the sigmoid function.
- Multi-label classification model: the model has several outputs that can be assigned to one of two possible classes each one. In this case, the ANN should have the same number of neuron as output variables in the output layer with an activation function, typically the sigmoid function.
- Multi-class classification model: the model has one output that can be assigned to one of several possible classes. In this case, the ANN should have the same number of neuron as possible classes of the output with the softmax function.

4.2.4 Learning process

The learning process of ANNs involves adjusting the weights of the network to minimize the error between the predicted output (\hat{Y}_i) and the actual target values (Y_i). This is



typically achieved through the gradient descent, where the model iteratively adjusts the weights and biases of the neurons to reduce the loss function.

4.2.4.1 Loss function

The loss function is a fundamental aspect in the training of ANNs. It quantifies the error of the predicted outputs of the network compared to the actual target values. The objective of the loss function is to guide the training process by providing a measure of network's performance intended to be improved.

There are several types of loss functions, each suitable for different kinds of problems. Among them, the following are highlighted:

- Mean Squared Error (MSE): Commonly used in regression models, it calculates the average of the squares of the errors between the predicted and actual values.

$$\text{MSE} = \frac{1}{N_s} \sum_{i=1}^{N_s} (\hat{Y}_i - Y_i)^2 \quad (4.2)$$

- Log Loss: Often used in classification models, it measures the performance of a classification model whose output is a probability value between 0 and 1.

$$\text{LogLoss} = -\frac{1}{N_s} \sum_{i=1}^{N_s} (Y_i \ln \hat{Y}_i + (1 - Y_i) \ln (1 - \hat{Y}_i)) \quad (4.3)$$

4.2.4.2 Backpropagation

Backpropagation is the algorithm most used in the training of ANNs. The algorithm calculates the gradient of the loss function with respect to the neural network's weights and biases. During the training process, the input data pass through the network, layer by layer, until the predicted output is obtained. Then, the loss function is evaluated comparing the predicted output and the actual target value. The error is propagated backward through the network, while the gradient of the loss function with respect to each weight and bias in the network is evaluated. Finally, the calculated gradients are used to update the parameters of the network, with the aim of reducing the loss in the next iteration. From a mathematical point of view, backpropagation uses the chain rule from calculus to compute the gradients of the loss function, which results in a very efficient process.

Since the ANN training is reduced to an optimization problem, many algorithms have been developed to update network's parameters. Some of them are:

- Gradient descent: The parameters are updated in the opposite direction of the gradient of the loss function over the entire training dataset. This is the simplest version.



- Stochastic gradient descent: The parameters are updated using only a single training example at a time. The convergence can be faster, but it presents more noise.
- Mini-batch gradient descent: It is a combination of the two previous methods. The parameters are updated using a small, random subset of the training data, known as a mini-batch.
- Momentum: This method reduces the oscillation of Stochastic gradient descent by incorporating part of the gradient in the previous sample to the current one.
- Adaptive moment estimation (Adam): This method adjusts the learning rates of each parameter during the training process, and uses momentum to reduce oscillation.

4.2.4.3 Regularization

Regularization is a technique used to prevent overfitting, that is, when the model is adjusted to the training data but cannot be applied to other (test) data. Some of the most used regularization techniques are the following:

- L1 Regularization (Lasso): Adds a penalty to the loss function equal to the absolute value of the magnitude of network's parameters.
- L2 Regularization (Ridge): Adds a penalty to the loss function equal to the square of the magnitude of network's parameters.
- Early Stopping: Analyse the model's performance on a validation set not used for gradient computation and stops training when validation performance starts to decay.
- Dropout: Randomly, some neurons outputs are set to zero during training time.
- Data Augmentation: Increases the amount of training data using information only in the training data, through transformations like rotation, scaling, etc.
- Noise Injection: Adds noise to inputs or weights during training.

4.2.4.4 Learning paradigm

In machine learning, there are three learning paradigms that differ in the way the model generate knowledge from data:

- Supervised learning: the model learns the information from labelled available data, being able to extrapolate to new data. For this purpose, a dataset with correlated inputs and outputs is required.
- Unsupervised learning: the model extracts knowledge from unlabelled data.

- Reinforcement learning: the model learns directly from the rewards obtained through a dynamic environment coupled to the model.

4.3 Ensemble model

Ensemble models are a fundamental technique in machine learning that improve the overall performance by combining the predictions from individual models. This approach is based on the collaboration of several models to achieve an aggregate performance superior to the originals. Therefore, the ensemble model manages to both improve accuracy and reduce overfitting. Some ensemble strategies are:

- Bagging: Several independent models are trained with different sub-sets of the dataset. The ensemble prediction is obtained by aggregating the constituent models.
- Boosting: Several models are trained sequentially, aimed to correct the prediction of the previous one.
- Stacking: A metamodel is trained to predict the target data from the outputs of several independent models.

4.4 Surrogate model for pile stiffness estimation

The aim of this section is to develop an ANN-based model capable of reproducing the equivalent linear stiffness of a pile foundation in non-homogeneous soil according to a continuum model. This is an initial approach to the implementation of Machine Learning techniques to the study of the compatibility of forces and movements between these deep foundations and the structure they support.

4.4.1 Problem statement

This surrogate model aims to characterize the static stiffness of pile foundations in non-homogeneous soils, such as the one represented in Figure 4.3. The pile is considered as a tubular element embedded in a vertical position. The geometric variables that define it are the embedded length (L_{pile}), the diameter (D_{pile}), and the thickness (T_{pile}). For the static analysis, the material characteristics needed are the Young's modulus (E_{pile}) and Poisson's ratio (ν_{pile}). The soil is considered as a non-homogeneous vertical half-space with mechanical properties defined by a shear wave velocity that increases continuously with depth following a generalized power law function [57]. As this work focuses on the static stiffness of foundations, this power law is rewritten in terms of Young's modulus as:

$$E_s(z_p) = E_s^L \left(b + (1 - b) \frac{z_p}{L_{pile}} \right)^{2ns} \quad \text{with} \quad b = \left(\frac{E_s^0}{E_s^L} \right)^{\frac{1}{ns}} \quad (4.4)$$

where L_{pile} is the pile length (used as reference depth), E_s^0 and E_s^L are the Young's modulus at the free surface and at the reference depth, respectively, and n_s is a dimensionless parameter that determines the Young's modulus profile between the free surface and the reference depth.

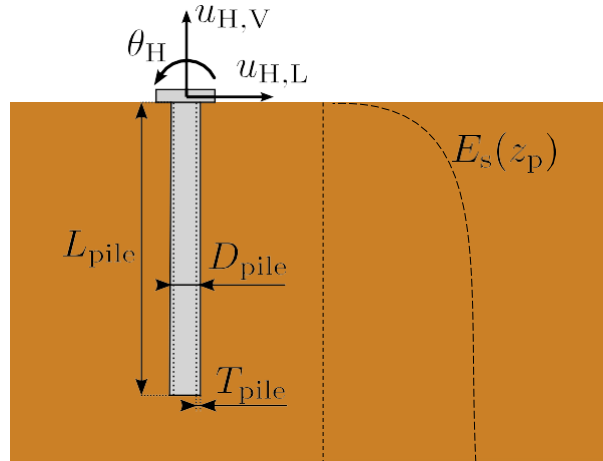


Figure 4.3. Single hollow pile embedded in non-homogenous halfspace

The stiffness of the pile is associated with three degrees of freedom: lateral displacement ($u_{H,L}$), rotation (θ_H) and vertical displacement ($u_{H,V}$) of the head (Figure 4.3). Due to the radial symmetry that the problem presents, it is redundant to determine what happens to the lateral displacement and the rotation in the perpendicular plane. In this way, the pile stiffness matrix presents the following structure:

$$\begin{bmatrix} F_{H,L} \\ M_H \\ F_{H,V} \end{bmatrix} = \begin{bmatrix} K_{hh} & K_{hr} & 0 \\ K_{hr} & K_{rr} & 0 \\ 0 & 0 & K_v \end{bmatrix} \begin{bmatrix} u_{H,L} \\ \theta_H \\ u_{H,V} \end{bmatrix} \quad (4.5)$$

where K_{hh} is the horizontal stiffness (lateral force on pile head owing to a unitary lateral displacement), K_{rr} is the rocking stiffness (bending moment on pile head owing to a unitary rotation), K_{hr} is the horizontal-rocking coupling stiffness (bending moment on pile head due to an unitary lateral displacement and lateral force on pile head owing to a unitary rotation), and K_v is the vertical stiffness (vertical force owing to a unitary vertical displacement).

Once the system is defined, applying Buckingham's theorem [58], the problem is dimensionless treated in order to reduce the number of variables. The dimensionless variables used to define the system under study are:

$$L_r = \frac{L_{pile}}{D_{pile}} \quad (4.6a)$$

$$\delta = 1 - \frac{2T_{pile}}{D_{pile}} \quad (4.6b)$$

$$\nu_{pile} \quad (4.6c)$$

$$E_r = \frac{E_{\text{pile}}^{v_s}}{E_s^L} (1 - \delta^4) \quad (4.6d)$$

$$E_r = \frac{E_s^0}{E_s^L} \quad (4.6e)$$

$$\gamma_s = \frac{E_s^0}{E_s^L} \quad (4.6f)$$

$$n_s \quad (4.6g)$$

while the dimensionless stiffnesses are:

$$\hat{K}_{hh} = \frac{K_{hh}}{E_s^L D_{\text{pile}}} \quad (4.7a)$$

$$\hat{K}_{hr} = \frac{K_{hr}}{E_s^L D_{2 \text{ pile}}} \quad (4.7b)$$

$$\hat{K}_{rr} = \frac{K_{rr}}{E_s^L D_{3 \text{ pile}}} \quad (4.7c)$$

$$\hat{K}_v = \frac{K_v}{E_s^L D_{\text{pile}}} \quad (4.7d)$$

To focus the study within a coherent scenario according to the possible systems, lower and upper limits are established for each of the dimensionless variables that define the problem. These limits are shown in Table 4.1.

Table 4.1. Limits established for the dimensionless variables that define the problem.

Variable	Lower limit	Upper limit
L_r	0	100
δ	0	1
v_p	0.15	0.35
v_s	0.15	0.5
E_r	10	$5 \cdot 10^4$
γ_s	0	1
n_s	0	1

Note that the reliability of the surrogate model predictions is limited to those regions within the search space, decreasing closer to the boundaries. However, many scenarios are covered by this search space. The considered soil profile is a halfspace with a general power-law stiffness variability trough depth. The n_s and γ_s parameters allow reproducing different variations of the properties with depth, including



the homogeneous halfspace as a particular case. Regarding the pile geometry, from solid to thin-walled hollow piles are including, with very wide slenderness ratios. The Young's modulus of the soil can range from 4.2 MPa, if a solid steel pile is assumed ($E_p = 210$ GPa), up to 2.7 GPa if the pile is made of concrete ($E_p = 27$ GPa). With respect to the Poisson's ratio, in the case of the pile the search space includes the characteristic values of concrete ($\nu_p = 0.2$) and steel ($\nu_p = 0.3$), while for the soil it is extended to include saturated soils ($\nu_s \approx 0.5$).

4.4.2 Methodology

The ANN-based model capable of estimating the stiffness of the pile is built through a supervised learning process, that requires a dataset with example samples from which the neural network can learn. Owing to the difficulty of obtaining a sufficiently large volume of experimental data, a synthetic dataset is built from the numerical model detailed in Section 2.3.2. The numerical model used is formulated for layered soils. In order to reproduce a continuous variability of soil properties, the soil profile is discretized into enough layers of constant properties, achieving an equivalent global behaviour. For the generation of this dataset, the limits of the search space of the input variables must be defined. Next, using uniformly distributed random numbers, random samples are generated between the established limits, obtaining the input variables of the dataset. Finally, the continuum model, which is intended to be replaced by the neural network, is used to evaluate the dataset inputs and thus obtain the outputs.

Since the problem to solve corresponds to a regression problem with unstructured data (there is no spatial or sequential structure), fully connected networks (represented in Figure 4.4) are used. The NoP that the network will present, as well as its capacity to fit the data, will closely depend on the NoHL and the NoNpHL. Different architectures will be analysed by modifying the NoHL and the NoNpHL. To reduce architecture variability, all hidden layers are assumed to have the same number of neurons. In addition, at the output of each hidden layer, a normalization of the layer is performed to speed up its training [59], and the ReLU is used as activation function.

To reduce the differences in scale of the different input and output variables, they are normalized by subtracting the mean and dividing by the standard deviation. Next, the dataset is randomly divided for each ANN into two parts: a training dataset (80%) by which the error is minimized, and a validation dataset (20%) to stop the training and avoid overfitting.

The training of the neural network is carried out using the automatic differentiation algorithm already implemented in Matlab [45], and setting the MSE (Equation (4.2)) of the outputs as the loss function. For updating the parameters, the adaptive moment estimation (Adam) [60] is used with an initial global learning rate of 0.01, a gradient decay factor of 0.9, a squared gradient decay factor of 0.999, and a batch size of 5 000. The error of the validation data is continuously evaluated, stopping the training when it stabilizes. Next, the neural network is retrained, reducing the global learning rate by half, repeating this process until the new network does not improve the results of the previous one.

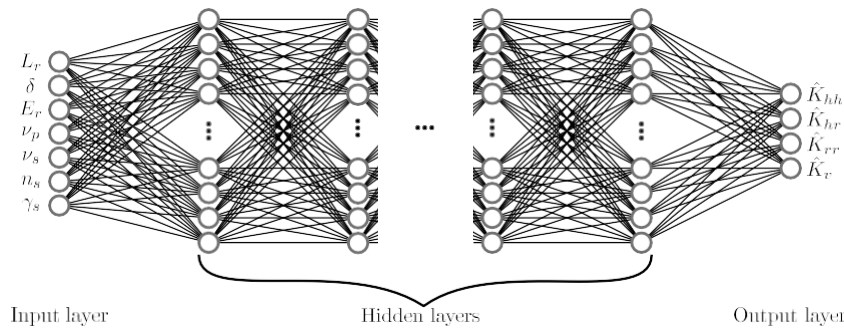


Figure 4.4. Conceptual diagram of the fully connected neural network used for the surrogate model for pile stiffness. Input and output variables included are properly defined in Section 4.4.1

Finally, once the training and evaluation of the ANNs have been carried out, it is proposed to combine the predictions of independent networks to build an ensemble model (see, for example, [61]). In this way, the output of the ensemble model would be defined as the mean of the predictions of the individual networks, so large local errors of some networks can be reduced by the agreement of others. In addition, a measure of prediction uncertainty can be obtained by evaluating the standard deviation of the individual ANNs outputs.

4.4.3 Architecture selection

To train the ANNs-based model, a dataset with 200 000 samples is generated (which will be divided into the training dataset and the validation dataset). In addition, for the required evaluation of the models, a test dataset of 150 000 samples is also generated. In a balance between computational cost and performance, a small study is performed to achieve sufficient predictive capacity in the resulting model while avoiding training an excessive number of oversized ANNs. To analyse the architecture relevance, 20 different architectures are defined. The NoHL and the NoNpHL is randomly selected within the intervals from 2 to 5 and from 50 to 200, respectively. Table 4.2 shows the NoHL and the NoNpHL of the generated architectures. For each of the established architectures, 3 repetitions are performed in order to reduce the statistical fluctuations due to the stochastic processes associated with these models.

Once the training of the 60 neural networks described has been completed, the aim is to compare their performance. To do this, the test dataset is evaluated, and the relative error in absolute value of the prediction related to the value of the continuum numerical model is obtained:

$$\left\{ \varepsilon \right\}_i (\%) = 100 \cdot \frac{1}{Y_i} \frac{Y_i - \hat{Y}_i}{1} \quad (4.8)$$

The 50th, 90th, 95th, and 99th percentiles of error distributions are selected as measures of the performance of the neural network. Figure 4.5 shows the results for the different

Table 4.2. Definition of architectures used for the architecture selection of the surrogate model for pile stiffness.

Id.	NoHL	NoNpHL	NoP
1	2	50	3 354
2	2	65	5 334
3	2	70	6 094
4	2	80	7 764
5	3	60	8 404
6	4	50	8 654
7	3	70	11 204
8	2	110	13 974
9	3	90	18 004
10	3	100	22 004
11	3	110	26 404
12	5	80	27 684
13	5	90	34 744
14	2	180	35 464
15	4	105	35 494
16	2	195	41 344
17	3	145	44 954
18	3	170	61 204
19	4	165	85 474
20	5	145	87 874

architectures used, where the different markers represent the value of the 50th, 90th, 95th, and 99th percentiles obtained for the ANNs trained. As expected, the error in the predictions decrease while the number of parameters increases, stabilizing over 40 000 parameters. Based on this trend, it is not necessary to increase the range of the architecture study. According to the results, the architecture with 3 hidden layers and 145 neurons per hidden layers is established for the pretended model, being their results surrounded by a dashed line in Figure 4.5. Also, to help the comparison, solid lines are used to mark the mean value among the three repetitions of each percentile of the selected architecture.

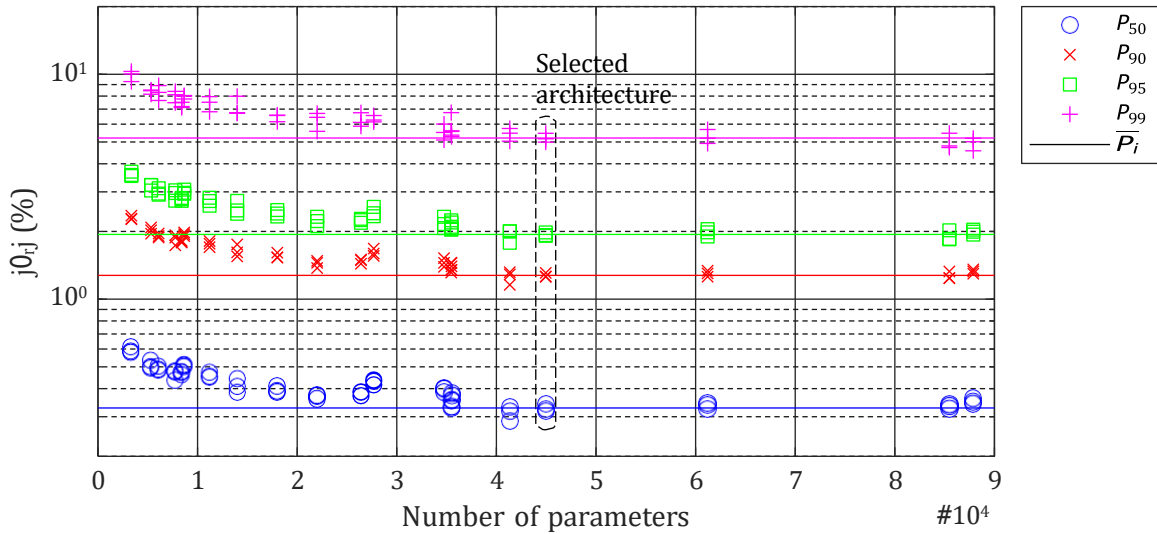


Figure 4.5. The 50th, 90th, 95th and 99th percentiles of the relative errors obtained by trained neural networks evaluated over test dataset.

4.4.4 Ensemble model performance

After defining the architecture of the neural network that will be used in the proposed model, 17 networks of the same topology are additionally trained to obtain a total of 20 independent ANNs. In this way, the prediction of each of them can be combined to obtain an ensemble model that consists of the mean value of each individual network. To evaluate the performance of the different networks and the ensemble model, the test dataset is evaluated, and the relative error in absolute value of each measurement is obtained (Equation (4.8)). Figure 4.6 represents the complementary cumulative distribution function of the error of the four stiffness terms of each one of the 20 networks individually evaluated and of the ensemble model built from them. It is observed that, from a statistical point of view, the ensemble model significantly improves the performance of individual networks. In a more detailed comparison, individual networks present an average error greater than 3.7% in the horizontal stiffness for only 1% of the samples, while the ensemble model presents an error greater than 2.4% for 1% of the samples. Similarly, this reference error is reduced from 4.6% to 2.3% for horizontal-rocking coupling stiffness, from 9% to 3.6% for the rocking stiffness and from 4.2% to 2.5% for vertical stiffness.

Figure 4.7 groups the complementary cumulative distribution function of the error of the ensemble model for the four stiffness estimated in order to be easily compared among them. It should be noted that the errors do not present a homogeneous distribution among them, where horizontal stiffness and rocking stiffness stand out. The former presents higher relative errors for a large percentage of samples, while the deviations it presents are smaller than for the other stiffness terms for the worst predicted samples. On the other hand, for rocking stiffness, the opposite occurs. In any case, this fact does not affect the global performance of the model, since only a 10% error in

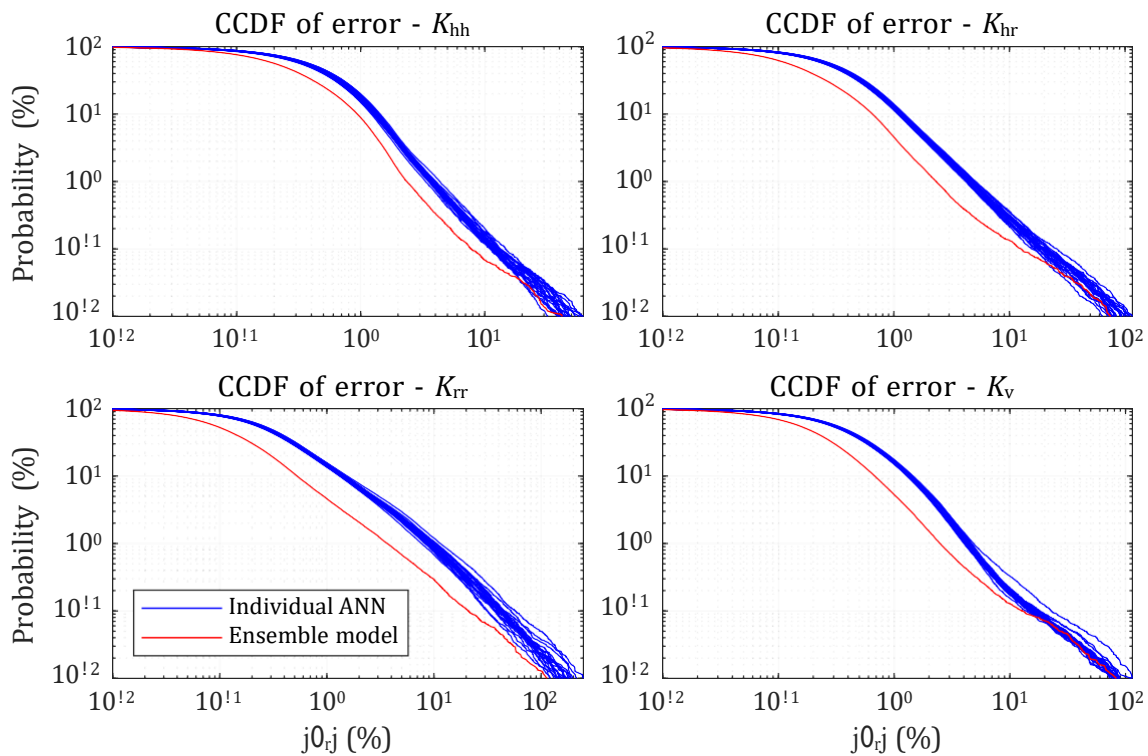


Figure 4.6. Complementary cumulative distribution function (CCDF) of the error in the predictions for the individuals ANNs and the ensemble model for pile stiffness prediction.

the prediction is exceeded in the 0.3% of the rocking stiffness, the 0.13% of the cross stiffness and the vertical stiffness, and the 0.07% of the horizontal stiffness. It should be mentioned that there are some samples for which errors of up to 100% are obtained, although with a very low prevalence (less than 0.013% in the most frequent case). However, the difference in computation times justifies using this surrogate model: the average execution time of the continuous model is around 61.25 s, while in the ensemble model it is around $1.04 \cdot 10^{-4}$ s, both executions performed parallelized in a 40-core (Intel® Xeon® Gold 6242R CPU @ 3.10GHz), 93 GB RAM computer.

Other advantage of the ensemble model is that it provides a measure of prediction uncertainty through the standard deviation of the results given by each individual net. The relationship between the prediction dispersion and the error of the surrogate model is analysed in Figure 4.8. This figure shows a heatmap of the number of observations of the relative error, in absolute value, and the coefficient of variation ($|CV|$) obtained from the ensemble model. The coefficient of variation is defined as the absolute value of the standard deviation of the individual predictions of each ANN divided by their mean value. A significant relationship between the relative error and the coefficient of variation is observed. The diagonal dashed line marks the points where both metrics coincide. Furthermore, those samples whose error is considerable larger than the model uncertainty (that is, points above the diagonal dashed line) correspond to small

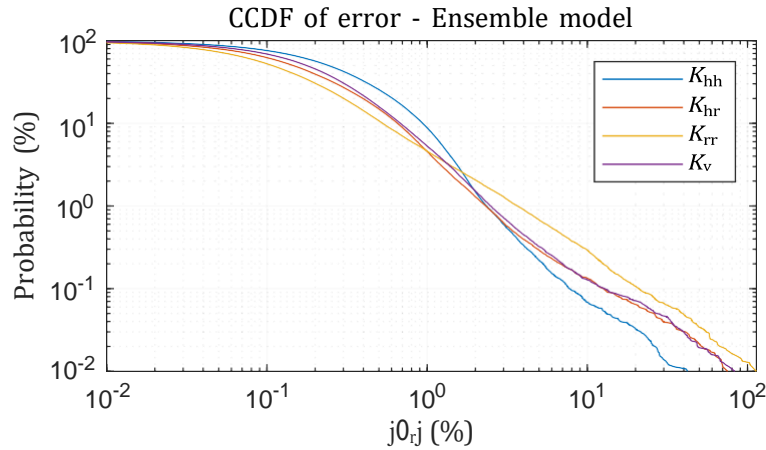


Figure 4.7. Complementary cumulative distribution function (CCDF) of the error in the predictions for the ensemble model for pile stiffness prediction.

relative errors, not compromising the reliability of the surrogate model. Note that the horizontal dotted line marks the limit of a relative error equal to 1%.

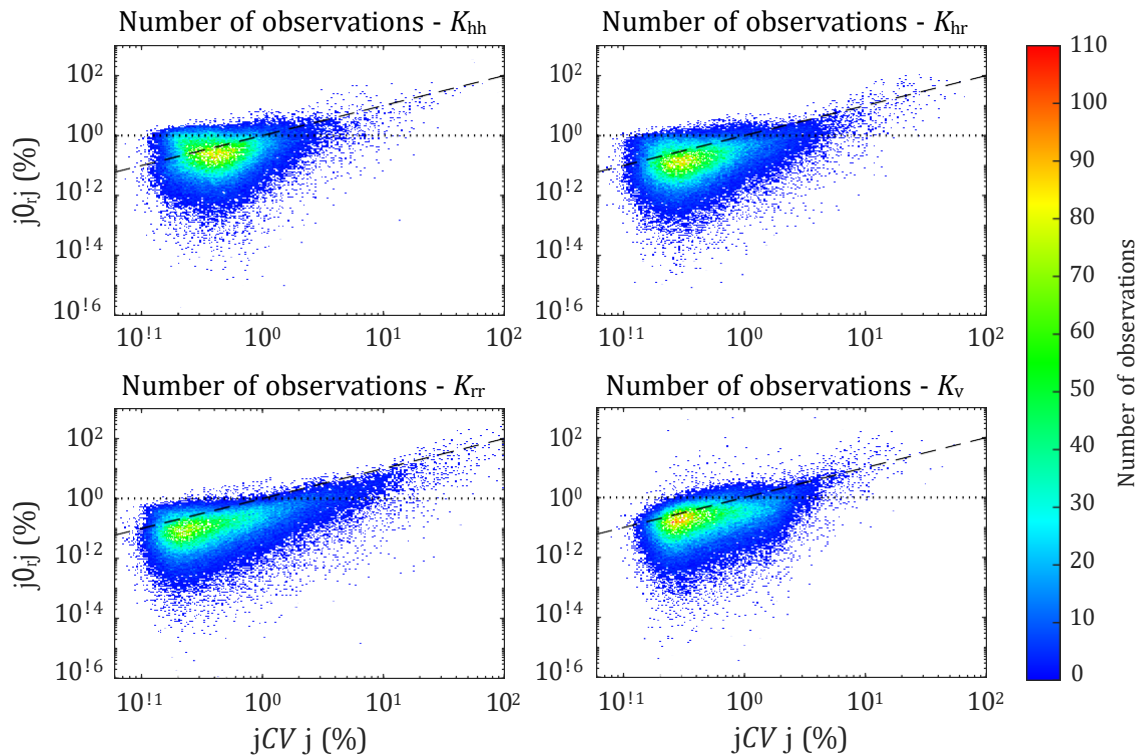


Figure 4.8. Heatmap of the number of observations of the relative error and the coefficient of variation of the surrogate model.

4.4.5 Application examples

To show the ability of the proposed surrogate model to reproduce the behaviour of single pile foundations in terms of its head stiffness, two application examples are presented.

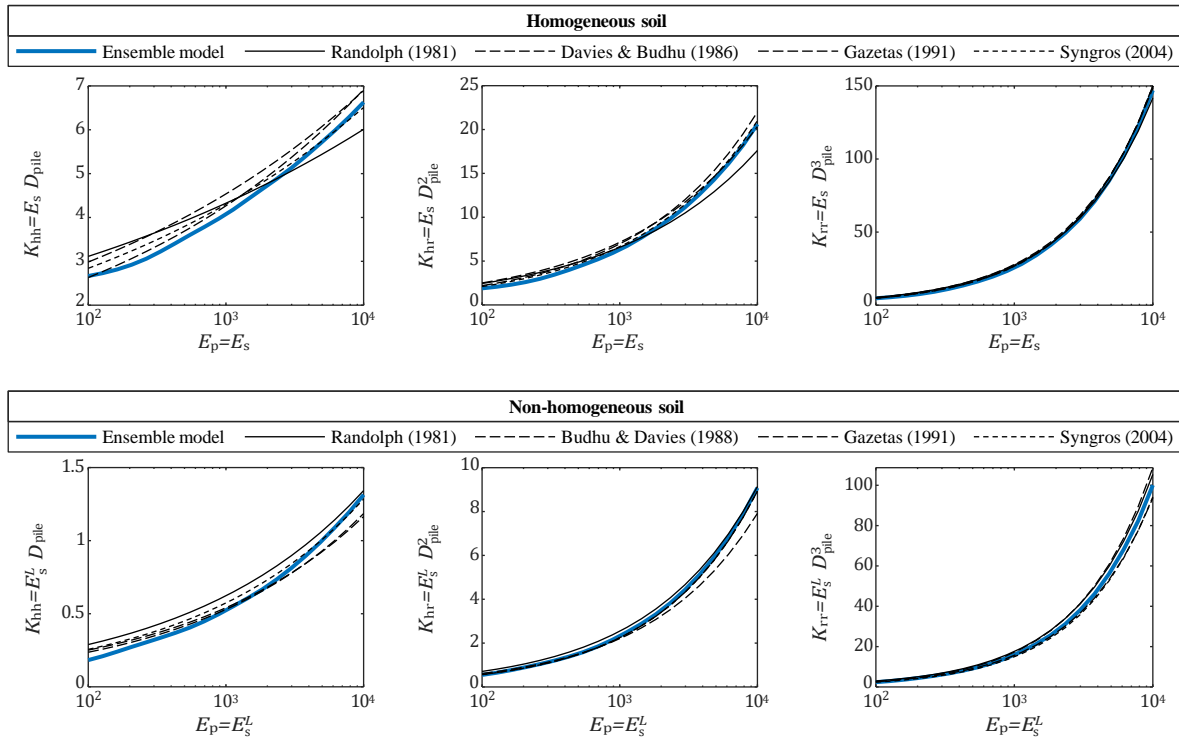


Figure 4.9. Pile head stiffness for the lateral behaviour of a single pile depending on the pile-soil relative stiffness. Comparison of the ensemble model against fitted expressions.

First, in Figure 4.9, the results of the ensemble model are compared with well-established fitted expressions [62–66] for the lateral, rocking and cross-coupled stiffness of a flexible pile embedded in homogeneous soils or soils with a linearly varying stiffness profile. These expressions, which define the head stiffness as a function of the pile–soil relative stiffness, can be consulted in the original works or in the recent review made by Mylonakis and Crispin [67]. In all this works, the soil with a linear variation of the Young’s modulus has zero stiffness at surface level ($\gamma_s = 0$, $n_s = 0.5$). The results of the ensemble model are obtained assuming $L_{pile}/D_{pile} = 50$, $\delta = 1$ (solid cross-section), $\nu_{pile} = 0.25$, and $\nu_s = 0.5$ (as in [66]).

The comparison presented in Figure 4.9 shows a nice agreement between the results computed by the ensemble model and those obtained by the different fitted expressions. Furthermore, the surrogate model is capable to smoothly reproduce the influence of the pile–soil relative stiffness on the three stiffness terms without noise or discontinuities. Discrepancies between the ensemble model and formulas are higher for the lateral stiffness, while for the rocking term almost all approaches converge into the same

values. The same level of good agreement is found both for the homogeneous and non-homogeneous profiles.

For the second application example, the dimensional problem of computing the pile head stiffness of a large-sized hollow monopile is handled. These foundations are typically used as the supporting structures for offshore wind turbines. The influence of both the pile length and soil profile on the four pile stiffness terms is analysed. For that purpose, three variable-with-depth soils ($n_s = 0.2, 0.5$ and 0.8) and one homogeneous soil ($n_s = 0$) are considered. All profiles present the same average stiffness over their first 30 m, $\bar{E}_{s,30} = 30$ MPa, and a constant Poisson ratio $\nu_s = 0.49$ (equivalent to a saturated soil). For the non-homogeneous media, a zero stiffness at surface level is assumed ($\gamma_s = 0$). The evolution with depth of the Young's modulus with respect to the average value is presented for the studied profiles in the right graphic area of Figure 4.10. The pile geometry is defined by the dimensional properties: $D_{pile} = 5$ m, $T_{pile} = 57$ mm (following API's recommendation [27]), $L_{pile} = 5-40$ m. Steel material properties are assumed for the pile: $E_{pile} = 210$ GPa, $\nu_{pile} = 0.25$.

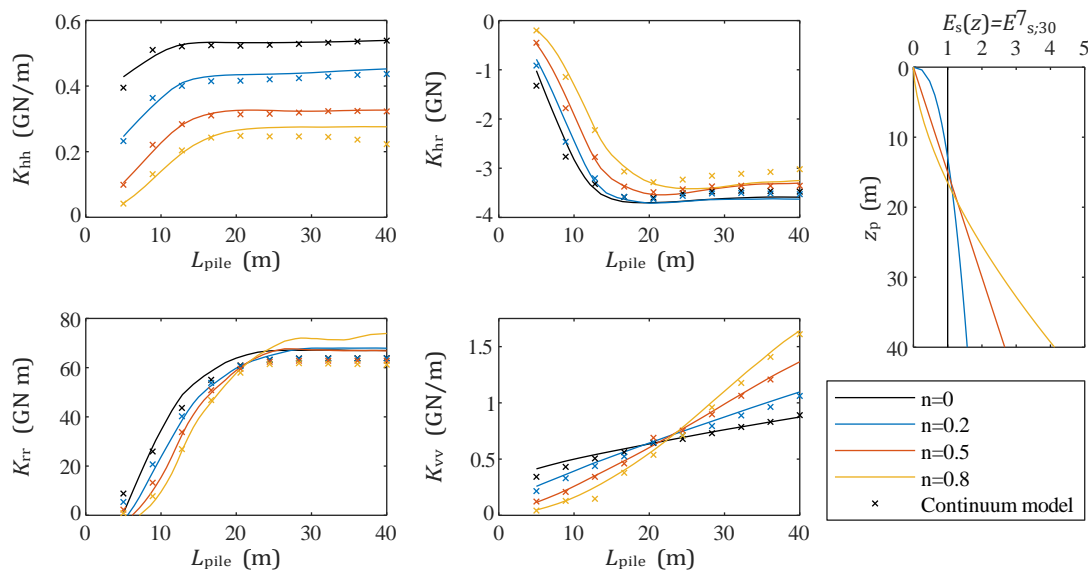


Figure 4.10. Influence of pile length on the head stiffness for large diameter monopiles embedded in several soil profiles with the same average stiffness. Results comparing the ensemble model and the continuum model.

Figure 4.10 presents the four pile head stiffness terms as functions of the pile length. The results of the ensemble model for each soil profile are shown by different line colours, while crosses are used to represent the reference values obtained with the numerical model. A great agreement is observed between the predictions made by the ensemble model and the numerical model, even in this example where a significantly flexible pile (close to the lower limit presented in Table 4.1) is considered. As in the previous example, the pile stiffness computed by the surrogate model present a smooth behaviour with the variation of the pile length. The convergence into a fixed stiffness when the pile active length is reached is clearly seen for the terms related to the lateral



behaviour (lateral, rocking and cross-swaying stiffness). Furthermore, the results show that the active length increases as the soil profile becomes softer near the free-surface, that is, n_s increases. This trend qualitative agrees with the expressions presented in [68]. The expected relation between pile stiffness and length is obtained: as the pile grows longer, it reaches stiffer soils which leads to an increment of the foundation stiffness. However, as the impact of deeper soil layers is not the same for all terms [69, 70], different behaviours are obtained. The horizontal stiffness, which is mainly influenced by the superficial soil properties, presents its maximum value for the homogeneous medium, and reduces its values as the soil becomes softer. The same trend is observed in the rocking and horizontal-rocking coupling terms for short piles. However, when the pile is long enough, the additional resistance of the deeper layers against the pile deflection reduce the difference of the rocking and coupled stiffness with respect to the homogeneous profile. The value of the active length for the rocking problem is larger than the one corresponding to the lateral problem. The extreme scenario is found for the vertical stiffness, which is affected by soil properties along the whole pile. Thus, the vertical stiffness constantly increases with the pile length. The ratio of this increment is proportional to the ratio of the increment of the soil Young's modulus with depth.

4.5 Surrogate model for dynamic characterization of off-shore wind turbine on jacket structure

The aim of this section is to build an ANN-based surrogate model which can predict the fundamental frequency of an OWT supported by a jacket structure with a pile foundation, considering the soil-structure interaction (SSI). This initial approach would allow to significantly reduce the computational cost of the dynamic characterization of the structure.

4.5.1 Problem statement

The dynamic system under study is a jacket-supported OWT, described in Chapter 2, which can be divided into three parts: wind turbine, jacket substructure (including the pile foundation), and the site conditions. Each one of them presents a wide number of properties necessary for a complete definition; however, not all these properties have the same relevance for calculating the fundamental frequency of the system. The main variables taken into account for this surrogate model are detailed below.

4.5.1.1 Wind turbine

From a structural point of view, the wind turbine is made up of the rotor-nacelle-assembly, which adds inertia to the system; and the tower, which provides stiffness. This last element can be sufficiently defined by a reduced number of variables. Assuming it as a tubular element with a linearly variable section, its geometry can be defined with bottom diameter (D_{bottom}), bottom thickness (T_{bottom}), top diameter (D_{top}), top



thickness (T_{top}), and height (H_{tower}). The tower is assumed to be made of steel, so the following material properties are considered: density of $7\,850\text{ kg/m}^3$, Young's modulus of 210 GPa , Poisson's ratio of 0.3 , and hysteretic damping coefficient of 0.5% .

On the other hand, rigorously describing the rotor-nacelle assembly (RNA) requires numerous parameters. This is because the variable geometry of the blades makes it necessary to indicate the dimensions of the section along the length (see, for example, [5]). In this case, RNA is described only from its inertial properties, since it is assumed that this simplification does not considerably affect the fundamental frequency of the system. Thus, the variables used are: mass (M_{RNA}), inertia about roll axis ($I_{RNA,roll}$), and inertia about yaw axis ($I_{RNA,yaw}$). Inertia about pitch axis is considered to be equal to inertia about yaw axis. In addition, a punctual hysteretic damping in the rotor of 6% in fore-aft direction and 0.75% in side-side direction is considered, following intervals proposed by Chen et al. [43].

4.5.1.2 Jacket substructure

The hyperparameters used for this surrogate model that define the topology of the jacket are: jacket height (H_{jck}), number of legs (n_{leg}), base leg spacing (S_{base}), top leg spacing (S_{top}), and the number of bracing levels (n_{br}). For the jacket platform, it is assumed to be a 20 cm thick solid plate that covers the entire area above the upper end of the legs.

In the case of the pile foundation, all the piles are considered equals to each other and in a vertical position. In this way, they are defined by to the diameter and thickness of the hollow circular section and the embedded length (L_{pile}).

As an initial approach of the problem and to reduce the size of the search space, only two types of circular sections are considered for the structural elements: one for the jacket's legs and the piles (D_{leg}, T_{leg}); and another for the elements of the different brace levels (D_{br}, T_{br}). All elements of the jacket structure and the foundation are assumed to be made of steel. The same material properties listed for the turbine tower are considered.

4.5.1.3 Site conditions

The soil is assumed to be a homogeneous, isotropic, linear, and viscoelastic domain. The properties that characterize the soil media are: shear wave propagation velocity (c_s), Poisson's ratio (ν_s), density (ρ_s), and hysteretic damping coefficient of 2.5% .

In the case of seawater, to define which elements are affected by inertial effects, the depth from the free surface (H_w) is established. It is assumed that the density of the medium is $1\,024.7\text{ kg/m}^3$ and that the presence of the water increases the damping of the steel elements up to 1.5% . Since it is considered that it will not have great relevance in the calculus of the fundamental frequency of the system, more complete (and expensive) models that rigorously incorporate the water-structure interaction, as well as the second-order phenomena of incidence of waves and ocean currents, are not implemented.

4.5.2 Ranges of variables established for analysis

Table 4.3. Search space for wind turbine, site, and jacket structure variables.

Variable	Lower limit	Upper limit
H_{tower}	80 m	145 m
D_{bottom}	$H_{\text{tower}}/16$	$H_{\text{tower}}/13$
T_{bottom}	$D_{\text{bottom}}/250$	$D_{\text{bottom}}/200$
D_{top}	$D_{\text{bottom}}/1.65$	$D_{\text{bottom}}/1.45$
T_{top}	$D_{\text{top}}/290$	$D_{\text{top}}/190$
M_{RNA}	$35 H_{\text{tower}}^2$	$60 H_{\text{tower}}^2$
$I_{\text{RNA,roll}}$	$0.1^2 H_{\text{tower}}^2 M_{\text{RNA}}$	$0.15^2 H_{\text{tower}}^2 M_{\text{RNA}}$
$I_{\text{RNA,yaw}}$	$0.6 I_{\text{RNA,roll}}$	$0.75 I_{\text{RNA,roll}}$
c_s	60 m/s	600 m/s
v_s	Equation (4.9a)	Equation (4.9b)
Q_s	Equation (4.10a)	Equation (4.10b)
H_w	25 m	60 m
H_{jck}	$1.1 H_w$	$1.6 H_w$
n_{leg}	3	5
S_{top}	D_{bottom}	$2.5 D_{\text{bottom}}$
S_{base}	Equation (4.11) $\alpha_{\text{leg}} \sim U(60^\circ, 90^\circ)$	
n_{br}	Equation (4.12) $\alpha_{\text{br}} = 70^\circ$	Equation (4.12) $\alpha_{\text{br}} = 30^\circ$
D_{leg}	0.5 m	3.5 m
T_{leg}	$D_{\text{leg}}/64$	$\min\{D_{\text{leg}}/16, 0.1\}$
D_{br}	$D_{\text{leg}}/5$	D_{leg}
T_{br}	$D_{\text{br}}/64$	$\min\{D_{\text{br}}/16, 0.1\}$
L_{pile}	5 m	40 m

In order to generate a dataset that allows to achieve the objective of this work, limits are established in the exploration of the described variables to avoid wasting computational capacity exploring regions in the search space that are not relevant from a technical point of view. These limits, summarized in Table 4.3, have been set based on analysing cases present in the bibliography.

For the variables that characterize the wind turbine, the limits are defined from the properties of four examples of 5, 8, 10, and 15 MW described in the bibliography

[5, 71–73]. Manually, a set of relationships that reduce the variability are identified, and a lower and upper limit are established for them. The height of the tower is taken as the starting variable, using a uniform distribution between 80 m and 145 m for its generation. For the diameter of the tower base, a uniform distribution is used that goes from $H_{tower}/16$ to $H_{tower}/13$. The same procedure is used for the different variables of the wind turbine, according to the limits specified in Table 4.3, depending on the variables previously defined.

To describe the soil, a value of the shear wave propagation velocity (c_s) between 60 m/s and 600 m/s is randomly established, excluding the extreme cases: soft soils, where a structure could not be founded, and hard soils, where the SSI phenomena lose relevance. Establishing the limits for the Poisson’s ratio and the density of the soil arises from the assumption of the extreme cases of the c_s . It is considered that in soft soil the Poisson’s ratio can vary between 0.4–0.499 and the density between 1 600–2 000 kg/m³; while in a hard soil, these intervals move to 0.25–0.35 and 2 000–2 500 kg/m³, respectively. Thus, the limits for different values of c_s are taken from a linear interpolation:

$$v_{s, \text{ lower limit}} = 0.4 + (0.25 - 0.4) \frac{c_s - 60}{600 - 60} \quad (4.9a)$$

$$v_{s, \text{ upper limit}} = 0.499 + (0.35 - 0.499) \frac{c_s - 60}{600 - 60} \quad (4.9b)$$

$$Q_{s, \text{ lower limit}} = 1600 + (2000 - 1600) \frac{c_s - 60}{600 - 60} \left(\frac{\text{kg}}{\text{m}^3} \right) \quad (4.10a)$$

$$Q_{s, \text{ upper limit}} = 2000 + (2500 - 2000) \frac{c_s - 60}{600 - 60} \left(\frac{\text{kg}}{\text{m}^3} \right) \quad (4.10b)$$

The limits of water height are 25 m and 60 m. Once these limits are established, the variables are generated using uniform distributions.

Jacket variables definition is carried out after analysing some structures present in the bibliography [36, 37, 74]. Following a process similar to that used for the wind turbine, some variables are generated from a uniform distribution between two previously defined limits (number of legs, leg diameter, and pile length), while, for the rest of the variables, these limits are specified from other variables already obtained (jacket height, top leg spacing, leg thickness, bracing diameter, and bracing thickness). Two variables follow a different process. First, for the spacing of the legs at the base (S_{base}), the angle of the jacket legs with respect to the sea bottom (α_{leg}) is defined between 60° and 90°, and the value of the variable is calculated as:

$$S_{base} = S_{top} + \frac{2H_{jck} \sin(\pi/n_{leg})}{\tan(\alpha_{leg})} \quad (4.11)$$

On the other hand, to determine the number of bracing levels, lower and upper limits are established based on the geometry of the jacket and assuming for them an angle

(α_{br}) between 70° (lower limit) and 30° (upper limit). The number of bracing levels that check these criteria is calculated as:

$$n_{br} = \begin{cases} \frac{S_{base} \frac{H_{jck}}{\tan(\alpha_{br})}}{\log(S_{top}/S_{base})} & \text{if } S_{base} = S_{top} \\ \log \left(1 - \frac{2 \tan(\alpha_{br})}{\frac{2H_{jck}}{S_{base} - S_{top}} + \frac{1}{\sin^2(\pi/n_{leg})} - 1 + \tan(\alpha_{br})} \right) & \text{if } S_{base} > S_{top} \end{cases} \quad (4.12)$$

All this is summarized in Table 4.3.

Variables are assigned a random value within the limits defined above because the homogeneous discretization of a 22-dimensional space requires a completely unaffordable amount of data. For illustration, if the space is discretized with a homogeneous mesh with only two nodes per dimension (which obviously does not reproduce the variability throughout it), more than four million samples would be needed. There are more complex sampling methods that can allow exploring the search space in a more effective way (see, for example, [53]), however, in this case, the use of uniform probability distributions between two established limits simplifies the procedure without compromising the accuracy of the obtained results (see Section 4.5.4).

4.5.3 Methodology

The intended ANN model must be able to capture the influence that each of the variables established for this analysis has on the dynamic characterization of the system, acting as a regression model. Therefore, the ANN should present 22 inputs (according to the variables specified in Subsection 4.5.2) and one output (the system fundamental frequency).

Because the data is not structured (spatial or sequential structure), fully connected networks are used. Architectures that have a visible input layer with 22 neurons, a visible output layer with 1 neuron, and a variable number of hidden layers with different numbers of neurons are considered (see Figure 4.11). The neurons in the hidden layers present the ReLU activation function.

To train the ANN, a synthetic dataset is built, generating random points within the limits established in Subsection 4.5.2 and using the structural model (Chapter 2) to calculate the fundamental frequency (Section 2.3.5). To homogenize the values of the different variables, a normalization of each of the input and output variables is performed by subtracting the mean and dividing by the standard deviation.

The obtained dataset is randomly divided into three groups: training set (70%), a dataset used to train the neural network, minimizing its error; validation set (15%), a dataset used to determine when the training process should be stopped, avoiding

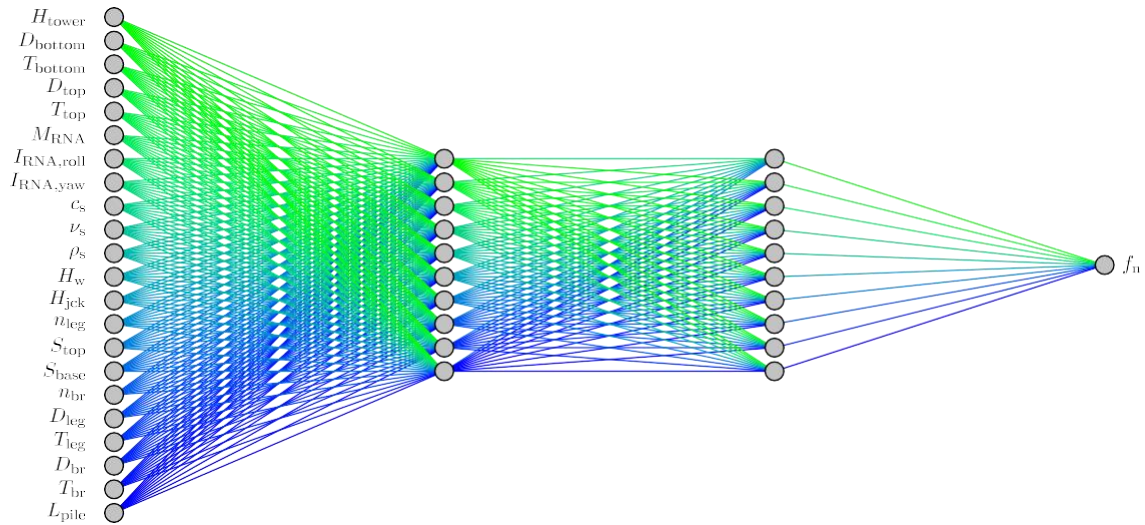


Figure 4.11. Representation of an ANN with 22 neurons in the input layer, 10 neurons in each of the two hidden layers, and 1 neuron in the output layer.

overfitting; and test set (15%), a dataset not used in any stage of training that helps to evaluate ANN prediction capacity.

The training of the network is carried out by automatic differentiation algorithm already implemented in Matlab [45], using the MSE (Equation (4.2)) of the fundamental frequency predictions as cost function. Parameter optimization is based on the adaptive moment estimation algorithm (Adam) [60] with a global learning rate of 0.01, a gradient decay factor of 0.95, and a batch size of 100. The validation data error is repeatedly evaluated to stop training when a trend to increase starts, avoiding overfitting.

4.5.4 Architecture selection

The performance of an ANN-based surrogate model depends on the number of ANN's internal parameters (related to the number of hidden neurons and how they are connected) and the size of the dataset used for its training. Therefore, a small study from these two perspectives is proposed to ensure that the case study is accurate enough to be able to work as a surrogate model. To modify the NoP of the ANN, the NoHL is modified from 1 to 4 and the NoNpHL by 10, 25, 50, 75, 100, 125 and 150. However, to reduce the analysis, only the cases that all hidden layers have the same number of neurons are considered. In addition, the size of the dataset available to be used in the training process described in Section 4.5.3 is modified, subdividing the complete dataset into sets of 1 000, 5 000, 15 000, 30 000, 50 000, 75 000, and 100 000 samples. In this way, each of the 196 combinations of these assumptions are analysed.

To evaluate the performance of the proposed ANNs, the relative error in absolute value (Equation (4.8)) of each of the predictions made by the network is calculated for the train, validation, and test sets. Using as an example the specific configuration of

the neural network with 4 hidden layers with 125 neurons each, trained with 100000 data; Figure 4.12 shows the Cumulative Distribution Function (CDF) of these errors over each one of the subsets. To better compare the error distributions, the 50th, 90th, 95th and 99th percentiles are marked in each of them. The error distributions obtained for the three data subsets show similar prediction errors for all of them, being slightly lower in the case of the training set, which is logical since it is the error in which the network has focused on minimizing. In all three cases the high precision of the predictions stands out, obtaining errors of less than 5% for more than 99% of the predictions made (marked by dashed green line).

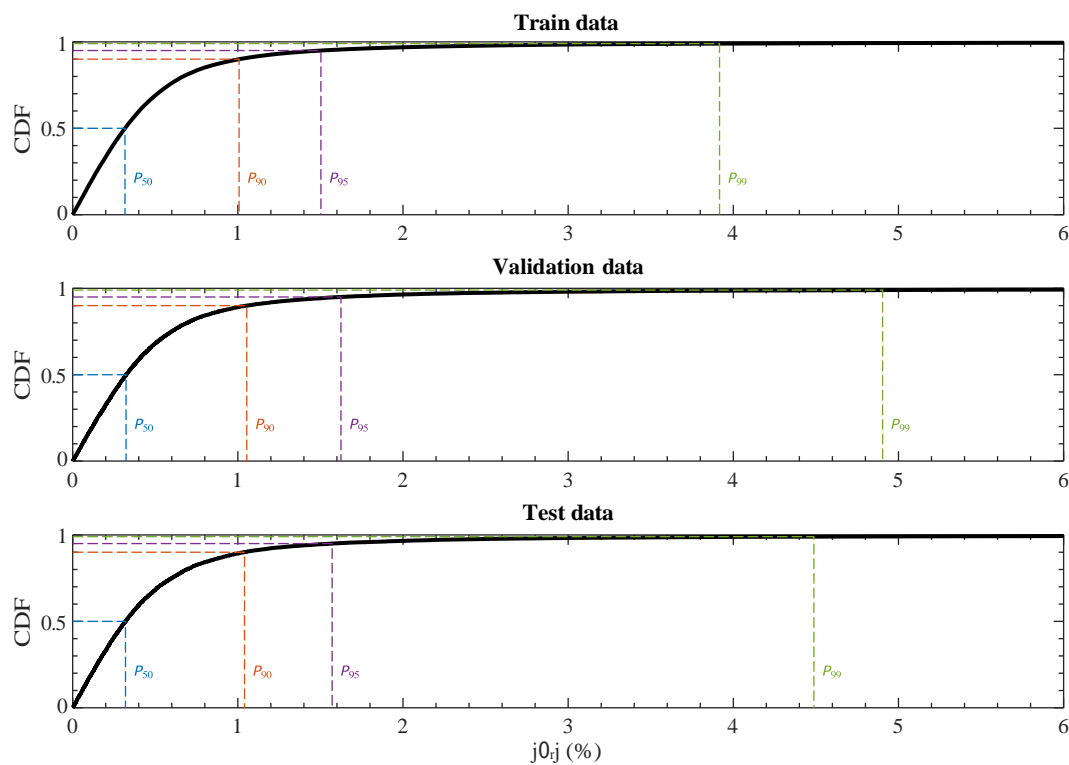


Figure 4.12. ANN’s error cumulative distribution function for training, validation, and test data. One selected network with 4 hidden layers and 125 neurons per hidden layer, trained with a 100 000 dataset.

However, the training of the ANNs described are subject to stochastic processes such as the random initialization of the ANN’s parameters and the division of the dataset. For this reason, a statistical approach to the study is carried out, executing 20 repetitions and obtaining the means of the results to be analysed. Focusing on the errors on the test set, which represents the network’s ability to generalize its learning, Figure 4.13 shows the 50th, 90th, 95th, and 99th percentiles for each of the 20 networks trained. The markers indicate the specific values of the percentiles for each of the networks obtained, while the dashed line marks the mean. Despite the expected variability due to random processes, a certain trend is observed that allows us to use the average values of the percentiles as indicators of the performance that would be

expected from a network trained under these considerations. Thus, if a new network were trained, the most probable situation would be that the 50%, 90%, 95%, and 99% of the predictions have an absolute relative error smaller than 0.4%, 1.3%, 1.9%, and 5.1%, respectively.

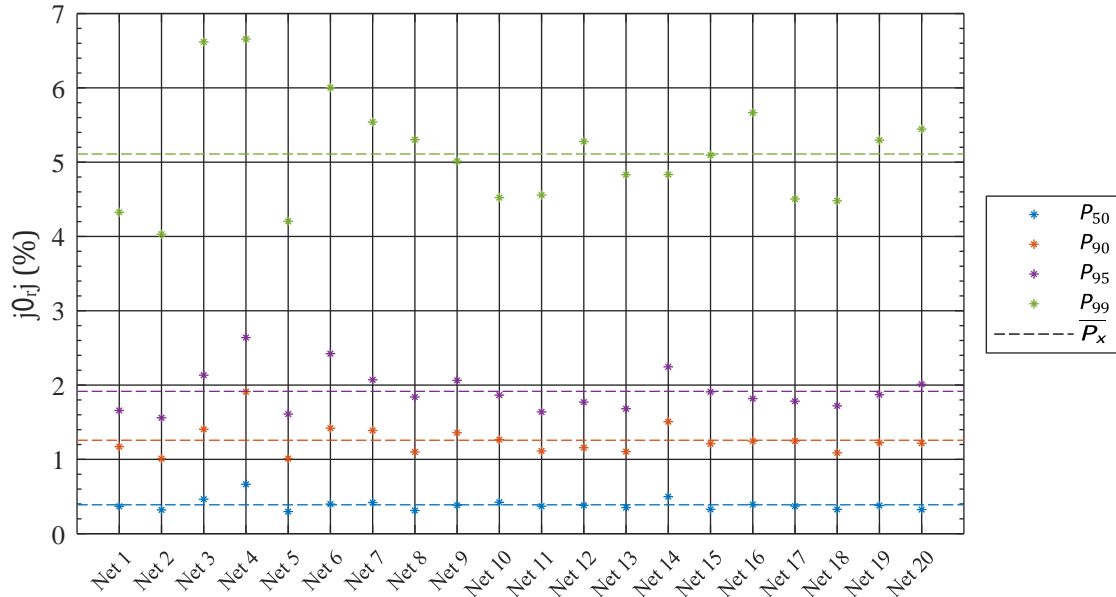


Figure 4.13. Error percentiles of different ANN with 4 hidden layers and 125 neurons per hidden layer, trained with a 100 000 samples.

Figure 4.14 shows the average 50th, 90th, 95th, and 99th percentiles of the rest of the configurations raised for this study against the NoP of each of the proposed architectures. As in any regression model, it can be seen that in general the error decreases as the NoP and the size of the dataset used for training increase. However, the error begins to stabilize with respect to both variables. The difference between the average percentiles is considerably reduced when the data volume 100 000 against 75 000. On the other hand, from about 10^4 parameters, the performance of the ANNs obtained shows some stabilization, presenting a variability more characteristic of random process noise than a defined trend. Among all the results, the one that has obtained the best results is the one previously used as an example, which has 4 hidden layers with 125 neurons each and has been trained with 100 000 data.

The computational cost of training the different neural networks must also be taken into account. It should be noted that the execution was carried out by parallelizing 20 process lines in a 40-core (Intel® Xeon® Gold 6242R CPU @ 3.10GHz), 93 GB RAM computer. The average training time of each architecture used is shown in Figure 4.15. There is an evident dependence of the time required against the number of ANN's parameters and the size of the dataset, observing convergence with respect to this last variable. However, there is no stabilization against the number of ANN's parameters, with an almost linear growth trend appearing from 10^3 parameters. This investment in ANN training can be clearly rewarded by exploiting the surrogate model on a large

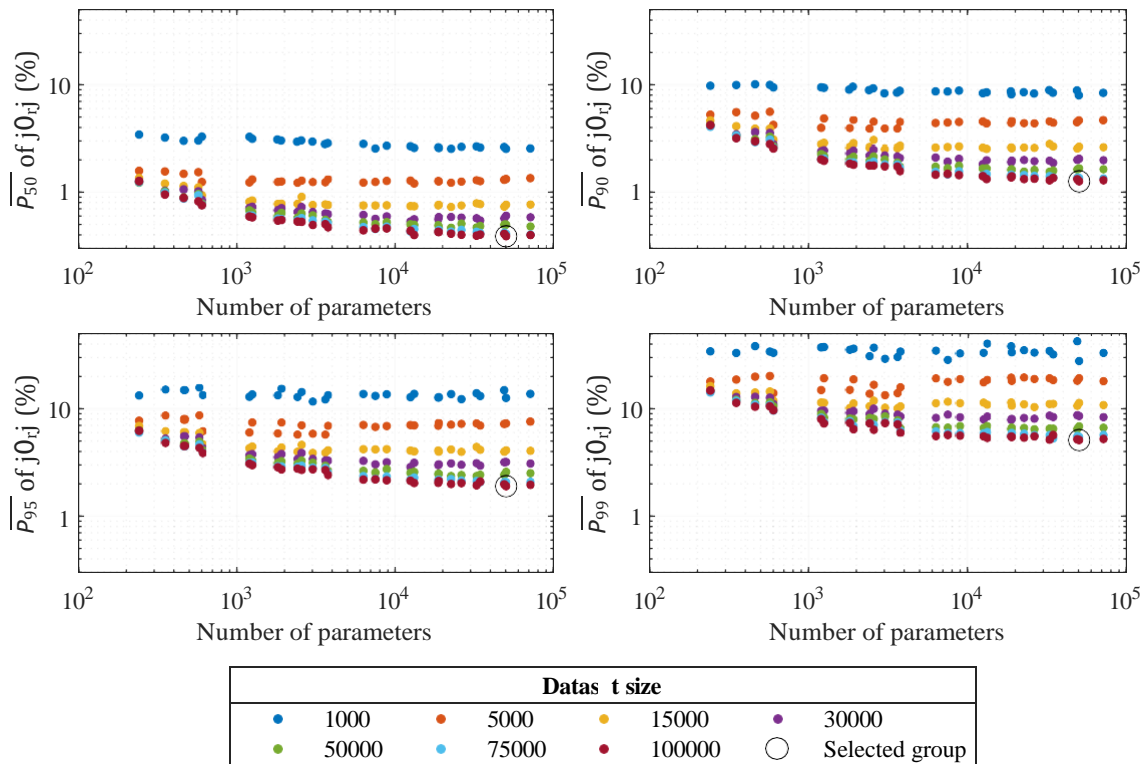


Figure 4.14. Mean of the error percentiles of the different configurations against the number of parameters, differentiating by the dataset size.

scale, since the average execution time for an input drops from 51 s in the structural model used to $2.4 \cdot 10^{-7}$ s by the neural network.

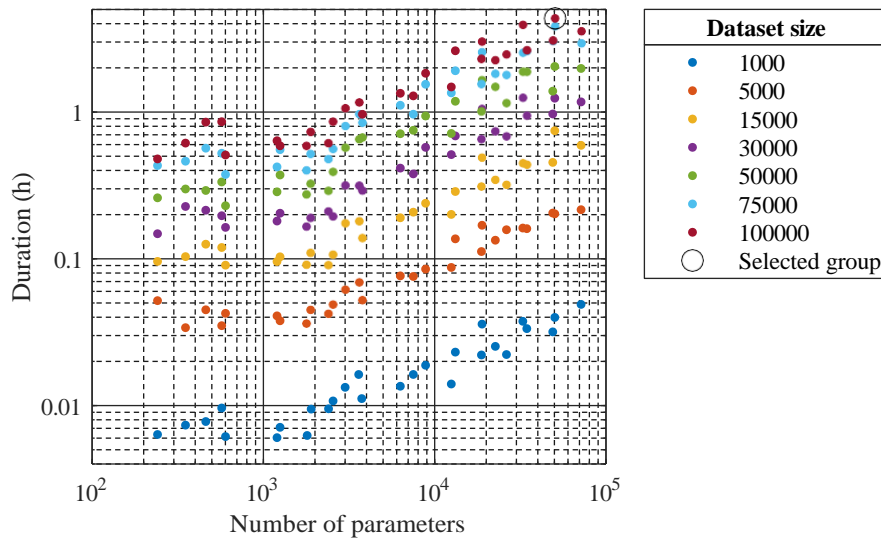


Figure 4.15. Training duration of the different configurations against the number of parameters, differentiating by the dataset size.

4.5.5 Ensemble model performance

An ensemble model is build and compared against individual networks using the 20 networks trained for the selected case with 4 hidden layers with 125 neurons each, trained with the 100 000-samples dataset. For this test, a new dataset of 10 000 samples is generated because the ANNs have been trained with different subsets of the initial dataset, and it is intended to evaluate the real ability to generalize the knowledge learned to new data never seen before. Figure 4.16 shows the 50th, 90th, 95th, and 99th percentiles for each of the 20 networks trained and the ensemble model. The asterisks indicate the specific values of the percentiles for each of the networks obtained, the dashed line marks its mean and the squares and solid line the results of the ensemble model. An evident reduction of the error percentiles is observed for the ensemble model, achieving an error less than 0.15%, 0.58%, 1.02%, and 3.36% for the 50%, 90%, 95%, and 99% of the samples, respectively.

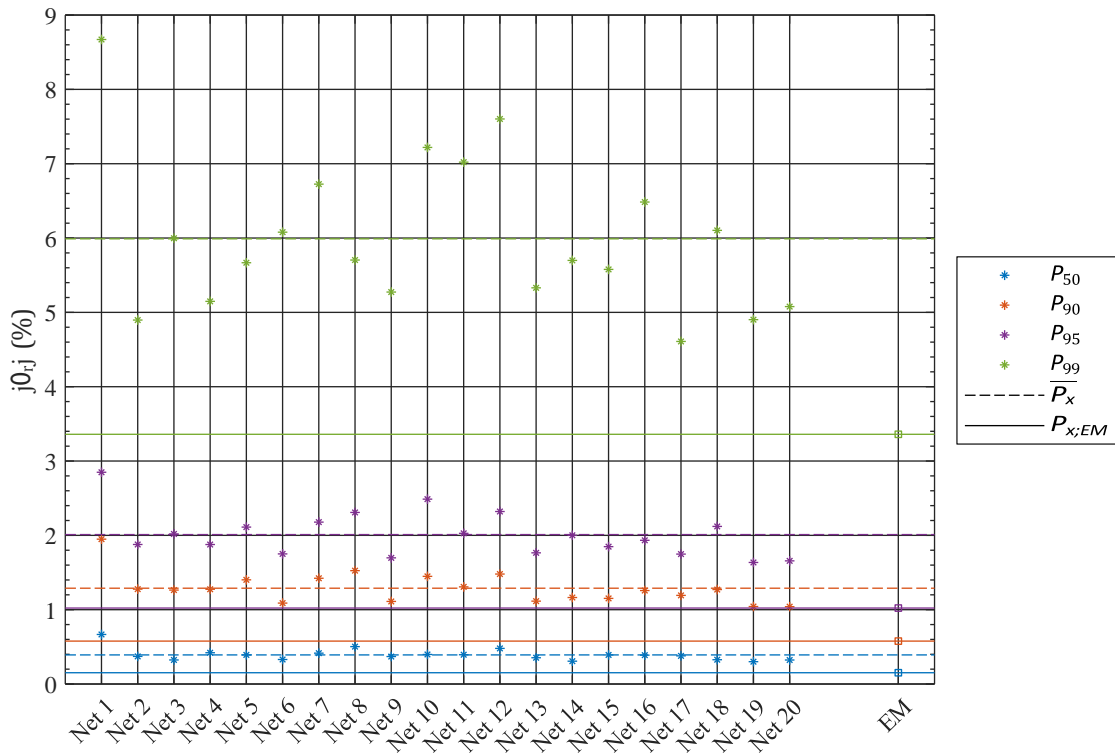


Figure 4.16. Comparison of error percentiles between individual ANNs and ensemble model (EM).

4.5.6 Application example

In order to verify the predictive capabilities of the proposed ANN surrogate model, a brief parametric study is conducted. Three different cases of wind turbines supported on jackets are adapted from the bibliography, calculating the fundamental frequency of the system using the structural model and the surrogate model. The parametric study, described in Table 4.4, analyse how the natural frequency of the structure varies against a change in the soil's shear wave propagation velocity. To do this, a density of 2 000 kg/m³ and a Poisson's ratio of 0.4 are set constant for the soil, and the shear wave propagation velocity is ranged from 60 to 600 m/s.

For this test, only the group of networks selected in Section 4.5.4 is used because it is the one that achieved the best results. It is the set that has: NoHL = 4 and NoNpHL = 125, and it was trained with 100 000 data. In addition, the ensemble model composed by 20 trained networks is used to better reproduce the structural response and establish a confidence interval.

Figure 4.17 shows the results of the fundamental frequency evaluated by both models. In the graphs above, the dashed black line represents the frequency calculated by the structural model, the solid blue line shows the mean prediction of the ensemble model, and the dashed blue lines mark the confidence interval for these set by twice the standard deviation. This interval is taken since, assuming a normal distribution, 95.44% of the predictions generated by neural networks trained under these assump-



Table 4.4. Parametric study cases of OWTs supported on jackets adapted from bibliography.

	5MW-Couceiro et al. [37]	5MW-Vorpahl et al. [74]	10MW-Stolpe et al. [36]
H_{tower} (m)	90	90	119
D_{bottom} (m)	6	6	8.3
T_{bottom} (mm)	27	27	38
D_{top} (m)	3.87	3.87	5.5
T_{top} (mm)	19	19	20
M_{RNA} (kg)	$350 \cdot 10^3$	$350 \cdot 10^3$	$869 \cdot 10^3$
$I_{\text{RNA,roll}}$ (kg m ²)	$354 \cdot 10^5$	$354 \cdot 10^5$	$156 \cdot 10^6$
$I_{\text{RNA,yaw}}$ (kg m ²)	$230 \cdot 10^5$	$230 \cdot 10^5$	$974 \cdot 10^5$
c_s (m/s)	60–600	60–600	60–600
v_s (-)	0.4	0.4	0.4
Q_s (kg/m ³)	2000	2000	2000
H_w (m)	50	50	50
H_{jck} (m)	70.15	70.15	76
n_{leg} (-)	4	4	4
S_{top} (m)	9.153	8	16
S_{base} (m)	13.862	12	33
n_{br} (-)	4	4	4
D_{leg} (m)	0.614	1.2	1.52
T_{leg} (mm)	17.1	38.8	42
D_{br} (m)	0.5	0.8	0.76
T_{br} (mm)	11.7	20	20.5
L_{pile} (m)	10	10	6

tions will be found within it. On the other hand, the graphs below show the relative error in absolute value (Equation 4.8) of the mean of the predictions (solid line) and the limits of the confidence interval (dashed line).

From a structural point of view, in the three cases analysed the natural frequency of the structure decreases as the soil becomes softer, which was expected. On the other hand, predictions made by the ensemble model show accurate predictions, since the midline error is considerably low with some peaks that do not reach 2.5%, al-

lowing to obtain very similar results than structural model in a much shorter time: 1.6 s/evaluation for structural model against $8.8 \cdot 10^{-5}$ s/evaluation for ensemble model.

All the frequency values calculated with the structural model are within the confidence interval established by the ensemble model, allowing it to be used as a measure of uncertainty. What's more, the width of this confidence interval is not homogeneous in the three cases, being narrower in 10MW-Stolpe et al. study case. This is because the quality of the network predictions are dependent on the position of the study case within the search space that was treated in the training.

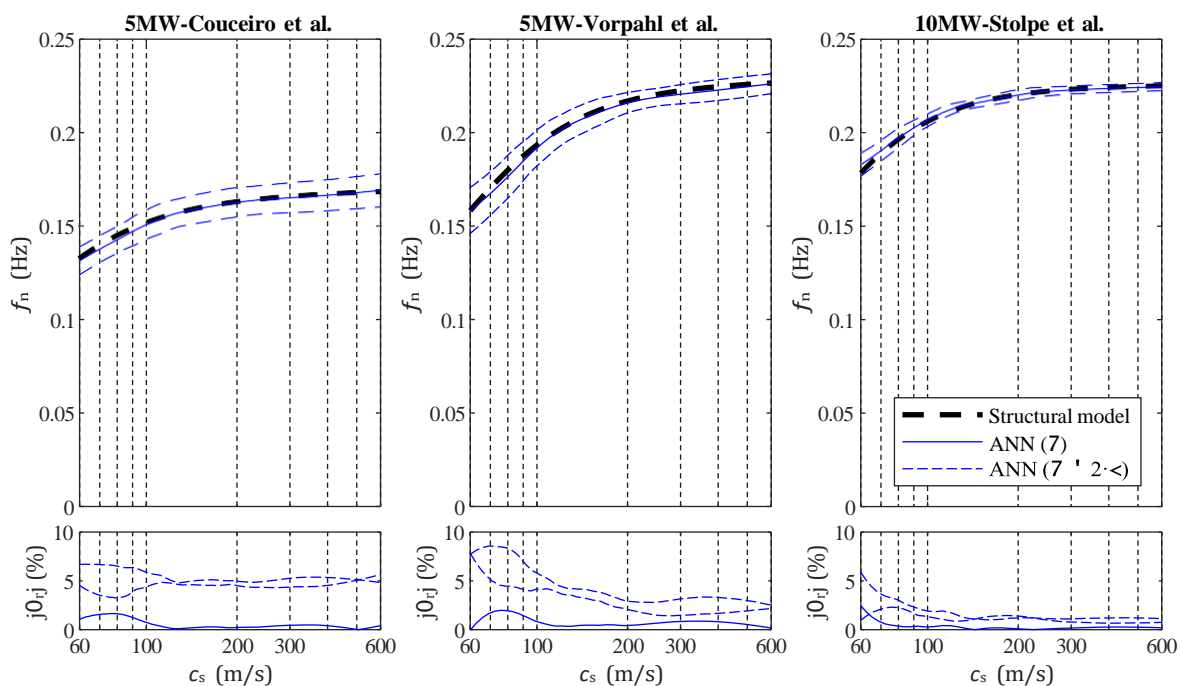


Figure 4.17. Fundamental frequency (f_n) of the three cases described in Table 4.4 with respect to soil's shear wave velocity (c_s). Comparison between the structural model and the ANN-based surrogate model.

4.6 Conclusions

In this chapter, ANNs are described, and two ANN-based surrogate models for structural problems are presented. In Section 4.4, a surrogate model which allow reproducing the pile foundation stiffness is presented. The ensemble model reaches a high performance, obtaining relative errors less than 10% for 99.7%, 99.87%, and 99.93% of the validation samples for the rocking stiffness, cross and vertical stiffness, and lateral stiffness terms, respectively. This performance is achieved with a significant reduction in the computational cost, allowing the evaluation of a thousand samples in less than one second.

Two application examples are included to illustrate the performance of the surrogate model with specific cases. First, the output of the model is compared with limited-




range expressions present in the bibliography, showing a great agreement with them. In the second example, the evolution of the pile stiffness as its length increases is studied, while comparing the results of the surrogate model and the continuous model. A great agreement is shown between both models. The stabilization of the pile stiffness derived of reaching the active length is adequately reproduced by the surrogate model, allowing to determine this critical aspect of the foundation. In both examples, the surrogate model presents a smooth behaviour, which makes it a useful tool to propose previous parametric studies or perform fast estimations in first stages of studies that require the evaluation of a large volume of samples.

In Section 4.5, a surrogate model for obtaining the fundamental frequency of an offshore wind turbine supported on a jacket structure, including SSI, is developed. The results obtained on the performance of neural networks reflect that, in this problem, a wide range of architectures and available dataset sizes reach an error of less than 5% for 90% of their predictions. In some cases, performance is considerably improved, reaching errors of less than 2% for 90% of samples. Moreover, the combined use of individual neural networks in an ensemble model further improves the prediction and allows incorporating its uncertainty through their mean and standard deviation values. To test the regression capacity of the model, a small parametric study is carried out. High performance of the surrogate model is observed, showing the potential uses that this methodology can develop.

From the analysis of both developed models, some relevant aspects to focus when implementing these ANN-based models are extracted:

- The definition of the dataset is a fundamental task for the training process. Regions with higher density of training samples tend to show better performance. Whether a synthetic dataset is generated, the defined search space must contain the relevant cases of the problem.
- Several architectures must be tested and compared to identify efficient design. In addition, some repetitions of the architecture should be evaluated in order to mitigate randomness in the process.
- The ensemble model offer two advantages against individual ANNs: first, it improves the results and, secondly, it allows to obtain a measure of the uncertainty.

This work confirmed the capability of ANNs-based surrogate models for predicting structural problems. In fact, both developed models have achieved good levels of accuracy for most of the test samples, showing errors less than 5%, usually considered in engineering. Furthermore, despite the computational cost of network training, the reduction in the execution time make this type of surrogate model relevant for replacement of high-resources-consumption models when many executions are required, such as in optimization procedures or extensive parametric studies.



5. Surrogate models for jacket evaluation

- 5.1 Introduction
- 5.2 Problem statement
- 5.3 Synthetic dataset
- 5.4 Classification model
- 5.5 Regression model
- 5.6 Classification and regression models comparison
- 5.7 Conclusions





5.1 Introduction

The design of the support structures of OWTs is a process with high consumption of computational resources, because it requires a structural analysis where many load cases are evaluated and many checks must be verified [34]. In case that a jacket is used as the support structure, the computational cost considerably increases due to the large number of structural elements that constitute the system. As commented in Chapter 3, many authors have developed optimization procedures capable of achieving jacket support structures that reduce the amount of material needed to verify the requirements (see, for example, [34–38]). However, the structural models used still were high time-consuming, so they are not extensively used in parametric studies that would allow a better understanding of the behaviour of the structure and the relationships between the design variables. In this line, the few parametric studies that focused on jacket support structures for OWT usually dealt with very specific problems by analysing a few variables (see, for example, [75–77]).

For this reason, different authors use low time-consuming surrogate models or meta-models, generated from other more rigorous ones, which are capable of providing sufficiently accurate results. For example, Zwick et al. [78] and Häfele et al. [79] used a multivariate linear statistical model and a Gaussian process regression, respectively, for estimating the fatigue damage to jacket structures. Within the structural engineering field, other techniques have been used to build surrogate models, as can be Kriging models [47–49] or ANNs [49, 50, 80]. This trend extends to other areas of civil engineering, where soft computing techniques have been used to approximate complex problems. In recent years, the use of Machine Learning techniques (including Deep Learning) have increased their presence in the field [46, 81, 82].

In this chapter, ANN-based surrogate models for estimating the feasibility of a jacket structure acting as the support structure for any given wind turbine in a specific emplacement is developed. A synthetic dataset is generated to train the ANNs, and different strategies to build the surrogate models are tested. First, the problem definition is established in Section 5.2. Then, the generation of the synthetic dataset used to train the ANNs is detailed in Section 5.3. Section 5.4 and Section 5.5 describe all the characteristics and show the performance results of the classification and regression models, respectively. Finally, classification and regression models are compared in Section 5.6, followed by the main conclusions in Section 5.7.

5.2 Problem statement

The structural system considered for this surrogate model is an OWT supported by a jacket structure, as presented in Chapter 2. Completely define this structural system is a very extensive task, so some acceptable simplifications are considered to reduce the large number of necessary variables. This complex system can be conceptually divided in three independent parts to be more comprehensible: the wind turbine, the characteristics of the emplacement, and the jacket substructure. For all these elements,

the main variables that define the system properties, the loads affecting the structure, and the capacity resistance must be considered.

This surrogate model aims to replace the structural evaluation model. Therefore, feasibility under the technical verifications imposed on the structure are considered as the structural response metric.

5.2.1 Wind turbine

The wind turbine is composed by the rotor-nacelle-assembly, which groups the energy production subsystem; and the tower, which is the structural element that supports it. In this model, the rotor-nacelle-assembly is defined by the rotor diameter (D_{rotor}), the mass (M_{RNA}), and the moment of inertia about roll axis $I_{RNA,roll}$ and yaw axis $I_{RNA,yaw}$. Inertia about pitch axis is considered to be equal to inertia about yaw axis. A punctual hysteretic damping in the rotor is considered in order to represent aeroelastic damping. Values of 6% in fore-aft direction and 0.75% in side-side direction are considered, following intervals proposed by Chen et al [43].

The tower is assumed as a tubular element of length (H_{tower}) with a linearly variable section defined by the bottom diameter (D_{bottom}), the bottom thickness (T_{bottom}), the top diameter D_{top} , and the top thickness T_{top} . Steel properties are considered to the wind turbine's tower: density of 7 850 kg/m³, Young's modulus of 210 GPa, Poisson's ratio of 0.3, and hysteretic damping coefficient of 0.5%.

Some operating parameters of the wind turbine are also required to evaluate the effects of the wind loads on the structure: the rated wind speed (U_R), the minimum rotor speed ($f_{r,min}$), and the maximum rotor speed ($f_{r,max}$).

5.2.2 Site conditions

The site conditions that affect the structure considered in the model are the wind, the sea, and the soil. The wind conditions are established by the mean velocity of the wind at 10 m above sea surface ($u_{m,10}$) and the shape parameter of the Weibull distribution of wind (k_{wind}).

Sea influence is characterized by the water depth (H_w), the circulatory current $v_{v,circ}$ assumed in the same direction as wind, and the waves states: 1-y extreme sea state ($H_{ESS,1}$), 50-y extreme sea state ($H_{ESS,50}$), 1-y extreme wave height ($H_{EWH,1}$), and 50-y extreme wave height ($H_{EWH,50}$). An increment of one percentage point on the hysteretic damping of submerged structural elements is set.

Finally, soil is considered as a homogeneous halfspace defined by the shear wave propagation velocity (c_s), the Poisson's ratio (ν_s), the density (ρ_s), the angle of internal friction (ϕ_s), and a hysteretic damping ratio of 2.5%.

5.2.3 Jacket substructure

Following the global description of the jacket structure presented in Chapter 2, some hyperparameters are necessary to define the shape of the structure. These variables are

the number of legs (n_{leg}), the number of bracing levels (n_{br}), the jacket height (H_{jck}), and the spacing of the legs at the base (S_{base}) and at the top (S_{top}) of the structure.

The structural elements and the pile foundations are considered as tubular steel members, with the same properties as the wind turbine tower. In this case, elastic strength of the material f_y is also taking into account because affects the element capacity. For this surrogate model, different section typologies are allowed in the structure. Diameter (D_{leg}) and thickness (T_{leg}) of the legs during each bracing level, and diameter (D_{br_i}) and thickness (T_{br_i}) of each bracing level are considered. All piles present the same geometry, and are defined by their diameter (D_{pile}), thickness (T_{pile}), and length (L_{pile}). The mass of the jacket platform (M_{pltf}) is also included to extend the capabilities of the surrogate model.

5.2.4 Structural feasibility

The structural feasibility of the jacket structure is summarized by the utilization factors (η_j) described in Section 2.4, which allow a clear comparison of different checks. If this factor is less or equal than 1, the requirement is fulfilled.

To obtain a deeper knowledge of the feasibility, several utilization factors of partial checks are collected: non-resonance check (Section 2.4.4), foundation capacity (Section 2.4.2.3), maximum platform rotation (Section 2.4.3), pile head section capacity (Section 2.4.2.1), section capacity and buckling (combined) of each level of legs and braces (Sections 2.4.2.1 and 2.4.2.2), global buckling analysis (Section 2.4.2.2), welded joints geometry (Section 2.4.1.2), minimum jacket height (Section 2.4.1.1), minimum pile thickness (Section 2.4.1.3), and minimum pile length (Section 2.4.1.4). Also, a global utilization factor (η) of the structure is established as the maximum partial utilization factor.

$$\eta = \max(\eta_1, \eta_2, \dots, \eta_{N_{check}}) \quad (5.1)$$

5.3 Synthetic dataset

A synthetic dataset to train the surrogate model is obtained. This dataset is constituted by random-generated samples, where the wind turbine, the jacket foundation, and the site conditions are defined, and the partial utilization factors of the technical verifications imposed are computed by the structural model presented in Chapter 2. For most of the variables, lower and upper limits are not established for the sample generation. Instead, some relationships are identified to capture main dependencies among variables. Then, lower and upper limits are set for these relationships, and the random samples are defined by uniform distributions. This procedure allow generating more realistic samples, which increment the relevance of each sample of the dataset. This results in a more efficient dataset than an unrestricted one. The generation of each part of the dataset is described in the following subsections.

Two different datasets are generated: one for training the models with 300 000 samples, and another for testing the models with 50 000 samples. In both cases, the same procedure is followed.

5.3.1 Wind turbine

The search space for wind turbine variables is defined after analysing four examples of 5, 8, 10, and 15 MW described in the literature [5, 71–73]. Table 5.1 collects the lower and upper limits of the search space of the wind turbine variables. More complex

Table 5.1. Search space of the wind turbine variables.

Expression	Lower limit	Upper limit
H_{tower}	70	150
$D_{\text{rotor}}/H_{\text{tower}}$	1.3	1.9
$M_{\text{RNA}}/D_{\text{rotor}}^2$	15	25
$I_{\text{RNA,roll}}/M_{\text{RNA}} D_{\text{rotor}}^2$	0.05	0.15
$I_{\text{RNA,yaw}}/I_{\text{RNA,roll}}$	0.55	0.8
$H_{\text{tower}}^{1.2}/D_{\text{bottom}}$	34	40
$D_{\text{bottom}}/T_{\text{bottom}}$	200	260
$D_{\text{bottom}}/D_{\text{top}}$	1.45	1.65
$D_{\text{top}}/T_{\text{top}}$	190	290
U_{R}	10	14
$f_{\text{r,min}}$	Equation (5.2) $\lambda_{f_{\text{r,min}}} \sim \text{U}(30, 38)$	
$f_{\text{r,max}}$	Equation (5.3) $\lambda_{f_{\text{r,max}}} \sim \text{U}(0.1, 0.2)$	

expressions inspired in blade tip velocity and acceleration are used to obtain the rotor frequency ranges. In these cases, latent variables $\lambda_{f_{\text{r,min}}}$, $\lambda_{f_{\text{r,max}}}$ are obtained by uniform distributions, and then, the actual variables are evaluated. Minimum rotor speed is defined by the following expression:

$$f_{\text{r,min}} = \frac{\lambda_{f_{\text{r,min}}}}{2\pi^2 D_{\text{rotor}}} \quad (5.2)$$

While, maximum rotor speed is obtained as follows:

$$f_{\text{r,max}} = \frac{\lambda_{f_{\text{r,max}}} D_{\text{rotor}} + 60}{\pi D_{\text{rotor}}} \quad (5.3)$$

5.3.2 Site conditions

Site conditions can be segregated into wind conditions, sea states, and soil properties. All ranges considered are summarized in Table 5.2. Wind conditions are established

Table 5.2. Search space of the site conditions variables.

Expression	Lower limit	Upper limit
$u_{m,10}$	5	15
k_{wind}	1	3
λ_{wave}	0.1	4.5
k_{wave}	Equation (5.4a)	Equation (5.4b)
$H_{ESS,1}$	Equation (5.5) $T_R = 2$	
$H_{ESS,50}$	Equation (5.5) $T_R = 50$	
$H_{EWH,1}$	Equations (5.8a), (5.7), and (5.6)	Equations (5.8b), (5.7), and (5.6)
$H_{EWH,50}$	Equations (5.8a), (5.7), and (5.6)	Equations (5.8b), (5.7), and (5.6)
H_w	$\max(H_{ESS,50}, \frac{3}{4}H_{EWH,50}, 1)$	100
$v_{v,circ}$	0	2
c_s	60	600
v_s	Equation (4.9a)	Equation (4.9b)
Q_s	Equation (4.10a)	Equation (4.10b)
φ_s	20	50

between fixed limits. To define the sea state, first the Weibull distribution of waves is obtained. Scale and shape parameters are randomly generated from intervals extracted from estimations proposed in Appendix B of DNVGL-RP-C205 [2], represented in Figure 5.1. Scale parameter (λ_{wave}) is established between 0.1 and 4.5 m, and shape parameter (k_{wave}) limits are the following:

$$k_{wave,lower\ limit} = 1 + \frac{(\lambda_{wave})^3}{5} \tag{5.4a}$$

$$k_{wave,upper\ limit} = \begin{cases} 1.5 + \lambda_{wave} \frac{2.3 - 1.5}{2} & \lambda_{wave} \leq 2 \\ 23 + (\lambda_{wave} - 3) \frac{1.8 - 2.3}{4.5 - 3} & 2 < \lambda_{wave} \leq 3 \\ 23 + (\lambda_{wave} - 3) \frac{1.8 - 2.3}{4.5 - 3} & 3 < \lambda_{wave} \end{cases} \tag{5.4b}$$

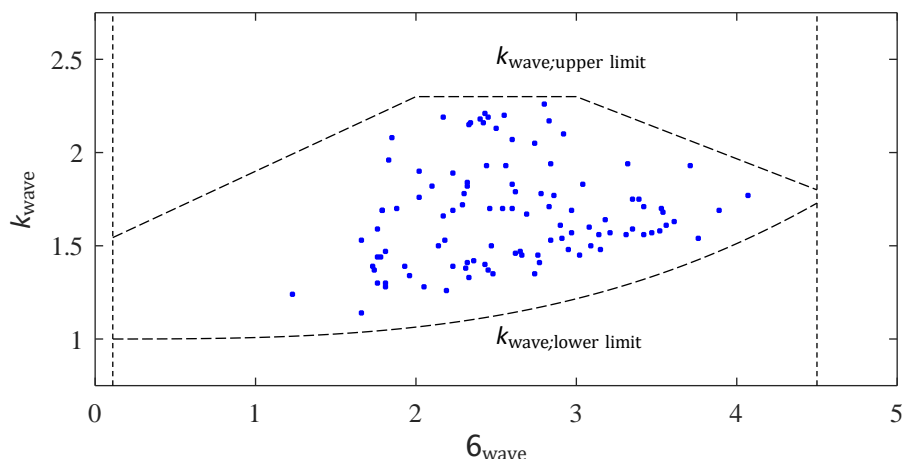


Figure 5.1. Values of the scale and shape parameters of Weibull distribution estimated for different nautic zones by Appendix B of DNVGL-RP-C205 [2]. Limits considered in this section for generating the dataset.

Once the Weibull distribution is defined, the significant wave height can be computed for different return periods (T_R) according to DNVGL-ST-0437 [4]:

$$H_{ESS, T_R} = \lambda_{wave} \left(-\ln \left(1 - \frac{1}{T_R} \right) \right)^{1/2920} \quad (5.5)$$

This expression is only valid for return periods greater than one year, so a return period of two years is assumed for computing the $H_{ESS,1}$. Then, DNVGL-ST-0437 [4] indicates that extreme wave height can be estimated by the following expression:

$$H_{EWH, T_R} = \sqrt{\frac{1}{2} \ln N_{wave} + \frac{0.2886}{2 \ln N_{wave}}} H_{ESS, T_R} \quad (5.6)$$

where N_{wave} is the number of waves, computed as

$$N_{wave} = \frac{3 \cdot 3600}{T_{wave}} \quad (5.7)$$

To set the lower and upper limits, wave period is considered as the limits shown in Equation (2.17):

$$T_{wave, lower\ limit} = 14.3 \sqrt{\frac{H_{ESS, T_R}}{g}} \quad (5.8a)$$

$$T_{wave, upper\ limit} = 11.1 \sqrt{\frac{H_{ESS, T_R}}{g}} \quad (5.8b)$$

Once waves scenarios are obtained, water depth is limited from the maximum value among $H_{ESS,50}$, $\frac{3}{4} H_{EWH,50}$, and 1 m to 100 m. Circulational currents are generated between zero and 2 m/s.



Table 5.3. Search space of the jacket substructure variables.

Expression	Lower limit	Upper limit
n_{leg}	3	5
$H_{jck} - H_{jck, min}$	0	10
$S_{top}/S_{top, min}$	1	2.5
S_{base}	Equation (4.11) $\alpha_{leg} \sim U(60^\circ, 90^\circ)$	
n_{br}	clamp {1, Eq. (4.12) $\beta_{br} = 70, 10$ }	clamp {1, Eq. (4.12) $\beta_{br} = 30, 10$ }
$D_{leg_{i+1}}/D_{leg_i}$	0.8	1.2
$\overline{D_{leg_i}}$	0.3	3
T_{leg_i}	$D_{leg_i}/64$	$D_{leg_i}/16$
D_{br_i}	$0.2 D_{leg_i}$	D_{leg_i}
T_{br_i}	$D_{br_i}/64$	$D_{br_i}/16$
D_{pile}	0.2	4
T_{pile}	$(0.635 + D_{pile})/100$	$D_{pile}/16$
L_{pile}	Equation (5.11)	$20 D_{pile}$
f_y	$2 \cdot 10^8$	$7 \cdot 10^8$
M_{pltf}	Equation (5.12) $T_{pltf} = 0$	Equation (5.12) $T_{pltf} = 0.2$

Finally, for the soil properties search space, the same limits of Section 4.5.2 are considered. In addition, the angle of internal friction (φ_s) is included, with limits established from 20° to 50° .

5.3.3 Jacket substructure

Established ranges for jacket variables are summarized in Table 5.3. First, hyperparameters about external shape of the jacket are defined. The number of legs is set between three and five. The jacket height is limited between the minimum jacket height, according to Equation (2.26), and 10 m higher. This minimum height is computed as:

$$H_{jck, min} = H_w + H_{EWH, 50} + \max(0.2 H_{ESS, 50}, 1) \quad (5.9)$$

Similar consideration is taken for top legs spacing, which is generated from 1 to 2.5 times its minimum value. This minimum value is assumed as the side of the regular polygon with n_{leg} sides circumscribed in the diameter of the base of the wind turbine tower:

$$S_{top, min} = D_{bottom} \tan(\pi/n_{leg}) \quad (5.10)$$

Legs spacing at the base of the jacket and number of bracing levels are generated by the same consideration as in Section 4.5.2. This last variable includes an additional appreciation. Each lower and upper limit obtained must be clamped between one and ten, because a maximum of ten different sections are considered for legs and bracings.

Second, the dimensions of the tubular elements in the structure are generated. The ratio between leg diameters for consecutive bracing levels is set between 0.8 and 1.2. An average value of leg diameters among all bracing levels ($\overline{D_{leg}}$) between 0.3 m and 3 m is considered. Legs thicknesses, bracings diameters, and bracing thicknesses are directly limited from previously obtained variables. Regarding to pile dimensions, pile diameter is limited from 0.2 m to 4 m, pile thickness is set from the minimum allowed value according Equation (2.29) to $D_{pile}/16$, and pile length is established between the minimum length ($L_{pile,min}$) recommended by Equation (2.30) and twenty times pile diameter.

$$L_{pile,min} = D_{pile} \sqrt{\frac{E_{pile} \frac{64 J_{pile}}{\pi D_{pile}^4}}{G_s \left(1 + \frac{3}{4} \nu_s\right)}} \quad (5.11)$$

Third, some extra variables must be defined. The elastic strength of the material is limited from 200 to 700 MPa. This range is set based on DNVGL-OS-B101 [83], to allow different steel grades. The mass of the jacket platform (M_{pltf}) is estimated as the mass of a steel plate filling the area closed by the upper extremes of legs with a thickness (T_{pltf}) between zero and 20 cm.

$$M_{pltf} = 7850 \frac{n_{leg} \left(\frac{S_{top}}{2}\right)^2}{\tan\left(\frac{\pi}{n_{leg}}\right)} T_{pltf} \quad (5.12)$$

During the jacket variables generation, lower limits for jacket height, pile thickness, and pile length are set from the minimum feasible value, according verifications imposed. This implies that the dataset implicitly satisfy these requirements and, therefore, the surrogate model cannot be trained to detect these fail criteria. However, as these checks are easy and fast to verify, they can be computed apart from the proposed surrogate model. Thus, the search space of the dataset is reduced and focused on more relevant regions.

5.3.4 Structural feasibility

Once the variables that define the wind turbine, the site conditions, and the jacket structure with the pile foundation are established, the structural model presented in Chapter 2 is used for evaluating the structural feasibility of each sample. All partial utilization factors are collected to completely define the synthetic dataset. Owing to the large search space explored and the numerous verification criteria, the dataset results very unbalanced. Over all the samples generated and evaluated, only 0.295% of the samples are feasible structures.



5.4 Classification model

In this section, a classification ANN model for jacket evaluation is developed. Two different classes are considered for the model output, to predict whether the technical checks imposed are verified or not.

5.4.1 Architecture

To be able to make a prediction, the surrogate model needs to collect information about the evaluated samples. In this case, the input layer of the ANN presents 74 input neurons, according to all variables described in Section 5.2. These variables are collected in Table 5.4, and they are 12 variables that describe the wind turbine and its operating conditions, 12 variables that describe the site conditions, and 50 variables that define the jacket structure.

Table 5.4. Input variables of the surrogate model for jacket feasibility evaluation.

Subsystem		Input variables
Wind turbine	Rotor-nacelle	$D_{\text{rotor}}, M_{\text{RNA}}, I_{\text{RNA,roll}}, I_{\text{RNA,yaw}}$
	Tower	$H_{\text{tower}}, D_{\text{bottom}}, T_{\text{bottom}}, D_{\text{top}}, T_{\text{top}}$
	Operating	$U_{\text{R}}, f_{\text{r,min}}, f_{\text{r,max}}$
Site conditions	Wind	$u_{\text{m,10}}, k_{\text{wind}}$
	Sea	$H_{\text{w}}, v_{\text{v,circ}}, H_{\text{ESS,1}}, H_{\text{ESS,50}}, H_{\text{EWH,1}}, H_{\text{EWH,50}}$
	Soil	$c_{\text{s}}, v_{\text{s}}, Q_{\text{s}}, \varphi_{\text{s}}$
Jacket structure	Hyperparameters	$n_{\text{leg}}, n_{\text{br}}, H_{\text{jck}}, S_{\text{base}}, S_{\text{top}}$
	Legs' sections	$D_{\text{leg}_i}, T_{\text{leg}_i} \mid i = 1, 2, \dots, 10$
	Bracings' sections	$D_{\text{br}_i}, T_{\text{br}_i} \mid i = 1, 2, \dots, 10$
	Pile foundation	$D_{\text{pile}}, T_{\text{pile}}, L_{\text{pile}}$
	Material	f_y
	Transition piece	M_{pltf}

Regarding model's output, two different architectures are considered. First, an ANN with one global output that indicates whether the jacket structure verifies all requirements or not. Second, an ANN with 26 partial outputs that indicate whether each one of the requirements imposed is verified or not. Partial checks considered are summarized in Section 5.2.4. However, minimum jacket height, minimum pile thickness, and minimum pile length are not included owing to these checks are easy and low-consumption evaluations. Both cases are classification models with two classes, so a sigmoid function is used as activation function in output layer to force binary output.

For this model, fully connected networks are used. The NoHL and the NoNpHL are modified to obtain architectures with different NoP, allowing to analyse the fitting capacity of the ANN. To reduce the variability, the same number of neurons is established for each hidden layer. Thus, architectures of increasing size are developed, both in NoHL and NoNpHL, ranging from 2 Hidden layers with 100 neurons per hidden layer to 8 hidden layers with 400 neurons per hidden layer, with a step of 1 hidden layer and 50 neurons per hidden layer. At the output of each hidden layer, a normalization of the layer is implemented to speed up the training of the ANN [59] and the ReLU is used as activation function.

5.4.2 Training process

To uniform the scale of the values of the different input variables, each variable is normalized by subtracting the mean and dividing by the standard deviation. For non-existing variables, that is, the diameters and thicknesses of legs and bracings for levels higher than the number of bracing levels, the input value is set to zero to remove their influence. Then, the training dataset is randomly divided in two sets: for training (80%) and for validation (20%), avoiding overfitting.

As the trained model is a classification model, the Log Loss (Equation (4.3)) is used as loss function. In the case of the model for partial checks, there are also non-existing outputs, corresponding to the ULS of legs and bracings for levels higher than the number of bracing levels. The loss of these outputs is removed, so the fitting capacity of the model is not wasted.

Twenty ANNs for each combination of the described architectures are trained by the automatic differentiation algorithm already implemented in Matlab [45]. The ANN parameters are updated by the adaptive moment estimation (Adam) [60], using an initial global learning rate of 0.01, a gradient decay factor of 0.9, a squared gradient decay factor of 0.999, and a batch size of 5 000. The validation data error is continuously evaluated, stopping the process when it stabilizes. Next, the neural network is retrained, reducing the global learning rate by half, repeating this process until the new network does not improve the performance of the previous one.

5.4.3 Model prediction

The implemented surrogate model is a classification model that predicts whether the jacket belongs to one of two classes: feasible or non-feasible. However, the output of the sigmoid function, used as activation function in the output layer, is a continuous value ranged from zero to one. This can be understood as the probability of belonging to one of the two classes, in this case, the probability of being a feasible jacket.

This initial approach becomes more complex when considering two aspects: the model trained through partial checks does not generate the global probability of being a feasible jacket, and how the prediction of several individual ANNs are combined in an ensemble model. The nomenclature $\hat{Y}_{i,j}^k$ is used to mathematically show the different



aggregations and ensemble strategies of the probabilities. This can be read as the probability, given by the ANN k , of verifying the check j for the sample i .

5.4.3.1 Partial predictions aggregation

The output of the model trained through the global check can be directly treated as the probability of being a feasible jacket. For the model trained to predict the partial checks, the global probability must be built using the partial probabilities. Different aggregation strategies are considered in this section:

- Conjunction of independent events: the global probability of feasibility is considered as the probability of the conjunction of all partial checks, assuming they are independent events. That is, the product of all partial probabilities.

$$\hat{Y}_i^k = \prod_{j=1}^{N_{\text{check}}} \hat{Y}_{i,j}^k \quad (5.13)$$

- Minimum of partial check: the global probability of feasibility is considered as the probability of the partial check having the least expectation of being feasible.

$$\hat{Y}_i^k = \min \left(\hat{Y}_{i,1}^k, \hat{Y}_{i,2}^k, \dots, \hat{Y}_{i,N_{\text{check}}}^k \right) \quad (5.14)$$

- Geometric mean: the global probability of feasibility is considered as the geometric mean of the partial check probabilities.

$$\hat{Y}_i^k = \left(\prod_{j=1}^{N_{\text{check}}} \hat{Y}_{i,j}^k \right)^{1/N_{\text{check}}} \quad (5.15)$$

This assumption is included as an attempt to average the partial verifications. Arithmetic mean does not represent the problem nature, because it treats feasible and non-feasible cases the same. However, the geometric mean tends to be zero if any of the partial checks is close to zero.

5.4.3.2 Ensemble model

As aforementioned, the output of the ANN can be understood as the probability of verifying the check. However, to build the ensemble model, the ensemble strategy of the probabilities provided by different ANNs must be defined. The following ensemble strategies are implemented:

- Mean: the combined probability of feasibility is considered as the mean of the probabilities predicted by each model.

$$\hat{Y}_{i,j} = \frac{1}{N_{\text{ANN}}} \sum_{k=1}^{N_{\text{ANN}}} \hat{Y}_{i,j}^k \quad (5.16)$$

- Voting: the combined probability of feasibility is considered as the proportion of ANNs that predict the check is verified. It is computed as the mean of the nearest integer (nint) of the prediction.

$$\hat{Y}_{i,j} = \frac{1}{N_{ANN}} \sum_{k=1}^{N_{ANN}} \text{nint}(\hat{Y}_{i,j}^k) \quad (5.17)$$

- Bayesian inference: the combined probability of feasibility is updated by the evidences given by individuals ANNs, following the Bayesian inference:

$$\begin{aligned} \hat{Y}_{i,j} &= \text{IP}(\eta_{i,j} \leq 1 | \hat{Y}_{i,j}^1, \hat{Y}_{i,j}^2, \dots, \hat{Y}_{i,j}^{N_{ANN}}) = \\ &= \frac{\prod_{k=1}^{N_{ANN}} \text{IP}(\hat{Y}_{i,j}^k | \eta_{i,j} \leq 1) \text{IP}(\eta_{i,j} \leq 1)}{\prod_{k=1}^{N_{ANN}} \text{IP}(\hat{Y}_{i,j}^k | \eta_{i,j} \leq 1) \text{IP}(\eta_{i,j} \leq 1) + \prod_{k=1}^{N_{ANN}} \text{IP}(\hat{Y}_{i,j}^k | \eta_{i,j} > 1) \text{IP}(\eta_{i,j} > 1)} = \\ &= \frac{\prod_{k=1}^{N_{ANN}} LR_{i,j}^k \text{IP}(\eta_{i,j} \leq 1)}{\prod_{k=1}^{N_{ANN}} LR_{i,j}^k \text{IP}(\eta_{i,j} \leq 1) + 1 - \text{IP}(\eta_{i,j} \leq 1)} \end{aligned} \quad (5.18)$$

where $\text{IP}(\eta_{i,j} \leq 1)$ is the prior probability of verifying the check j for the sample i , assumed as the prevalence of the feasible samples in the dataset for check j , and $LR_{i,j}^k$ is the likelihood ratio, which compare the probabilities of obtaining prediction $\hat{Y}_{i,j}^k$ knowing that the check is verified versus knowing the check is not verified. This last term can be expressed in terms of the individual predictions of the ANNs:

$$\begin{aligned} LR_{i,j}^k &= \frac{\text{IP}(\hat{Y}_{i,j}^k | \eta_{i,j} \leq 1)}{\text{IP}(\hat{Y}_{i,j}^k | \eta_{i,j} > 1)} = \frac{\text{IP}(\eta_{i,j} \leq 1 | \hat{Y}_{i,j}^k) \text{IP}(\hat{Y}_{i,j}^k)}{\text{IP}(\eta_{i,j} > 1 | \hat{Y}_{i,j}^k) \text{IP}(\hat{Y}_{i,j}^k)} = \\ &= \frac{\text{IP}(\eta_{i,j} \leq 1 | \hat{Y}_{i,j}^k)}{\text{IP}(\eta_{i,j} > 1 | \hat{Y}_{i,j}^k)} = \frac{\hat{Y}_{i,j}^k}{1 - \hat{Y}_{i,j}^k} \frac{1 - \text{IP}(\eta_{i,j} \leq 1)}{\text{IP}(\eta_{i,j} \leq 1)} \end{aligned} \quad (5.19)$$

In the cases of the ANNs trained to predict the global feasibility, these ensemble strategies can be only applied to the global probabilities of individuals ANNs. However, for ANNs trained for partial checks, assembly can be performed for the partial checks and then combined to obtain the global feasibility, or all the partials checks can be combined for each ANN and then assembled. Both options are analysed in this study.



5.4.4 Model performance

To evaluate the performance of the ANN-based models, the test dataset is evaluated, and the predictions made by the models are compared to the actual targets. The structural evaluation performed consists in a binary classification: feasible or non-feasible jacket. Therefore, a default decision threshold of 0.5 is used to assign the class of the output from model's probabilities, considering positive samples the feasible jackets ($\hat{Y}_i \geq 0.5$) and negative samples the non-feasible jackets ($\hat{Y}_i < 0.5$).

Confusion matrix is often used to analyse binary classification problems. This matrix is constituted by:

- True positives (TP): correctly predicted positive samples.
- False negatives (FN): positive samples incorrectly predicted as negative.
- False positives (FP): negative samples incorrectly predicted as positive.
- True negatives (TN): correctly predicted negative samples.

To easily evaluate the proportion of these metrics into the test dataset, the following relative metrics are used:

- True positive rate (TPR): proportion of positive samples correctly predicted.

$$\text{TPR} = \frac{\text{TP}}{\text{TP} + \text{FN}} \quad (5.20)$$

- True negative rate (TNR): proportion of negative samples correctly predicted.

$$\text{TNR} = \frac{\text{TN}}{\text{TN} + \text{FP}} \quad (5.21)$$

- Positive predictive value (PPV): proportion of positive predictions that are actually correct.

$$\text{PPV} = \frac{\text{TP}}{\text{TP} + \text{FP}} \quad (5.22)$$

- Negative predictive value (NPV): proportion of negative predictions that are actually correct.

$$\text{NPV} = \frac{\text{TN}}{\text{TN} + \text{FN}} \quad (5.23)$$

Owing to low prevalence of feasible jackets (0.295%), Matthews Correlation Coefficient (MCC) is also evaluated:

$$\text{MCC} = \sqrt{\frac{\text{TP TN} - \text{FP FN}}{(\text{TP} + \text{FP})(\text{TP} + \text{FN})(\text{TN} + \text{FP})(\text{TN} + \text{FN})}} \quad (5.24)$$

This metric is specially indicated for evaluating unbalanced data without overestimating one class over the other. This coefficient ranges from -1 to 1 , where 1 indicates perfect accuracy, 0 indicates no relation between predictions and actual values, and -1 indicates that all predictions are wrong.

Figure 5.2 shows the boxplots of the TPR, PPV, NPV, TNR, and MCC of all the classification models trained. Also including the different strategies of partial checks aggregation and ensemble. An initial analysis shows a wide range in TPR and PPV metrics. However, different results are obtained for TNR and NPV owing to the unbalance in the dataset. For TNR, the great proportion of non-feasible jackets produce that for most models, almost all negative samples are correctly assigned. Regarding NPV, all models are successful in almost all of their negative predictions, with a minimum NPV of 0.997 . Taking this into account, no more analysis of NPV will be done. The MCC also shows great variability, achieving values greater than 0.6 .

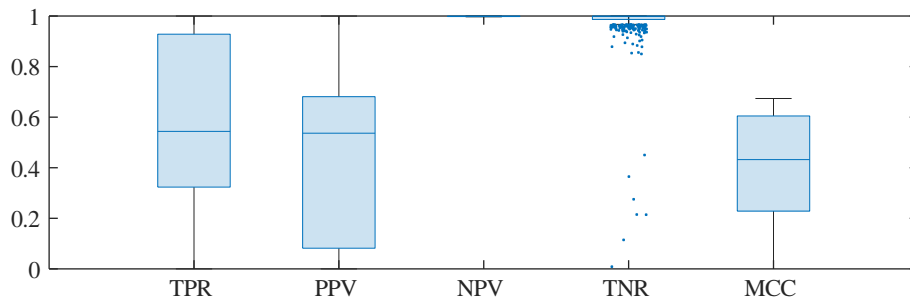


Figure 5.2. Boxplots of the classification metrics of all classification models, considering all the partial predictions aggregations and ensemble strategies.

Figure 5.3 shows the boxplots of TPR, PPV, MCC, and TNR of all classification models. Models are grouped depending on the ANN output: global check (GM) or partial check (PM); and ensembled variable: individual ANN (SANN), ensemble in partial checks (PE), or ensemble in global check (GE). In general terms, models for partial checks show better performances measured by MCC. This is mainly explained by the increase in TPR that they present. Regarding the benefits of combining several models, a slight increase in MCC is obtained by for the models for global check, but not consistently. However, the models for partial checks, ensembled in partial checks, show a consistent increase in the MCC.

An analysis of the influence of the size of the ANNs is shown in Figure 5.4. A significant decrement in MCC appears for ANNs with 8 hidden layers and 400 neurons per hidden layer, which is probably produced by overfitting. This effect occurs for smaller NoP values in models for global check. Generally, the ANNs with 5 hidden layers and 250 neurons per hidden layer show slightly better performance than other architectures.

The models implemented to combine the partial checks predictions to obtain the global feasibility, detailed in Section 5.4.3.1, are compared in Figure 5.5. The first aspect that must be highlighted is that not all aggregation strategies implemented are applied to each model. Thus, these aggregation strategies are only applied to partial

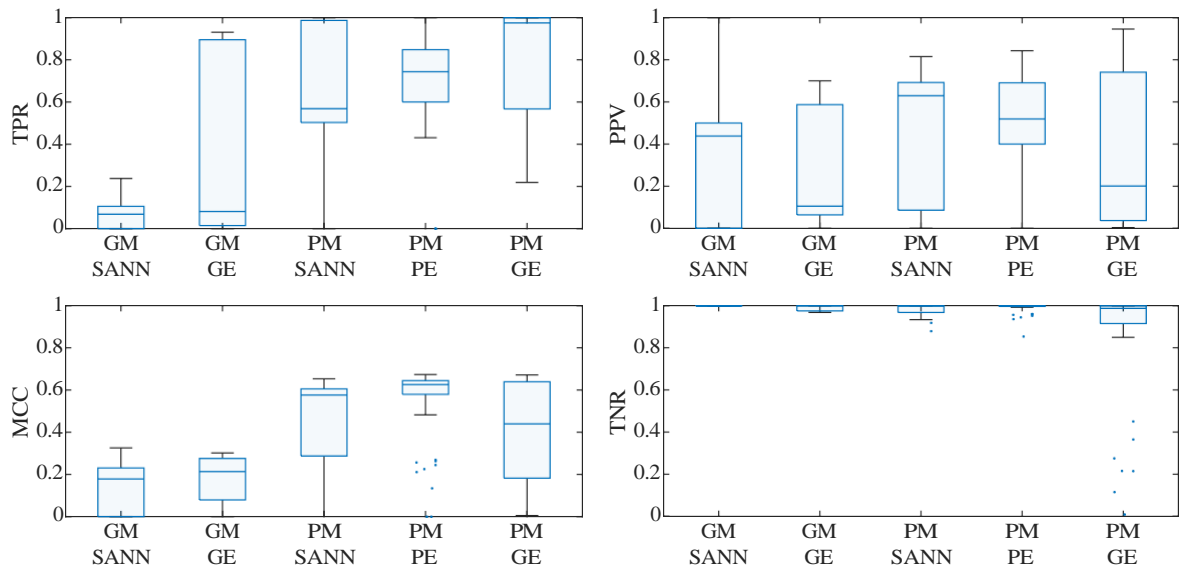


Figure 5.3. Boxplots of the classification metrics of all classification models.

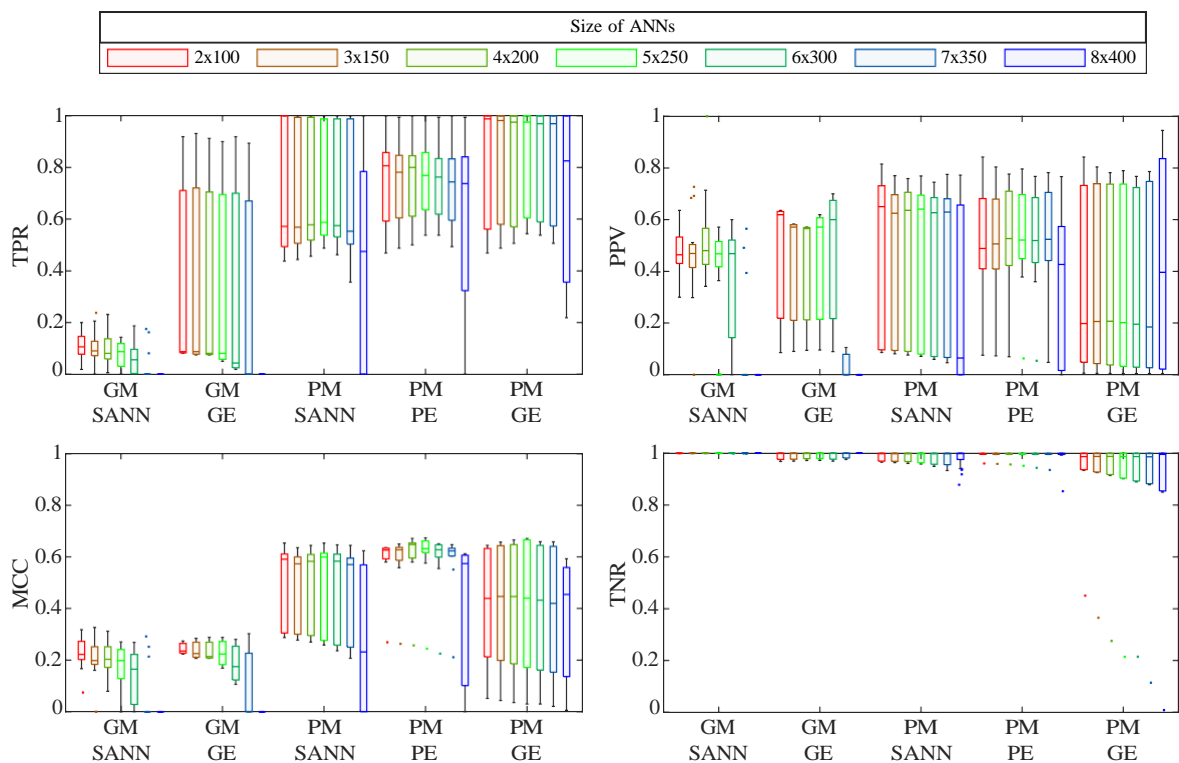


Figure 5.4. Boxplots of the classification metrics of all classification models. Different sizes of the ANNs are marked by colours.

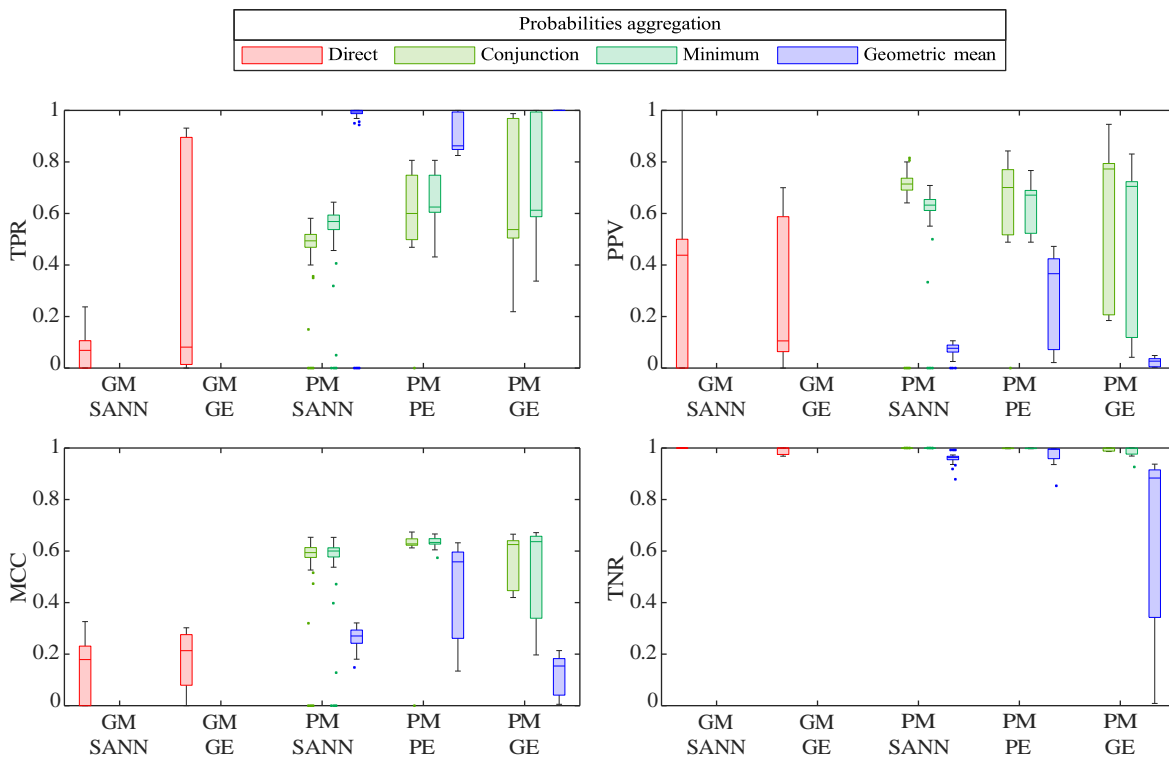


Figure 5.5. Boxplots of the classification metrics of all classification models. Different partial checks aggregation strategies are marked by colours.

checks models, while in global check models the probability of feasibility is obtained directly. Using the geometric mean to combine the partial checks results in lower MCC values, owing to an overestimation of the probability of feasibility. This can be concluded from the increment of TPR and the decrement of PPV and TNR. Comparing the use of conjunction of independent events and minimum partial check, no significant differences are observed in the MCC values. However, as can be expected, using the minimum partial check as the global check produces models with a slightly higher TPR and a slightly lower PPV.

Finally, the different ensemble strategies, described in Section 5.4.3.2, are analysed in Figure 5.6. Evidently, the ensemble strategies implemented do not apply to individual ANNs working alone. For the case of models for global check, using Bayesian inference increases the MCC values, owing to a great improvement of TPR without affecting the PPV and TNR in such a proportion. For the cases of models for partial checks, different tendencies arise. When the ensemble is made in global check, Bayesian inference produces lower MCC values. However, when the ensemble is applied in partial checks, Bayesian inference produces similar MCC values than other strategies. As happened in models for global check, Bayesian inference tends to increment the TPR while decreasing PPV and TNR. Comparing results of ensembles made by the mean or voting, both cases obtain similar metrics, although using the average presents greater dispersion.

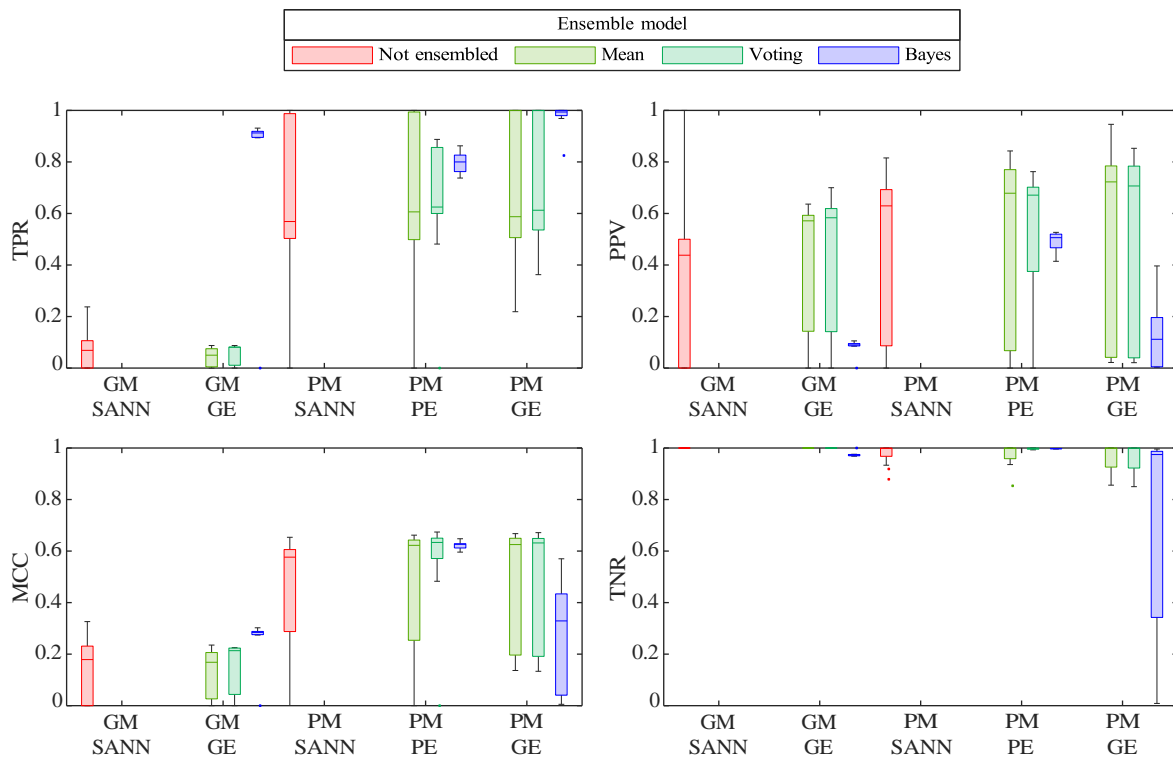


Figure 5.6. Boxplots of the classification metrics of all classification models. Different ensemble strategies are marked by colours.

To provide an idea of the actual values of the metrics, the model with the highest MCC is detailed. This model has 5 hidden layers and 250 neurons per hidden layer trained for partial checks. The ensemble is implemented in partial checks by voting, and the global feasibility is computed as the conjunction of independent events. This model obtains a TPR of 0.631, a PPV of 0.721, a NPV of 0.999, a TNR of 0.999, and a MCC of 0.674.

5.5 Regression model

In this section, a regression ANN model for jacket evaluation is developed. The model is trained to predict the value of the utilization factor that measures how close is the jacket structure to verifying the imposed technical checks.

5.5.1 Architecture

For the regression ANNs, the architectures are the same as implemented for classification ANNs, detailed in Section 5.4.1. The only difference between both is that the sigmoid activation function in output layer to force binary output is removed, because a binary output is not required.

5.5.2 Training process

For the training of regression ANNs, the process implemented for classification ANNs, detailed in Section 5.4.2, is followed. Two differences are considered owing to the difference on the nature of model's output. First, since the output variables are positive continuous variables, the natural logarithm is applied to the utilization factor, and then are normalized by subtracting the mean and dividing by the standard deviation of each variable. Second, the MSE (Equation (4.2)) is used as loss function.

5.5.3 Model prediction

The implemented surrogate model is a regression model that predicts the magnitude of the feasibility jacket, according to technical verifications imposed. That is, the ANN output ($\hat{Y}_{i,j}^k$) is the estimated value, by the ANN k , of the natural logarithm of the check j for the sample i . The obtention of the global probability of feasibility from the estimation of the utilization factor is developed in this section.

To transform the utilization factors predictions to probabilities, a statistical outlook on the ANNs output is adopted. Assuming that the different ANNs predictions follow a Gaussian distribution with specific mean and standard deviation, the probability of verifying the check can be obtained by the CDF of Gaussian distribution. That is, evaluate the probability that the model output is less than or equal to zero.

The same strategy can be implemented for single ANNs, imposing that the standard deviation is zero. In this case, the probability of the model would act as a binary variable, since the probability would be one, if the output is less than or equal to zero, or zero, if the output is greater than zero.

Once the regression model output is transformed into a probability, the partial checks aggregation strategies implemented are equivalent to those used for classification model, detailed in Section 5.4.3.1.

5.5.4 Model performance

The strategy followed to evaluate the regression ANNs is the same as used for classification ANNs (see Section 5.4.4).

Figure 5.7 shows the boxplots of the TPR, PPV, NPV, TNR, and MCC of all the regression models trained. Also including the different models of partial checks aggregation strategies. An initial analysis shows a wide range in TPR and PPV metrics. However, not significant differences are obtained in TNR and NPV among different models, being the minimum values obtained 0.997 and 0.989, respectively. No relevant analyses can be extracted from these metrics, so the same figure layout as in Section 5.4.4 is maintained for an easy comparison. The MCC also shows relevant variability, achieving values greater than 0.6.

Figure 5.8 shows the boxplots of TPR, PPV, MCC, and TNR of all regression models, dividing them by model for global check (GB) and for partial checks (PM), and by single ANNs (SANN), ensemble in global check (GE), and ensemble in partial

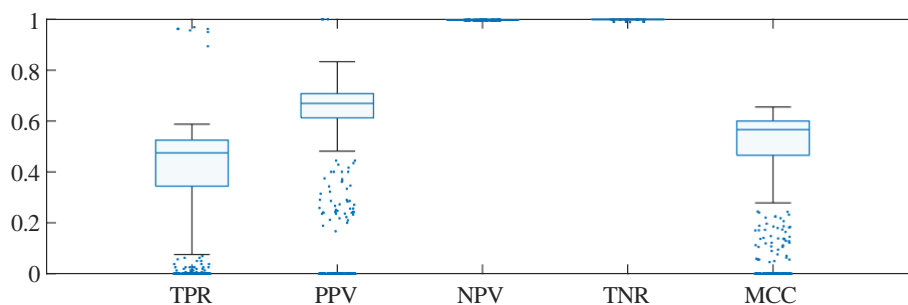


Figure 5.7. Boxplots of the classification metrics of all regression models, considering all the partial predictions aggregation and ensemble strategies.

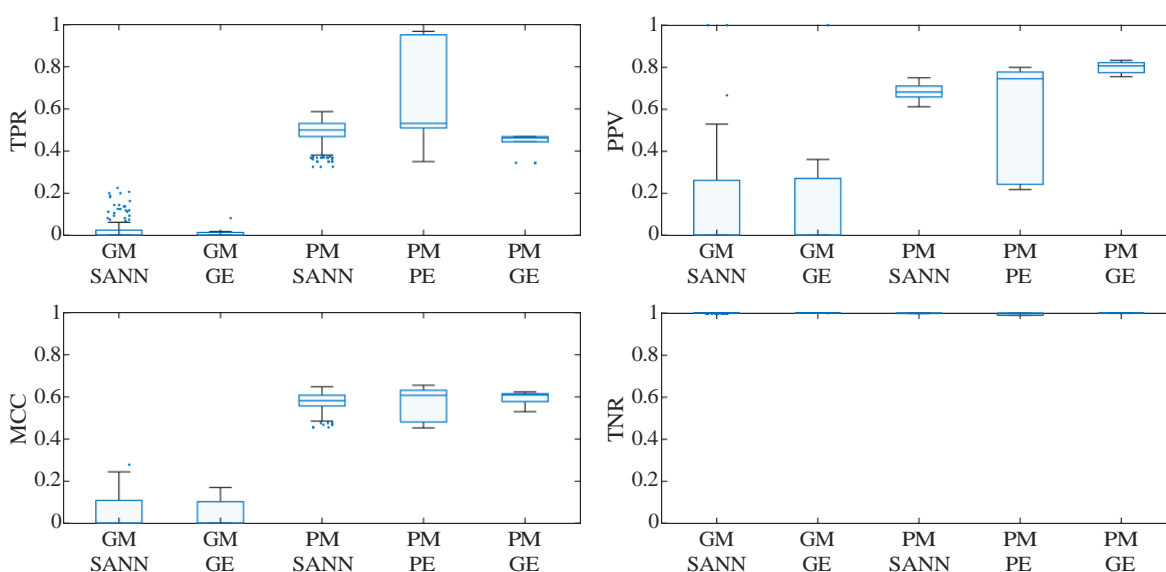


Figure 5.8. Boxplots of the classification metrics of all regression models.

checks (PE). Models for partial checks obtain clearly greater MCC values than models for global check. Higher TPRs are obtained for models for partial check, while most of them keep better results in PPV than models for global check. Among different ensemble strategies on models for partial checks, maximum MCC values are obtained when the ensemble is made in partial check, however not significant differences are observed in median cases.

The influence of the size of the ANNs on the performance is shown in Figure 5.9. Models for global checks only achieve decent MCC values for smallest ANNs. In models for partial checks a smooth tendency can be observed. Maximum values of MCC, TPR, and PPV are achieved by ANNs with 4 hidden layers and 200 neurons per hidden layer, or 5 hidden layers and 250 neurons per hidden layer. Worse performances are obtained for smaller and larger networks, being more pronounced in smaller networks.

The strategies implemented to combine the partial checks predictions to obtain the global feasibility are compared in Figure 5.10. As occurs on classification models, aggregation strategies implemented are only applied to models for partial checks. There

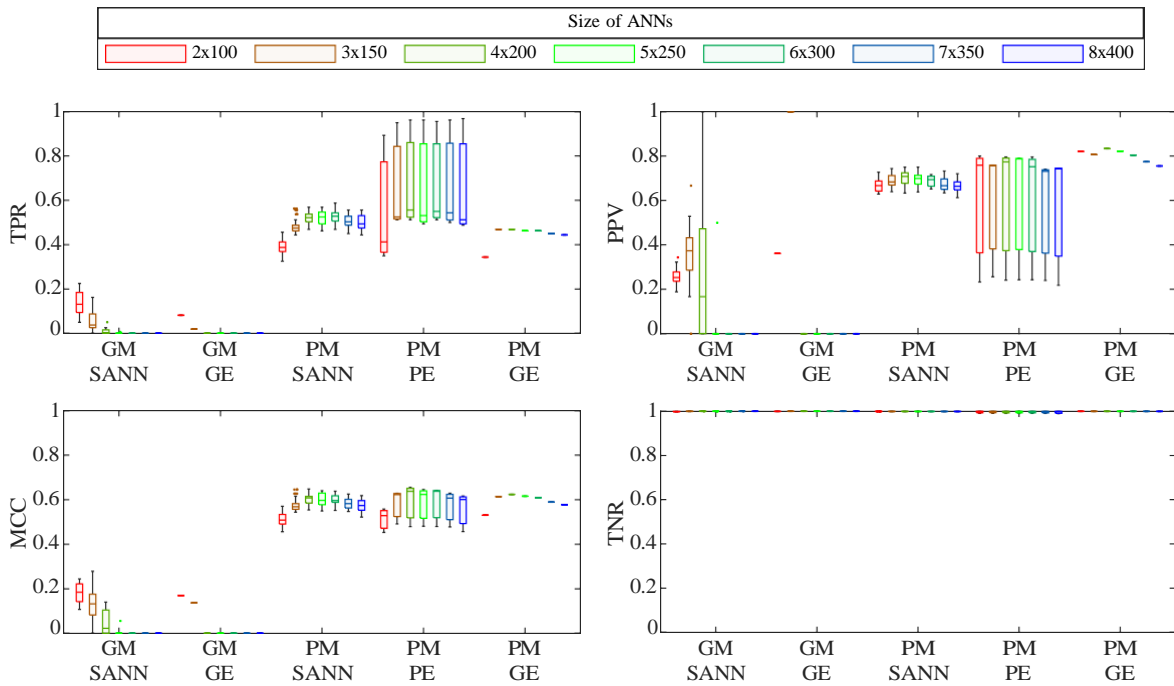


Figure 5.9. Boxplots of the classification metrics of all regression models. Different sizes of the ANNs are marked by colours.

are no differences among the different aggregation strategies in the models for partial checks that are not ensembled and ensembled in global check, because the probability of partial checks in these cases are binary: zero or one. That means that every aggregation strategy gives the same result. Analysing the models for partial checks ensembled in partial checks, lower MCC values are obtained when geometric mean is used, producing significant increments in TPRs and decrements in PPVs. Similar performances are shown by using the conjunction of independent events and minimum partial checks, observing slightly better MMC values when minimum partial check is considered.

To provide an idea of the actual values of the metrics, the model with the highest MCC is detailed. This model has 4 hidden layers and 200 neurons per hidden layer trained for partial checks. The ensemble is implemented in partial checks, and the global feasibility is computed as the minimum of partial checks probabilities. This model obtains a TPR of 0.556, a PPV of 0.774, a NPV of 0.999, a TNR of 0.999, and a MCC of 0.655.

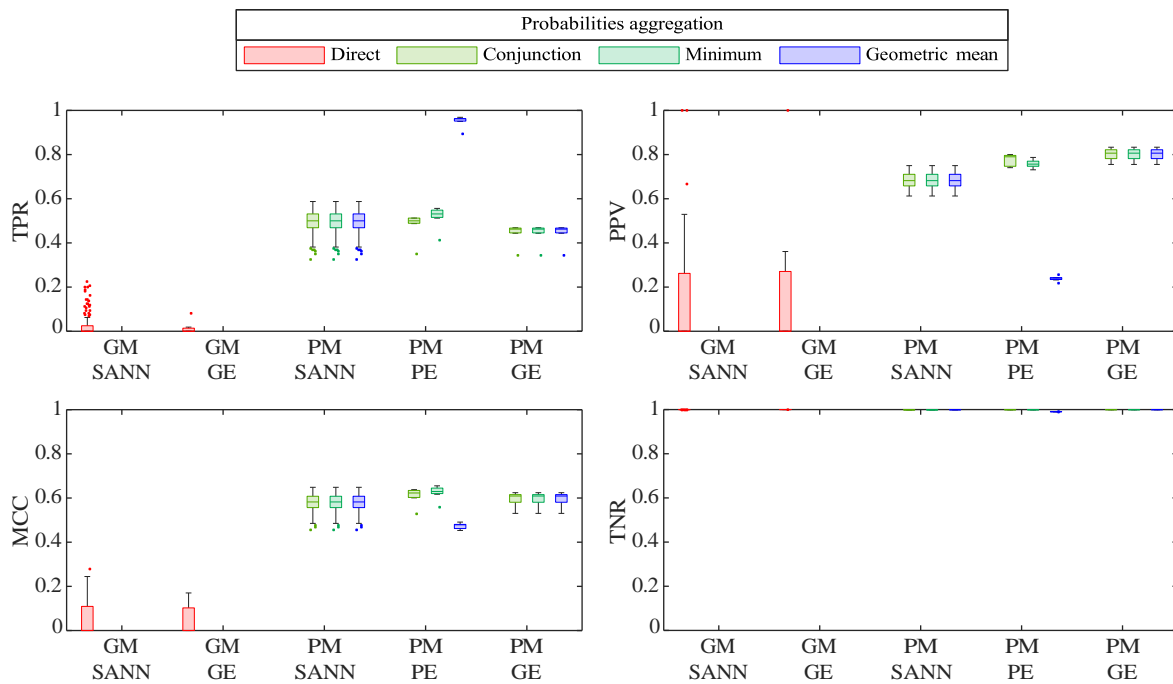


Figure 5.10. Boxplots of the classification metrics of all regression models. Different partial checks aggregation strategies are marked by colours.

5.6 Classification and regression models comparison

In this chapter, two surrogate models of different nature of their output have been developed: a classification model and a regression model. In both cases, the models trained for partial check achieve better performances than the models trained for global check, which can be explained because the ANN has more information. This difference is even clearer in the case of regression models. Generally, models trained for partial checks and ensembled in partial checks present higher MCC values than other models. In addition, using the geometric mean to aggregate partial checks results in models with higher TPR and lower PPV, also decreasing in MCC.

Table 5.5 collect the metrics of the classification and regression models with the highest MCC. Classification model achieve higher TPR and lower PPV the regression model. Almost same metrics are obtained in NPV and TNR. This results in a slightly higher MCC value for the classification model. Incorporating a new point of view, the probability of feasibility given by the model and the utilization factor of the jacket structure should be related. Figure 5.11 shows boxplots of utilization factors of global feasibility of the jacket in test dataset, grouped by the probability of feasibility predicted by the surrogate models. Blue boxplots are for predictions made by the maximum MCC classification model, and red boxplots are for predictions made by the maximum MCC regression model. In both cases, jackets with greater expectations of being feasible shows significantly lower utilization values. However, the regression model presents a better agreement between uncertain samples for the surrogate model

Table 5.5. Metrics of the classification and regression models with the highest MCC.

Model	TPR	PPV	NPV	TNR	MCC
Classification	0.631	0.721	0.999	0.999	0.674
Regression	0.556	0.774	0.999	0.999	0.655

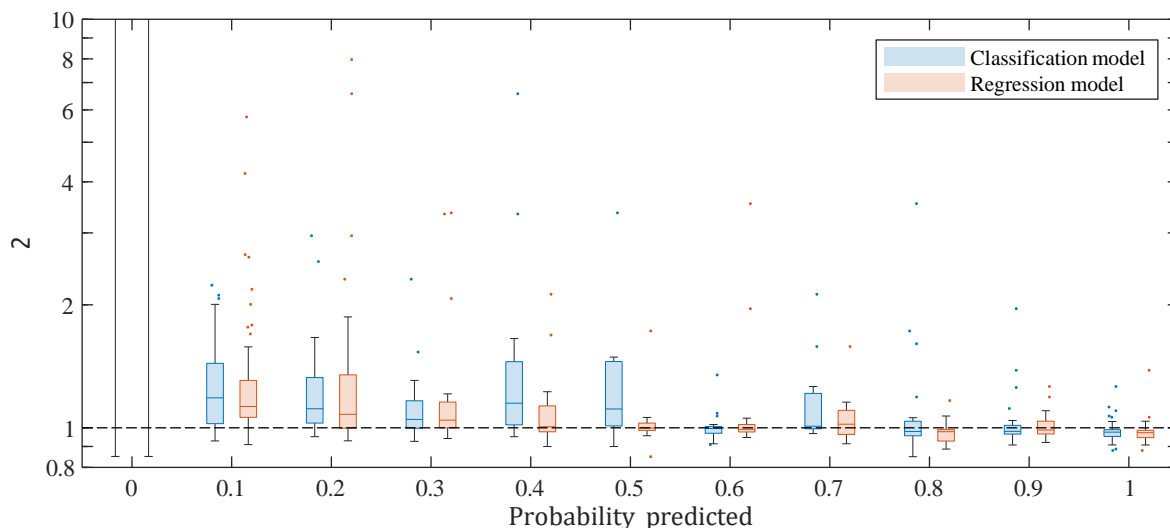


Figure 5.11. Boxplots of utilization factors of global feasibility of the jacket in test dataset, grouped by the probability of feasibility predicted by the surrogate model. Blue boxplots are for predictions made by the maximum MCC classification model, and red boxplots are for predictions made by the maximum MCC regression model.

and jacket structures close to the feasibility border.

Furthermore, the regression model returns a specific estimation of the utilization factor, which increases the scope of application of this model compared to the classification model.

5.7 Conclusions

In this chapter, ANN-based surrogate models for estimating the feasibility of a jacket structure acting as the support structure for any given wind turbine in a specific emplacement is developed. To train the ANNs, a synthetic dataset is generated using the structural model presented in Chapter 2. In order to obtain a sufficiently accurate surrogate model, different strategies are followed: first, both classification and regression ANNs are generated. Second, eight specific sizes for ANNs are tested. Third, ANNs are trained considering different outputs: the global feasibility of the jacket or the feasibility of partial checks imposed to the structure. Fourth, for this last case, different strategies to obtain global feasibility from the partial checks are implemented. Fifth,



different alternatives to combine the predictions of single ANNs in ensemble models are considered.

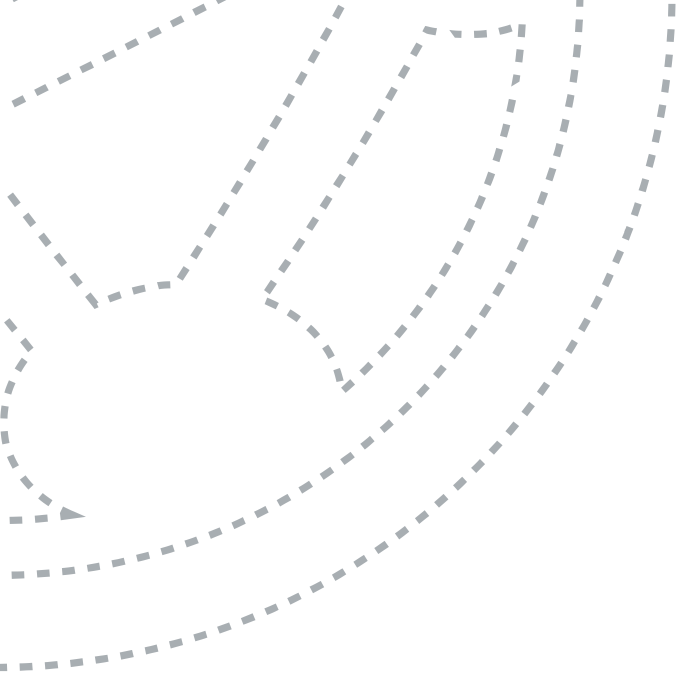
The best obtained models achieve great performances, presenting a MCC higher than 0.65. It should be taken into account that the prevalence of feasible jackets in the generated synthetic dataset is only 0.295%. Generally, models trained for partial checks show better performance than models trained for global check. When ensemble is applied on partial checks, it usually predicts slightly better. No major differences in performance are observed when aggregation of partial checks is made assuming the conjunction of independent events or the minimum probability of partial checks. However, considering the geometric mean overestimates the predictions, resulting in higher TPR and lower PPV, and also decreases the MCC. In all tested models, a decrease in performance for the largest size of the ANN is observed, not being necessary to test larger ANNs.

Comparing the classification and the regression models that achieved the maximum MCC, both present similar performances. In a more detailed analysis, regression tends to underestimate the feasible probability, showing lower TPR and higher PPV. A slightly higher MCC value is obtained by the classification model. However, when actual utilization factors of test dataset samples are analysed instead the binary feasible or not feasible states, the regression model achieves better agreement. Furthermore, regression model returns an estimation of the utilization factor, complementing the information that the classification model would provide.



6. Metamodel- assisted optimization

- 6.1 Introduction
- 6.2 Case study
- 6.3 Methodology
- 6.4 Jacket design
- 6.5 Conclusions





6.1 Introduction

As introduced in Section 5.1, structural models developed to evaluate jacket-supported offshore wind turbines use to be high time-consuming, reducing the extension of parametric studies. However, several authors have developed low time-consuming surrogate models or metamodels capable of replacing structural models with sufficient accuracy. Many other fields in civil engineering have also adopted this methodology.

The same trend has been observed in engineering optimization, where metamodel-assisted optimization acts as a useful strategy to decrease computational resource consumption [44]. Essentially, this optimization process begins with sampling initial solutions, and evaluating them with the reference model to build the metamodel. Then, any optimization strategy can be used to perform the optimization through the metamodel. Until this step, it would be a case of off-line optimization. If the solutions obtained and evaluated with the reference model are used to update the metamodel and repeat the process, an on-line optimization would be implemented [44].

Some recent studies that implemented metamodel-assisted optimization processes to address the design of support structures for wind turbines are the following. Stiang et al. [84] optimized the monopile foundation of an OWT using analytical gradient-based methods through a Gaussian process regression matamodel. Mathern et al. [85] performed a multi-objective optimization of a reinforced concrete foundation of a wind turbine, accelerating the simulated annealing algorithm by a Kriging metamodel. Shen et al. [86] implemented a random forest method to build a metamodel for reproducing the behaviour of the reinforced concrete foundation of a wind turbine, then, a multi-objective non-dominated sorting genetic algorithm was used to obtain the designs.

In this chapter, a metamodel-assisted optimization process is developed to obtain jacket designs to support a wind turbine under specific site conditions. The ANNs-based surrogate model obtained in Chapter 5 is used for accelerating the feasibility evaluation of the structures during the optimization. The objective of the study presented in this chapter is to compare the performance of this optimization procedure to the process followed in Chapter 3. First, the case study is introduced in Section 6.2. Then, a description of the metamodel-assisted optimization process implemented is presented in Section 6.3. Results of the optimization process and comparison with those obtained in Chapter 3 are shown in Section 6.4. Finally, the main conclusions of this study are summarized in Section 6.5.

6.2 Case study

To be able to analyse the metamodel-assisted optimization process developed in this chapter, the same case study as used in Chapter 3 is assumed. That is, all the characteristics considered for the wind turbine supported by the jacket and the site conditions where the device is located are defined in Section 3.2.

6.3 Methodology

As aforementioned, the metamodel-assisted optimization process must follow the same considerations as the optimization procedure implemented in Chapter 3 to both be comparable. Therefore, the jacket structure and the design variables are those detailed in Section 3.3. As in that section, the designs are separated by number of legs and bracing levels, obtaining a candidate solution for each case. Also, instead of directly optimize the structural variables, the relationships between them presented in Table 3.2 are the ones used as optimized variables.

The objective of the optimization process is defined by Equation (3.1). The total mass of the jacket structure is the objective function to be minimized. The optimized variables are again subjected to the boundaries restrictions (lower and upper limits), as well as to comply with the structural requirements in terms of utilization factors. The main difference between this optimization procedure and the one implemented in Chapter 3 is that the technical requirements are evaluated through the surrogate model developed in Chapter 5, instead of by the structural model presented in Chapter 2. Nevertheless, the restrictions according to minimum jacket height, minimum pile thickness, and minimum pile length are additionally computed because they were not considered for the surrogate model owing to the low computational cost that they present.

The specific optimization procedure implemented is represented in Figure 6.1. The central core of the process is based on the gradient descent method, using the “fmincon” function already implemented in Matlab [45]. The values and gradient of both the objective function and the nonlinear constraints are provided. The utilization factors are computed using the regression ANN-based surrogate model of maximum MCC, developed in Section 5.5. Thus, five jacket designs are obtained for each combination of number of legs and bracing levels from random initialization points. Then, the best design among repetitions is selected, and this winner solution for each combination of number of legs and bracing levels is evaluated using the structural model to obtain the actual utilization factors. The criterion to select the best jacket design is the following: the feasible jacket with the lowest mass or, if no candidate solution is feasible, the jacket with the lowest utilization factor. As in any surrogate model, the predicted values present some errors, so the ANNs are retrained with the new evaluated samples, and the optimization procedure is repeated for 20 iterations.

The same procedure followed in Section 5.5.2 is used for retraining the ANNs. To maintain information from the original training dataset, limiting the resources consumption, a portion of the training dataset is also incorporated in the retraining process. Thus, for each combination of number of legs and bracing levels, the 100 samples that are closest in Euclidean distance, within the normalized space, to any of the evaluated solutions in the metamodel-assisted optimization process are used for retraining the ANNs. However, to increase the relative relevance in the retraining process of the optimization solutions, an over-sampling is applied. That is, the optimization solutions are repeated 1 000 times in the retraining dataset. These ratios are an initial attempt to make the results converge.

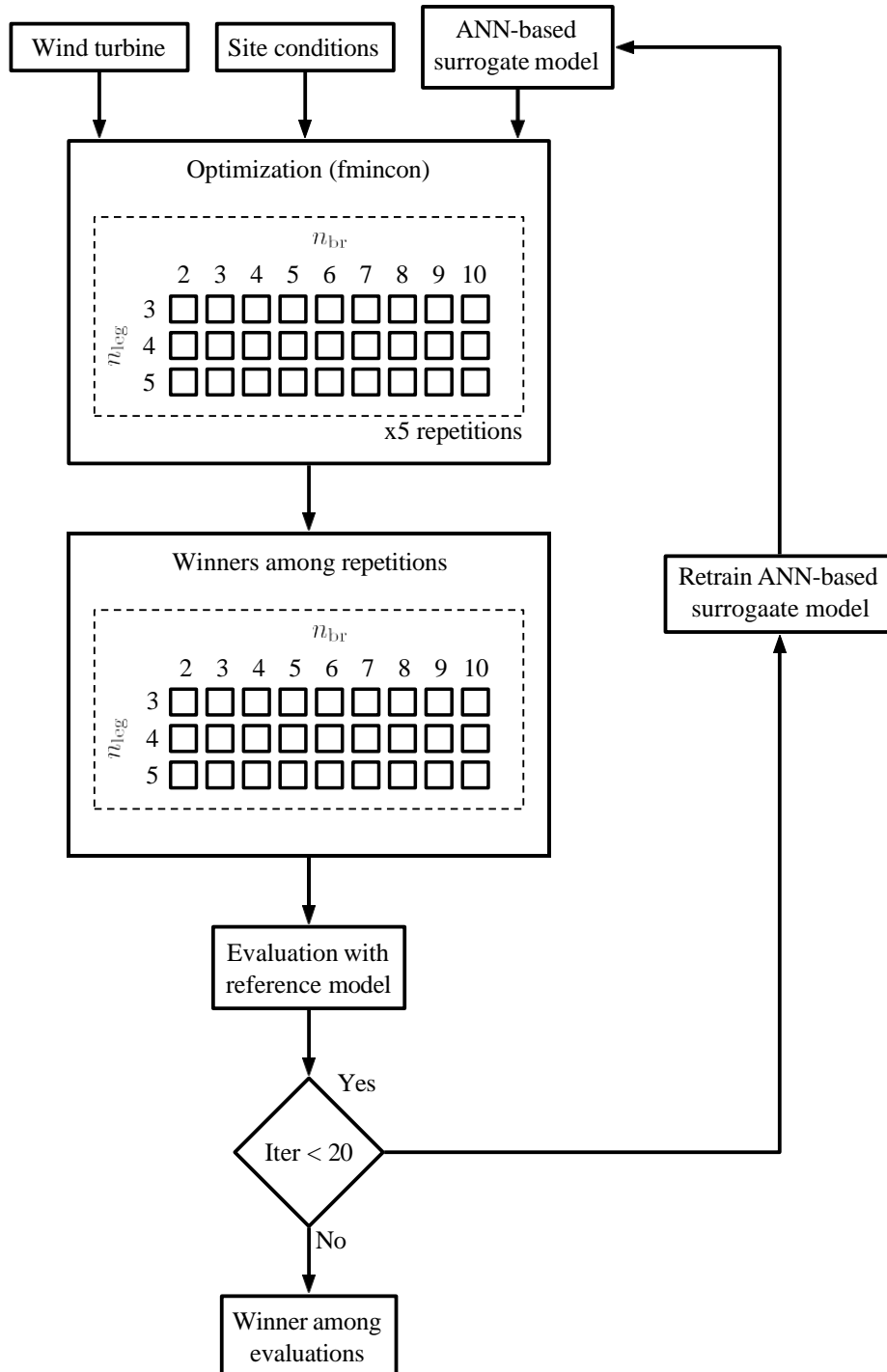


Figure 6.1. Diagram of the metamodel-assisted optimization process.

6.4 Jacket design

The described metamodel-assisted optimization procedure is repeated 5 times to estimate the convergence of the process. Then, the results are compared to those obtained in the optimization implemented in Chapter 3. It should be mentioned that both optimization processes are assisted by surrogate models to reduce the number of evaluation of the structural model. However, the key difference between them is that the surrogate model integrated in the optimization process presented in Chapter 3 is a general radial basis interpolation, while the one used in this chapter has been specifically developed to estimate the feasibility of jacket structures.

Figure 6.2 shows the masses of the obtained designs grouped by the numbers of legs and bracing levels. The cases are separated on the x-axis according to the number of bracing levels; crosses are used for three-legged jackets, squares for four-legged jackets, and diamonds for five-legged jackets. Green markers are used to indicate the designs obtained verify all requirements imposed, while red markers represent non-feasible designs. Black markers represent the mass of the jacket designs obtained in the optimization process implemented in Chapter 3. The results show that most of the designs obtained are feasible jackets, specifically 83% of the designs. Furthermore, between 3 and 7 bracing levels, most of the designs obtained through the implemented optimization process present lower masses than the obtained in Chapter 3. However, this is not observed for 2, 8, 9, and 10 bracing levels.

To analyse the variability of the performance of the optimization process implemented by the number of bracing levels, the angle of the bracings is computed. Figure 6.3 shows the angle of the bracing levels of jacket designs. The same markers criteria than the previous figure are followed. Black dashed lines mark the lower and upper limits imposed to the angle of bracing during the synthetic dataset generation for training the surrogate model. Generally, for cases with 3 legs and 5 or more bracing levels, 4 legs and 6 or more bracing levels, and 5 legs and 7 or more bracing levels, most designs obtained present lower angles for bracings than considered for the dataset generation. In addition, design obtained within these cases using the surrogate model present greater angles for bracings than design obtained using the structural model, which shows the trend of the surrogate model to move to explored regions. This explains the significant loose in performance of the optimization process from 8 to 10 bracing levels. Taking into account that designs with many bracing levels increase the cost of the structure owing to the large number of welded joints, it is considered an acceptable failure of the process. Nevertheless, the masses greater than expected obtained for 2 bracing levels are not justified by angles of bracings out of search space. This case could be explained by the reduced feasible region of the search space, which makes it difficult for the surrogate model to find feasible designs with less mass. The significant increment of the mass of jacket with 2 bracing levels, shown in Figure 6.2, suggests that the feasible region is smaller compared to other scenarios.

According to considerations explained in Section 3.4, four-legged jackets that have from four to six bracing levels are selected as most efficient design. To analyse the evolution of the metamodel-assisted optimization process, the intermediate results of

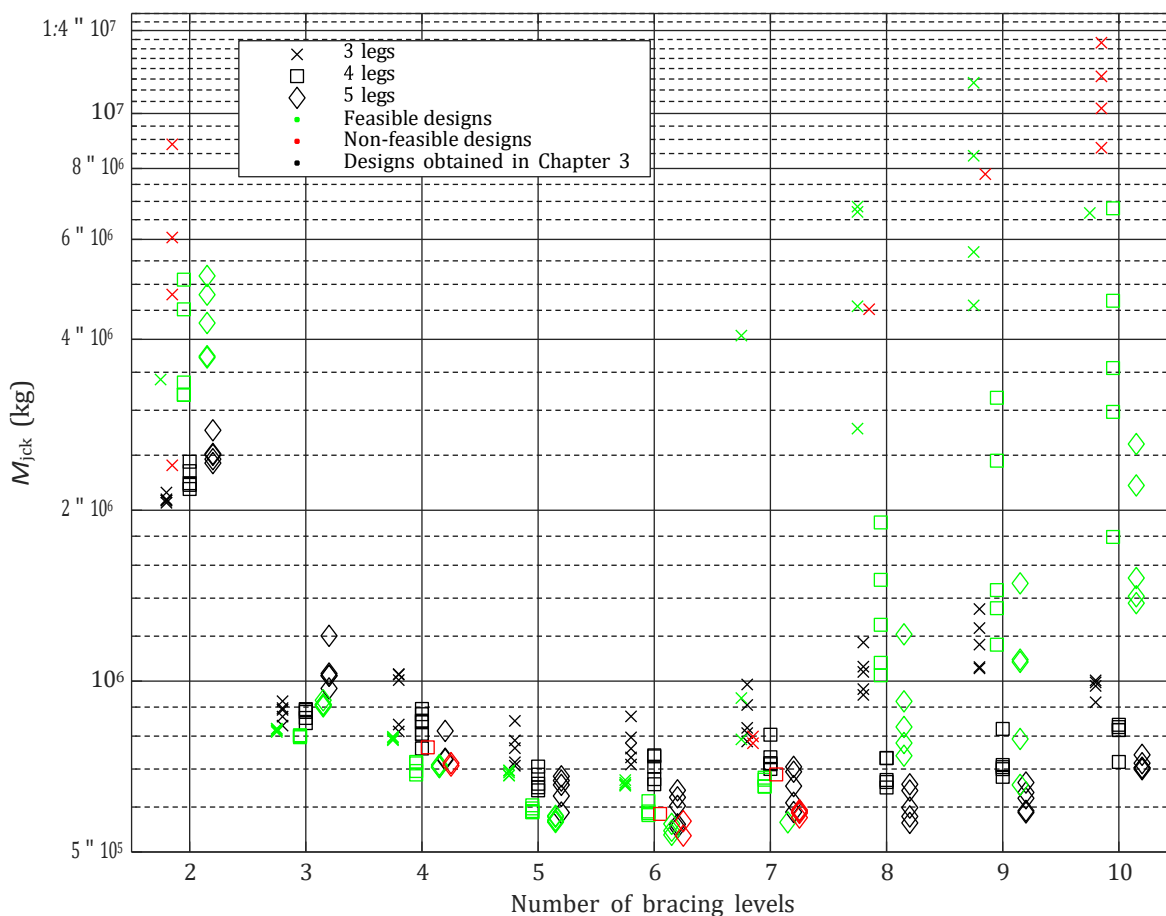


Figure 6.2. Mass of jackets obtained in the metamodel-assisted optimization process, differentiated by number of legs (markers) and bracing levels.

these cases are shown in Figure 6.4. Evolution of the mass of the design obtained during the iterations for each repetition is represented. Green curve fragments show feasible jacket designs, and a transition from yellow to red indicates non-feasible jackets with utilization factors from lowest to highest. Black dashed lines represent the mass of the jacket designs obtained in Chapter 3. All designs in the first iteration show lighter but non-feasible jackets, which means that surrogate model developed in Chapter 5 tends to overestimate the feasibility of the jackets in these cases. The retrained ANNs then move the solutions to heavier designs with some oscillations, achieving feasible jackets. At the end of the process, lighter feasible designs are obtained. Comparing the lighter designs obtained with optimization process implemented in Chapter 3 to the lighter designs using the metamodel-assisted optimization process for each number of bracing levels, the mass is reduced by 10%, 8.4%, and 11.8% for four, five, and six bracing levels, respectively.

To compare computational requirements of both processes, the total number of evaluations of the structural model are counted. All individual optimization and repetitions of the optimization process implemented in Chapter 3 run the structural model

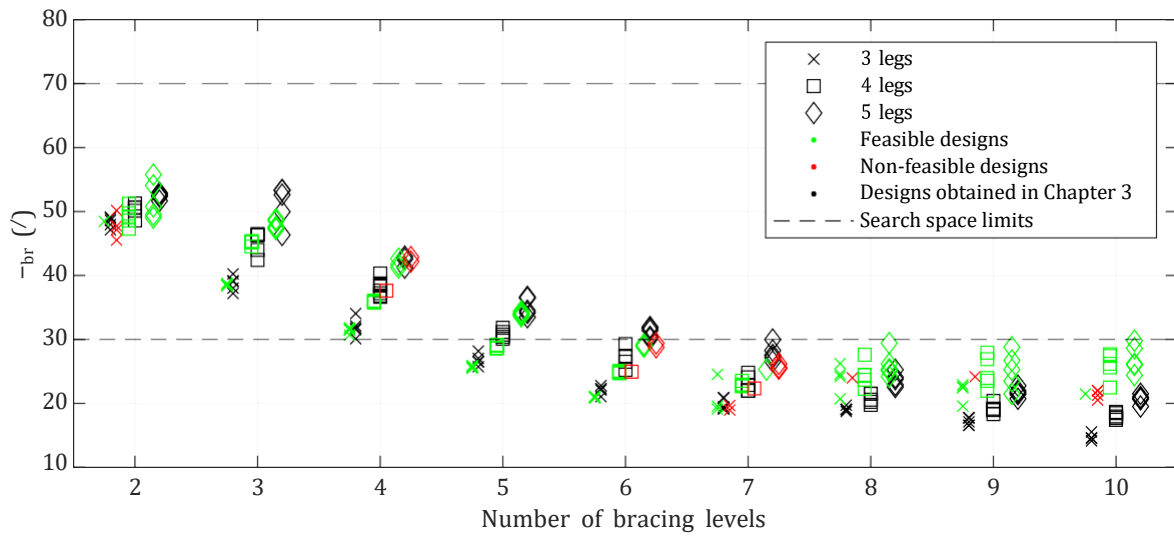


Figure 6.3. Angle of the bracings of the jackets obtained in the metamodel-assisted optimization process, differentiated by number of legs (markers) and bracing levels. Black dashed lines mark the lower and upper limits imposed to bracings angle in the synthetic dataset generation for training the surrogate model.

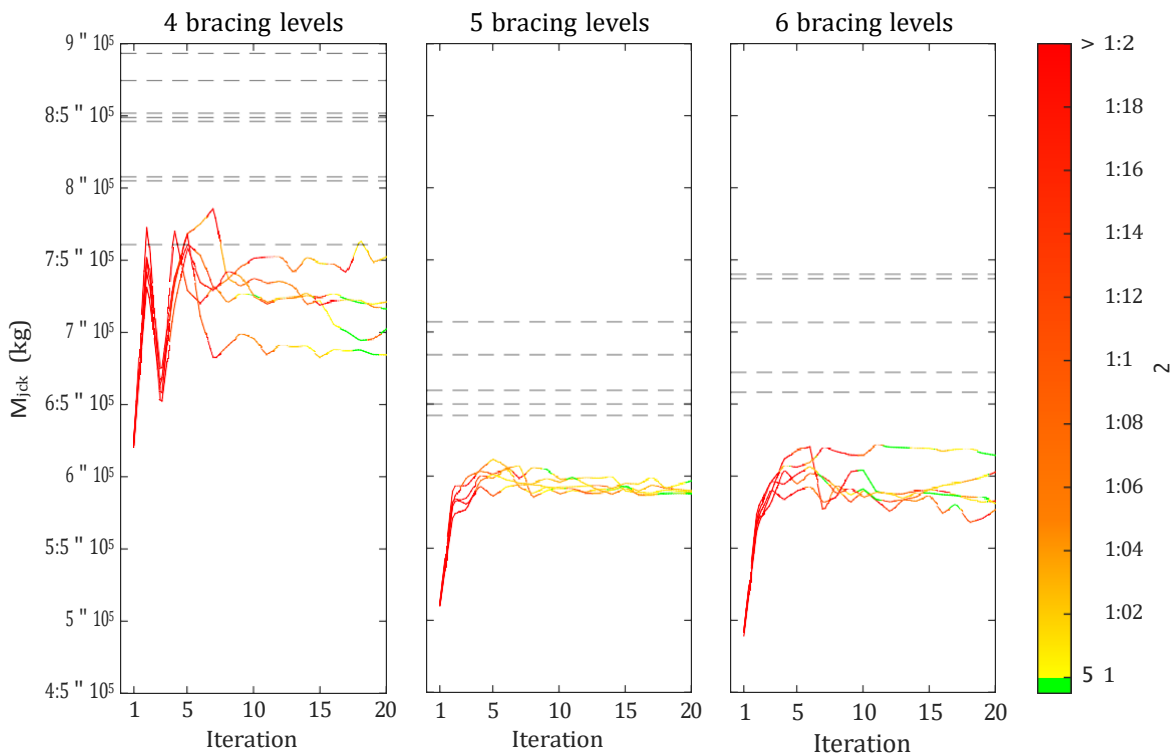


Figure 6.4. Evolution of the mass of the jacket designs obtained through the metamodel-assisted optimization process in each iteration. Green curve fragments show feasible jacket designs, and a transition from yellow to red indicates non-feasible jackets with utilization factors from lowest to highest. Black dashed lines represent the mass of the jacket designs obtained in Chapter 3.

88 800 times, while the optimization process developed in this chapter run the model 2 700 times. It should be taken into account that the ANNs trained required a dataset generation. In this case, a training dataset of 300 000 samples and a test dataset of 50 000 samples were generated. However, the surrogate model can be used again to solve other optimization problems, which makes it profitable if several optimizations are required.

6.5 Conclusions

In this chapter, a metamodel-assisted optimization process is developed to obtain jacket designs to support a wind turbine under specific site conditions. The ANNs-based surrogate model obtained in Chapter 5 is used for estimating the feasibility of the jacket structure instead of the structural model presented in Chapter 2. Within an iterative process, the best jackets designs are evaluated through the structural model while the surrogate model is retrained to improve its performance in the vicinity of the optimum.

The results of the optimization processes implemented in this chapter and in Chapter 3 are compared. Both optimization process are assisted by surrogate models. However, in this chapter, a surrogate model based on ANNs, specifically obtained for jacket feasibility evaluation, is used. The obtained results show a reduction of the total mass of the jacket for many of the cases optimized, that is, combination of number leg and bracing levels, being most of the designs feasible jackets. Worst performance of the optimization process is observed for jacket with eight, nine, and ten bracing levels, owing to the angle of bracings of these cases is lower than those explored in the search space of the synthetic dataset used for training the ANNs. Focusing on the four-legged jacket with four, five, and six bracing levels, a significant correction of the initial solutions is achieved by the iteration process. Finally, a mass reduction of 10%, 8.4%, and 11.8% are obtained for the four-legged jacket with four, five, and six bracing levels, respectively.

Analysing the mass and feasibility of the designs obtained in each iteration of the proposed optimization, the need to retrain the network is observed. The designs of the first iteration have a low mass but do not meet the requirements. This implies that the initial surrogate model overestimates the viability of these designs. After several iterations retraining the surrogate model with samples closer to the optimal design, the performance of the model is improved around the boundary between feasible and non-feasible designs. In this way, the optimization process is improved.

In addition to obtaining lighter feasible jackets using the developed surrogate model for jacket feasibility evaluation, a significant reduction of the number of evaluation with the structural model is observed. In this study case, the structural model was used about 97% fewer times than for the optimization process developed in Chapter 3. Even considered the computational resources used to generate the synthetic dataset and training the ANNs, the flexibility of the surrogate model allows the procedure to be made profitable if several structures are optimized. This is a fundamental aspect to

6 METAMODEL-ASSISTED OPTIMIZATION

be incorporated in parametric studies that analyse the influence of the wind turbine properties and site conditions in the jacket design variables.

A series of four concentric, dashed, light gray arcs are positioned on the left side of the page, partially overlapping the dark blue box and extending upwards and downwards.

7. Summary, conclusions, and future research directions

- 7.1 Summary and conclusions
- 7.2 Future research directions



7.1 Summary and conclusions

The present dissertation proposes an initial approach to the implementation of ANN-based models to assist in the analysis and design of jacket foundations structures for OWTs. This proposal raises the development of an ANN-based surrogate model capable of partially replacing the numerical model usually required for the analysis of structural feasibility. And, therefore, efficiently expand the study of these complex structural systems.

The presented numerical model allows the evaluation of the structural feasibility of the jacket support structure. This model is a compromise between extremely simplified methods and rigorous complex models, making it a suitable tool for the structural analysis of this type of complex structure using fewer computational resources. A reduced set of the most representative load states is established, and a static equivalent analysis is conducted to introduce all the relevant environmental loads. The jacket response is obtained, accounting for the effects of SSI owing to the pile foundation flexibility. Most relevant technical verifications required to ensure the jacket feasibility, according to international standard, are evaluated.

The structural model is used to obtain jacket designs for a wind turbine in specific site conditions, through a predefined optimization process. A complete convergence is not achieved owing to the complexity of nonlinear constraints and the large number of variables required to completely define the geometry. However, feasible jackets designs are obtained. Furthermore, an analysis of the importance of the SSI in the jacket optimization process is performed. Feasible jackets obtained from the optimization process are studied to obtain relevant conclusions, focusing in the influence that this assumption produce in the technical verifications imposed on these structures. Comparison against fixed-base jackets shows an increase in the stresses of some structural elements when the flexibility of the pile foundation is considered.

To explore the capability of ANNs to reproduce the response of complex structural systems that include SSI effects, two ANN-based surrogate models are developed. First, a surrogate model for estimating the pile foundation stiffness, and second, a surrogate model to predict the fundamental frequency of an OWT on a jacket structure. Both models confirm the utility that ANN models can provide to replace high-consumption numerical models. Great prediction accuracy, smooth behaviour, and extremely less time consumption are achieved.

Taking advantage of the great fitting capacities showed by ANNs models, surrogate models for evaluating the feasibility of the jacket support structure are built. To train the ANNs, a synthetic dataset is generated in two steps. First, a set of samples of many different wind turbines, site conditions, and jacket designs is randomly obtained from a predefined search space. This search space aims to limit the generation of samples to relevant cases. Then, the structural model presented in this Ph. D. Thesis is used for evaluating the feasibility of each sample in the dataset. Classification and regression surrogate models are obtained, which take into account most relevant variables that define the physical system: wind turbine, site conditions, and jacket structure. After testing the models, good classification between feasible and non-feasible jackets

is observed in both of them, even considering that the prevalence of feasible cases in the training dataset is about 0.295%. Comparing the classification and the regression models, small differences are observed in classification metrics. However, the better agreement between the feasibility prediction and the utilization factor achieved by the regression model increases its usefulness.

This regression model is incorporated into a metamodel-assisted optimization process to test the capabilities of using ANN-based models to assist in the design of jacket structures. The regression surrogate model is combined with a gradient-based optimization to obtain jacket designs. The optimization is implemented in an iterative process where the ANNs are updated using the previous jacket solutions. Comparing the jacket designs with those obtained by the optimization process with no specific-developed surrogate model, lighter feasible jackets with a mass reduction about 10% are obtained. Moreover, a significant reduction in the number of structural model evaluations is achieved, only requiring the 3% of them. Metamodel-assisted optimization strategies, such as the one implemented in this Ph. D. Thesis, increase the scope of parametric studies that analyse the influence of wind turbine properties and site conditions on the jacket design variables.

7.2 Future research directions

In this section, some future research direction that arise from the work developed and the results obtained during the Ph. D. Thesis are proposed. These proposals are grouped into four categories according to where the focus of each investigation is located. The first focuses on the direct application of the surrogate models for jacket evaluation developed in this work. The second and the third analyse different strategies that could enhance the surrogate model and the optimization process, respectively. The last proposes obtaining a model for the generation of jacket designs using the models and strategies developed in this dissertation.

Application of the surrogate model

The low computational resources consumed by the developed ANN-based surrogate model allow the evaluation of a large number jacket designs, even considering different OWTs and site conditions. This unlocked functionality can be used for performing large parametric studies that analyse the influence of the main variables established for the system, that is, the wind turbine, the site conditions, and the jacket structure, in the feasibility of different fail criteria considered. Through this strategy, a better understanding of the structural behaviour of jacket as support structures for OWTs could be achieved.

Similar strategy can be applied using the metamodel-assisted optimization. Defining several wind turbines and site conditions, the metamodel-assisted optimization process could be performed for obtaining jacket designs for each case. The influence of the characteristics of the wind turbine and the site conditions on the jacket design

variables could be studied. However, the size of this study would be reduced compared to the previous one owing to the increase of computational cost of the optimization process.

Enhancement of the surrogate model

A better knowledge of the structural behaviour of jacket foundations would affect the limits considered for the synthetic dataset generation for training the ANNs. The conclusions extracted from the aforementioned parametric studies could be used to modify the lower and upper limits established for dataset generation to include unexplored relevant regions of the search space and exclude explored non-relevant regions of the search space. Therefore, the ANNs could be focused on more relevant data during their training, enhancing their performance.

Other aspect of the model that should be taken into account is the structural model used to evaluate the jacket structures. Using a structural model which considers more load cases and implements nonlinear time-domain analysis, such as OpenFAST [87], can make conclusions from the surrogate model more relevant. However, higher computational cost of that model makes unaffordable generating the large dataset necessary for training ANNs. The proposal is to use the current model to filter a smaller set of great relevance samples. This small dataset could be evaluated with the new structural model and used to enhance the surrogate model prediction.

Enhancement of the optimization process

As commented in Chapter 3, the optimization of the jacket support structure for OWTs is a complex task. The large number of design variables that define the structure and the nonlinear constraints owing to the technical requirements produce numerous local minima that difficult the convergence. To enhance the optimization results, the implementation of a metaheuristic optimization algorithm is proposed, such as genetic algorithm, particle swarm optimization, or simulated annealing. These optimization algorithms usually require numerous evaluations. In this context, the utilization of the surrogate model can speed up the process without significantly affecting the performance of the optimization.

Furthermore, different optimization objectives may be considered. Many authors try to minimize the total mass of the jacket structure as it is a significant part of the cost of the foundation. However, other characteristics of the structure also increase the cost, without affecting the mass. In order to achieve more efficient structures in terms of economic cost, these aspects must be taken into account. Häfele et al. [79] performed the optimization of a jacket minimizing the total capital expenses, estimated as a linear combination of the following contributions:

- Material factor: Proportional to the mass of the structure. It is evaluated as the total mass of the jacket structure, not including the pile foundations and the transition piece.



- Fabrication factor: Includes the fabrication expenses that increase the jacket cost. It is assumed as the weld volume.
- Coating factor: Considers the cost of protecting the jacket from corrosion. It is proportional to the outer surface of the jacket structure.
- Transition piece factor: Takes into account the cost of the transition piece. It is evaluated as the product of the number of legs and the head radius.
- Transport factor: Includes the cost of the transport of the jacket structure from the port to the installation emplacement. It is assumed proportional to the material factor.
- Foundation and installation factor: Introduces the cost of the piles foundation and its installation. It is proportional to the number of legs.
- Fixed expenses factor: Expenses not dependent on the jacket variables. Established as a fixed value.

Considering the cost estimation and the unitary prices proposed by Häfele et al., the cost of the jacket designs obtained in Chapter 3 are shown in Figure 7.1. These results show an increment in capital expenses for jackets with more number of legs and bracing levels, which agree with engineering experience.

However, the unitary cost of these factors are estimations, which means that different assumptions could considerably change the outcome of the optimization process. Moreover, unit prices are expected to significantly vary in different regions of the world, as well as in the future. This does not deny the usefulness of cost estimation, but rather reinforces the need to explore more specific methodologies that allow a more reliable estimation to be included in optimization process.

Generation of a surrogate model for jacket designs

From the results obtained in the parametric studies proposed in first future research direction, a new surrogate model could be developed. Using the metamodel-assisted optimization process, many jacket designs for different wind turbines and site conditions are optimized. This set of design could be used to train an ANN to predict the optimum jacket design for a wind turbine in specific site conditions. Therefore, the surrogate model would use the characteristics of the wind turbine and the site conditions as inputs, and the jacket design variables would be the outputs. This would result in a surrogate model that, immediately, proposes a jacket design for the desired study cases. It must be taken into account that the jacket obtained could not be assumed as global optimum, but it could act as a predesign.

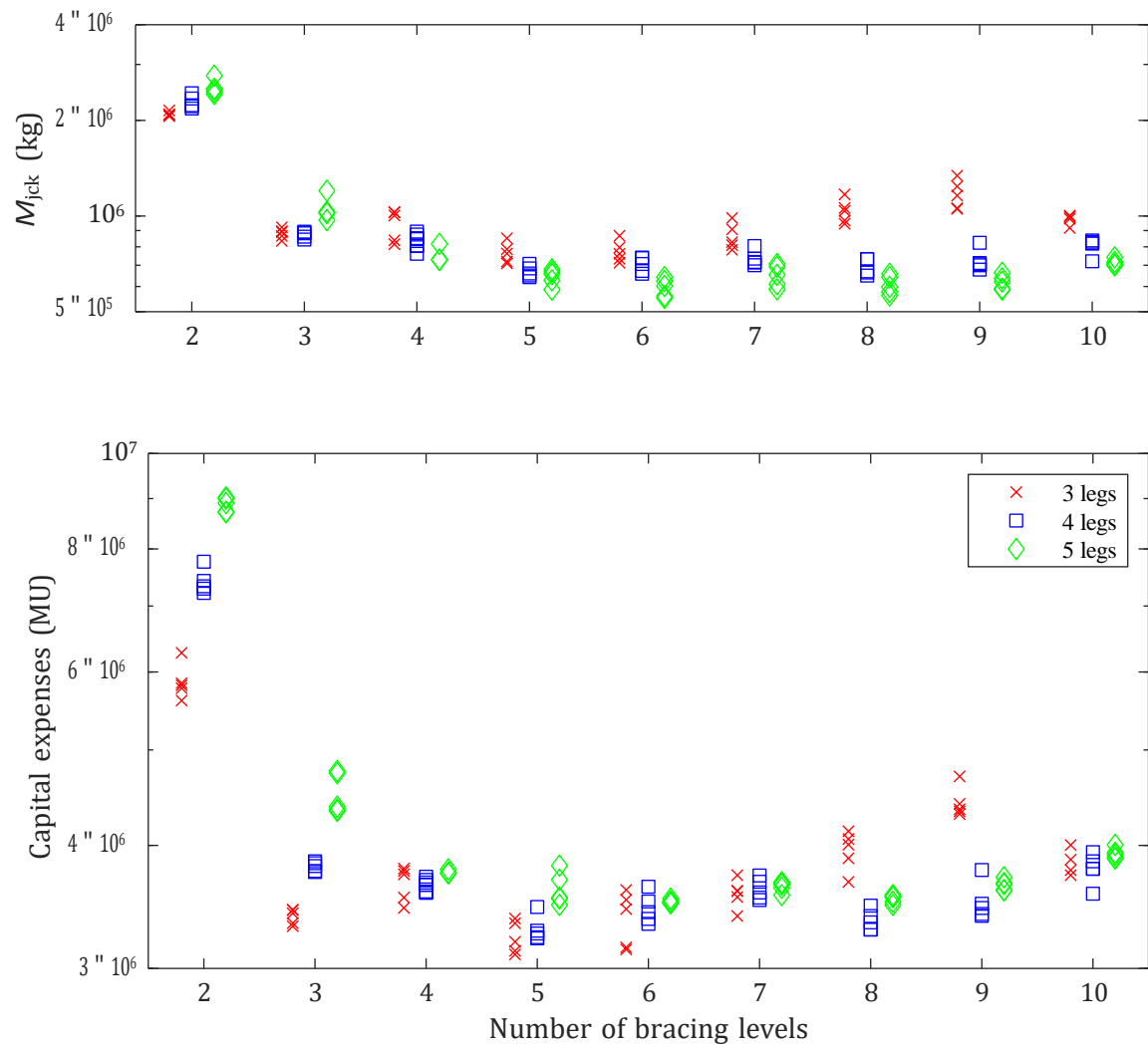


Figure 7.1. Mass (up) and capital expenses (down) of jackets obtained in the design process addressed in Chapter 3, differentiated by the numbers of legs (markers) and bracing levels.



A. Nonlinear Winkler springs model

A Nonlinear Winkler springs model

- A.1 Introduction and general hypotheses
- A.2 Model description
- A.3 Validation results





A.1 Introduction and general hypotheses

Many international standards recommend the use of load–deflection curves (p – y curves) to determine the ultimate lateral capacity of pile foundations (see, for example, [27,32]). This model takes into account the SSI by replacing the surrounding soil with springs that reproduce its stiffness. To introduce the plastic behaviour of the soil, these springs are formulated as nonlinear springs. By imposing compatibility of loads and deflections between the pile and the springs representing the soil, the displacements and internal forces of the pile can be evaluated.

A.2 Model description

This model implements the p – y curves to obtain the pile response under head loads. Assuming that the soil around the pile is sand, API Recommended Practice 2A-WSD [27] define the lateral resistance–deflection relation of the soil as follows:

$$p_s = A_h p_u \tanh \left(\frac{k_h z_p}{A_h p_u} u_p \right) \quad (\text{A.1})$$

where p_u is the sectional ultimate bearing capacity at depth z_p , k_h is the initial modulus of the subgrade reaction, u_p is the lateral deflection, and A_h is a factor taken as 0.9 if cyclic loading conditions are assumed.

Owing to the complex deformation modes of the embedded pile, the pile and the surrounding soil are discretized in sufficient elements. Pile elements are modelled using Timoshenko beam theory [29], and the distributed sectional reaction of the soil is concentrated as two local lateral springs at each node of pile element. Figure A.1 represents the modelling of the system. By applying the head loads, the system of equations is solved iteratively, and the response of the pile is obtained.

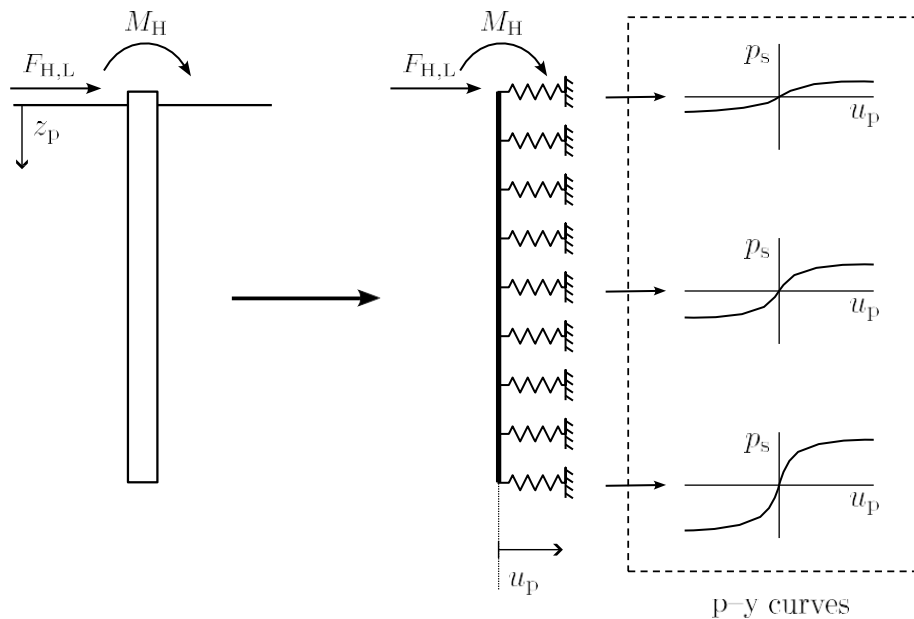


Figure A.1. Representation of static Winkler model used for the evaluation of lateral foundation capacity.

A.3 Validation results

To validate the implemented p-y model, a comparison with the Matlab toolbox Stabil [88] is performed. A simplified study case of an embedded pile with a diameter of 1 m, a thickness of 15.6 mm, and four lengths of 5, 10, 15, and 20 m is established. Steel properties are assumed, that is, a Young's modulus of 210 GPa and a Poisson's ratio of 0.3. Soil properties are considered homogeneous through depth, with constant values of $A_h p_u = 3 \text{ MN/m}$ and $k_h z_p = 10 \text{ MN/m}^2$. Lateral head load is applied to the pile, considering eccentricities of -2, 0, and 2 m. Figure A.2 shows the lateral head load against the lateral head displacement for different lengths piles (rows) and eccentricities (columns). Blue lines represent results obtained by the implemented model, while orange crosses are the validation results from Stabil. Great agreement is observed between both model, validating the use of the implemented nonlinear model. As expected, an increment in the lateral capacity is observed for longer piles, owing to the larger contact surface between pile and soil. Furthermore, the study case also shows that the load eccentricity produces a decrement in the lateral capacity.

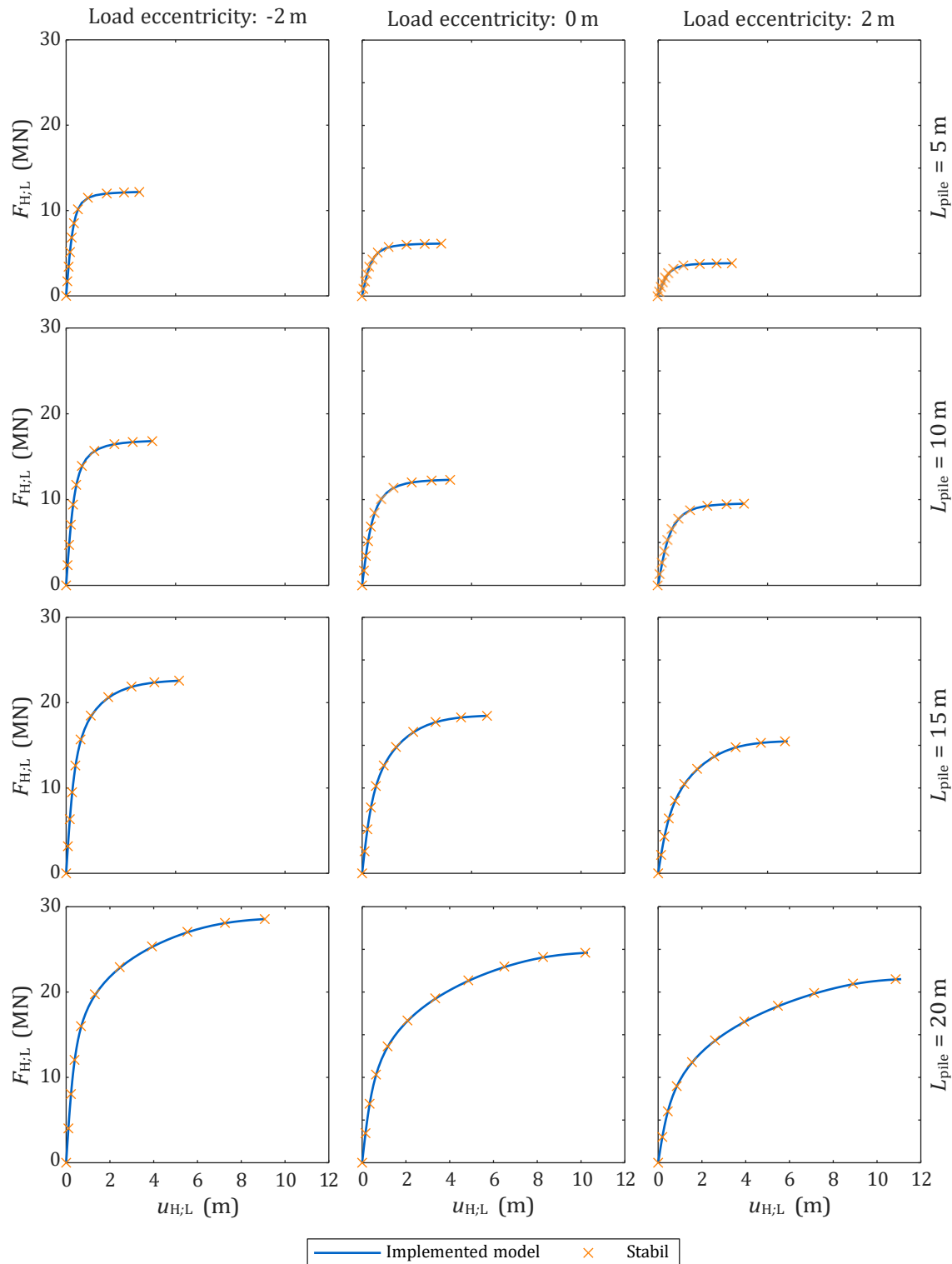


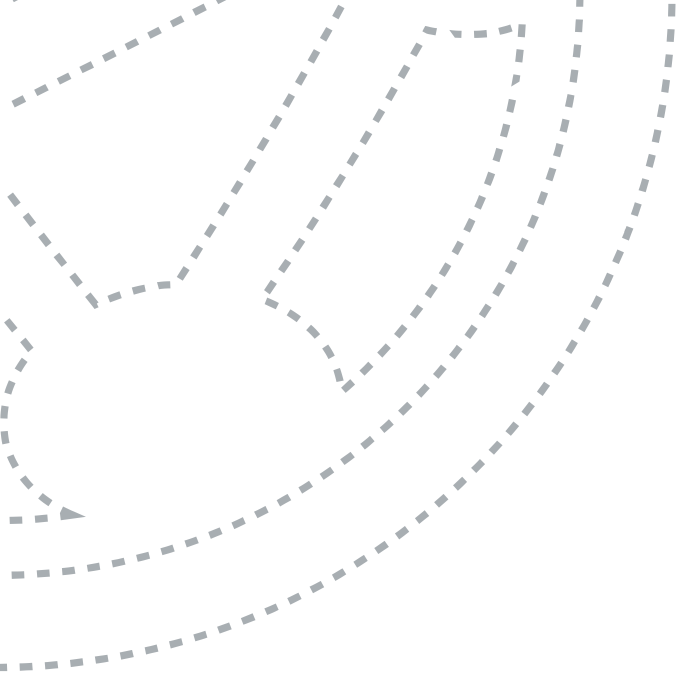
Figure A.2. Lateral head load against the lateral head displacement of the embedded pile. Rows represent different lengths of the pile, and columns represent different eccentricities of the lateral load.



B. Resumen en castellano

B Resumen en castellano

- B.1 Objetivos
- B.2 Modelo estructural
- B.3 Optimización del jacket
- B.4 Modelos subrogados basados en redes neuronales artificiales
- B.5 Modelo subrogado para la evaluación del jacket
- B.6 Optimización asistida por el modelo subrogado
- B.7 Conclusiones





Título de la Tesis Doctoral:

Implementación de modelos basados en redes neuronales artificiales para asistir en el análisis y diseño de cimentaciones jacket para aerogeneradores marinos

B.1 Objetivos

El objetivo de esta Tesis Doctoral consiste en explorar la implementación de modelos basados en redes neuronales artificiales (RNAs) para asistir en el análisis y diseño de estructuras tipo jacket como soporte de aerogeneradores marinos, teniendo en cuenta los fenómenos de interacción suelo–estructura. Para alcanzar dicho objetivo, se establecen dos objetivos parciales:

1. El desarrollo de un modelo estructural que permita el análisis de la respuesta del aerogenerador marino, incorporando los efectos de interacción suelo–estructura. De este modo, el modelo puede ser usado dentro de estrategias para el diseño de estructuras de soporte de aerogeneradores. Con la finalidad de evaluar la viabilidad del jacket como estructura de soporte del aerogenerador, este modelo tiene en cuenta:
 - Todos los elementos relevantes del sistema y sus interacciones mutuas: el fondo marino, la cimentación, la subestructura jacket, la torre y el conjunto góndola-rotor-palas.
 - Las cargas que se espera actúen sobre el aerogenerador y la estructura jacket, que son el peso de la turbina y los elementos estructurales, y las fuerzas de arrastre producidas por el viento y el mar.
 - Los requisitos técnicos impuestos por las guías y prácticas recomendadas para las estructuras de soporte de aerogeneradores marinos.
2. Explorar la utilidad de implementar modelos basados en RNAs para asistir en el proceso de diseño de estructuras de soporte jacket para aerogeneradores marinos. Estos modelos deben ser capaces de reemplazar el modelo estructural en algunas etapas del proceso de diseño. De esta manera, se espera una mejora del mismo, aprovechando el menor coste computacional de los modelos subrogados.

B.2 Modelo estructural

El modelo estructural desarrollado durante esta Tesis doctoral permite obtener la respuesta y evaluar la viabilidad estructural de la estructura jacket, al que se le asume cimentación pilotada, que actúa de soporte de un aerogenerador marino. El sistema estructural considerado se representa en la Figura B.1. Dicho modelo se puede diferenciar

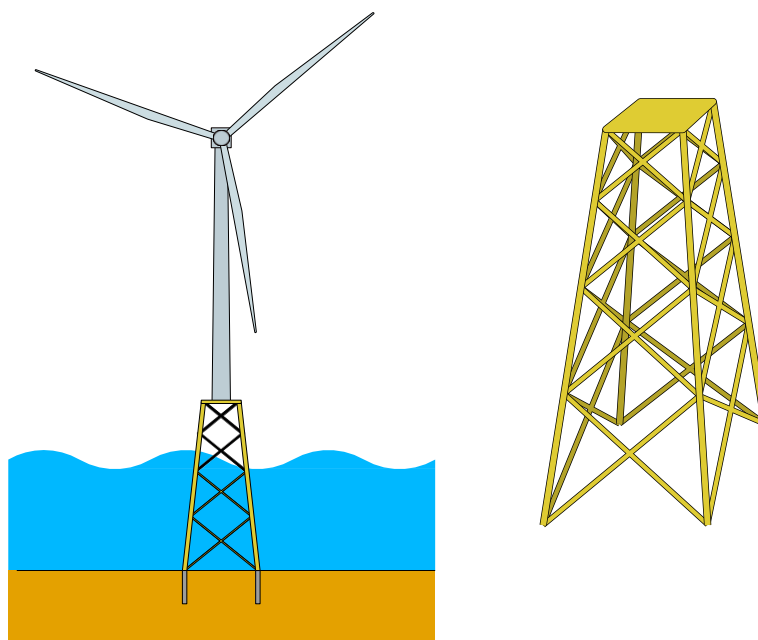


Figure B.1. Representación del sistema estructural. Aerogenerador soportado por una estructura jacket cimentada sobre el lecho marino.

en tres módulos que acometen distintas partes del proceso de análisis: evaluación de las cargas que actúan sobre la estructura, cálculo de la respuesta estructural y verificación de los criterios de diseño.

Cargas de diseño

El modelo estructural implementa las principales cargas que actúan sobre la estructura de soporte jacket. Se dividen en dos grupos:

1. Cargas gravitacionales. Cargas debidas al peso propio de la turbina eólica y los distintos elementos estructurales que componen el sistema, es decir, la torre del aerogenerador y los elementos tubulares que conforman la estructura jacket. También se tiene en cuenta la flotabilidad que presentan los elementos sumergidos.
2. Cargas ambientales. Cargas producidas por las fuerzas de arrastre del viento y del mar. Se considera el arrastre que produce el viento sobre la turbina eólica y los elementos estructurales sobre el nivel del mar, así como el arrastre del oleaje y las corrientes marinas sobre los elementos estructurales sumergidos.

Para reducir el coste computacional asociado al modelo estructural, únicamente se evalúa un set reducido de casos de cargas con las principales combinaciones de condiciones de funcionamiento del aerogenerador y características ambientales.



Repuesta estructural

La respuesta de la estructura jacket frente a las cargas externas, tanto en términos de los desplazamientos nodales como de los esfuerzos internos, se obtiene empleando el método de elementos finitos, considerando que la base de la torre del aerogenerador se vincula con la parte superior de las patas del jacket mediante elementos rígidos. La caracterización dinámica se extrae a partir de la resolución del problema de autovalores. Para introducir los efectos derivados de las cargas cíclicas, se realiza un análisis estático equivalente.

La interacción suelo–estructura se incorpora empleando un modelo previamente desarrollado. Dicho modelo asume el pilote como un elemento unidimensional tipo viga y se basa en la expresión integral del teorema de reciprocidad en elastodinámica y el uso de soluciones fundamentales que reproducen el comportamiento de suelos estratificados con superficie libre. De este modo, se obtiene la matriz de impedancia de la cimentación pilotada de forma eficiente, incorporando la interacción pilote–suelo–pilote. Por otro lado, la interacción agua–estructura se considera como una inercia extra sobre la del propio elemento. Finalmente, se considera el amortiguamiento histerético del material, así como un amortiguador puntual en el rotor para incorporar el amortiguamiento aeroelástico.

Criterios de diseño

Se verifican un conjunto de requerimientos impuestos a las estructuras de soporte para aerogeneradores marinos. En primer lugar, se evalúan algunas restricciones de carácter geométrico: la altura mínima permitida a la que se debe situar la plataforma del jacket, la viabilidad de las uniones soldadas y el espesor y longitud de los pilotes. En cuanto a los criterios de fallo, se verifica que los elementos estructurales resisten los esfuerzos internos que presentan, sin producir pandeo. Además, se evalúa la capacidad portante del terreno frente a las cargas recibidas por la cimentación pilotada. Finalmente, se comprueba que el aerogenerador mantenga su orientación vertical y que el giro del rotor no produce resonancia con la estructura.

B.3 Optimización del jacket

El modelo estructural desarrollado se emplea para diseñar la estructura jacket para un caso de estudio concreto. Para establecer el caso de estudio, se define el aerogenerador que soporta el jacket, tanto sus características como las condiciones de funcionamiento, y las condiciones del emplazamiento donde se ubica, que incluye las propiedades del suelo, las características meteoceánicas y las condiciones del viento.

Para la obtención de los diseños de jackets, se optimiza la geometría y las secciones de los elementos tubulares para las distintas configuraciones de número de patas y niveles de arriostamiento. Como criterio de diseño, se establece minimizar la masa de la estructura jacket, sujeto a que el diseño cumpla los requerimientos impuestos a las estructuras de soporte. Para asegurar la viabilidad estructural, se evalúa la estructura

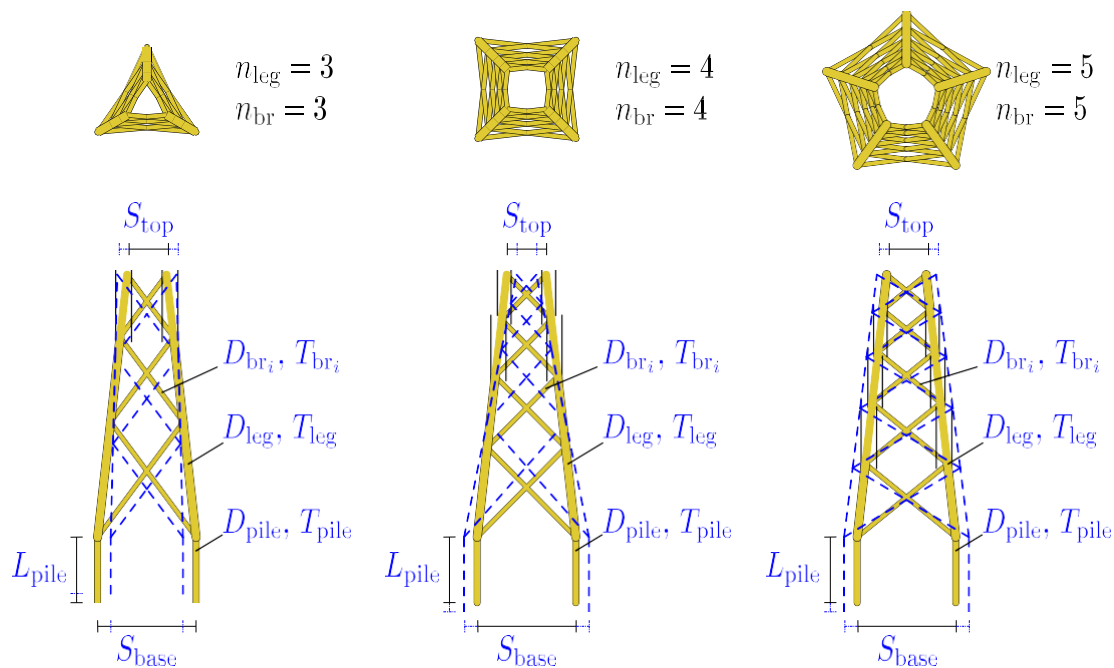


Figure B.2. Representación de tres ejemplos de diseño del jacket, indicando las variables incluidas (azul) o fijas (negro) en el proceso de optimización.

mediante el modelo estructural presentado. La optimización se realiza empleando la función “surrogateopt” ya implementada en Matlab. La figura B.2 muestra una representación de las variables optimizadas en tres ejemplos concretos de diferente número de patas y niveles de arriostamiento.

Haciendo uso del proceso de optimización, se evalúa la relevancia de la interacción suelo–estructura en el proceso de diseño de estas estructuras de soporte. Para ello, se obtienen diseños de estructuras jacket considerando la interacción suelo–estructura y asumiendo cimentación rígida. Seguidamente, se emplea el modelo estructural para evaluar la viabilidad de las estructuras con ambas consideraciones. De este modo, se analiza cómo afecta la consideración de la flexibilidad de la cimentación pilotada sobre los criterios de diseño impuestos en estructuras relevantes obtenidas tras un proceso de optimización.

B.4 Modelos subrogados basados en redes neuronales artificiales

Para explorar la utilidad de los modelos subrogados basados en RNAs, se desarrollan dos modelos subrogados para distintas aplicaciones relacionadas con el tema central de la presente Tesis Doctoral. El primero de ellos consiste en un modelo subrogado capaz de predecir la rigidez de un pilote enterrado en un suelo no homogéneo, mientras que el segundo estima la frecuencia fundamental de un aerogenerador marino cimentado sobre



una estructura jacket. En ambos, se alcanzan altos niveles de precisión, obteniendo modelos subrogados capaces de reproducir la respuesta de los sistemas.

B.5 Modelo subrogado para la evaluación del jacket

Para reducir el coste computacional tradicionalmente asociado a los modelos estructurales, se desarrolla un modelo subrogado basado en RNAs para la evaluación de la viabilidad del jacket. El objetivo de dicho modelo es determinar, a partir de las características del aerogenerador, del emplazamiento y de la estructura jacket, si la estructura de soporte verifica los requerimientos impuestos según las guías y prácticas recomendadas internacionales.

El entrenamiento de las RNAs se realiza mediante un proceso de aprendizaje supervisado. Para ello, se genera un dataset sintético en dos etapas. En primer lugar, se obtiene un set de muestras aleatorias de diferentes aerogeneradores, emplazamientos y diseños de jackets a partir de un espacio de búsqueda predefinido, que pretende limitar la generación de muestras a casos relevantes. Seguidamente, se emplea el modelo estructural presentado en esta Tesis Doctoral para evaluar la viabilidad de cada muestra en el dataset. Tras generar el dataset, se entrenan RNAs, tanto de clasificación como de regresión (de los factores de utilización), para estimar si la estructura jacket es viable o no es viable. Con respecto a la salida del modelo, se compara el rendimiento del modelo subrogado al considerar una única salida que estime la viabilidad o no viabilidad del conjunto estructural o, por el contrario, de establecer múltiples salidas dedicadas a estimar si se verifican o no cada una de las comprobaciones parciales impuestas. Del mismo modo, se analiza la utilidad de combinar diferentes RNAs en un modelo de conjunto para mejorar su rendimiento.

B.6 Optimización asistida por el modelo subrogado

Se estudia la mejora que supone incluir el modelo subrogado dentro del proceso de optimización. Para ello, se parte del mismo caso de estudio que en el proceso de diseño anterior, se optimiza la geometría y secciones del jacket para cada combinación de número de patas y niveles de arriostramiento. Se implementa una optimización basada en el descenso del gradiente donde las verificaciones impuestas sobre la estructura son evaluadas mediante el modelo subrogado.

Para asegurar la obtención de estructuras viables, las soluciones obtenidas se evalúan con el modelo estructural y se utilizan para reentrenar las RNAs. Este proceso se repite durante 20 iteraciones, permitiendo al modelo subrogado refinarse durante el proceso. La figura B.3 representa el esquema general de este proceso de optimización.

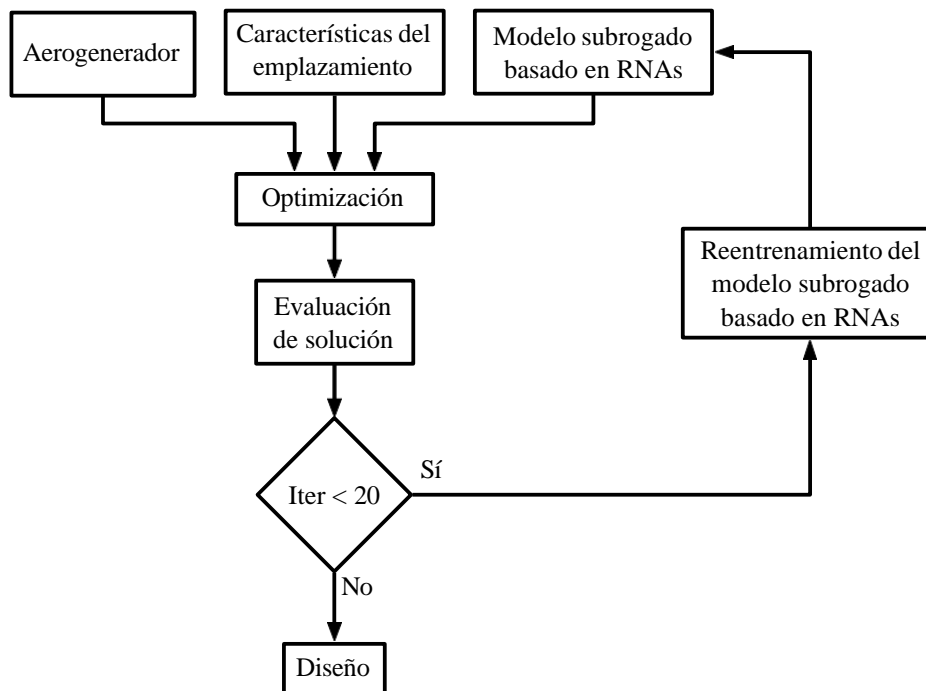


Figure B.3. Diagrama del proceso de optimización asistido por el metamodelo.

B.7 Conclusiones

El modelo numérico presentado permite la evaluación de la viabilidad estructural de la estructura de soporte jacket para aerogeneradores marinos. Este modelo es un compromiso entre los métodos extremadamente simplificados y los modelos rigurosos y complejos, haciéndola una herramienta adecuada para el análisis estructural de este tipo de estructuras complejas usando menos recursos computacionales. En dicha herramienta se establece un set reducido de casos de cargas y se lleva a cabo un análisis estático equivalente para introducir todas las cargas ambientales relevantes. La respuesta del jacket es calculada, teniendo en cuenta los efectos de la interacción suelo–estructura derivados de la flexibilidad de la cimentación pilotada. Finalmente, se evalúan los principales requerimientos técnicos impuestos a la estructura de soporte jacket para garantizar su viabilidad, de acuerdo con normas internacionales.

El modelo estructural se usa para obtener diseños de jackets para un aerogenerador en un emplazamiento concreto, a través de un proceso de optimización. No se logra una convergencia completa del proceso debido a la complejidad de las restricciones no lineales y al gran número de variables requeridas para definir completamente la geometría. Sin embargo, se obtienen diseños estructurales que verifican todas las restricciones impuestas. Adicionalmente, se realiza un análisis de la relevancia de la interacción suelo–estructura en el proceso de optimización, estudiando cómo afecta esta consideración en las restricciones impuestas a las estructuras de soporte en jackets viables obtenidos a través del proceso de optimización. Los resultados muestran un incremento en los esfuerzos internos en algunos elementos estructurales cuando se



considera la flexibilidad de la cimentación pilotada.

Se desarrollan dos modelos subrogados basados en RNA, para explorar su capacidad de reproducir la respuesta de sistemas estructurales complejos que incluyen efectos de interacción suelo–estructura. En primer lugar, un modelo subrogado para estimar la rigidez de una cimentación pilotada, y en segundo lugar, un modelo subrogado para predecir la frecuencia fundamental de un aerogenerador marino sobre una estructura jacket. Ambos modelos confirman la utilidad que los modelos de RNAs pueden proporcionar para reemplazar a los modelos numéricos de alto coste computacional, alcanzando una elevada precisión, un comportamiento suave y un coste computacional mucho menor que el modelo de referencia.

Aprovechando la gran capacidad de ajuste mostrada por los modelos de RNAs, se construye un modelo subrogado para la evaluación de la viabilidad de la estructura de soporte jacket. Para el entrenamiento del modelo, se genera un dataset sintético de muestras aleatorias representativas de diferentes aerogeneradores, emplazamientos y estructuras jacket; que se evalúa con el modelo estructural para determinar si las muestras generadas cumplen los criterios de diseño. Se obtienen modelos subrogados de clasificación y regresión que tienen en cuenta las variables más relevantes que definen el sistema. Tras analizar el rendimiento de los modelos, se observa una buena capacidad de discriminación entre jackets viables y no viables, incluso partiendo de un dataset de entrenamiento altamente descompensado donde la prevalencia de estructuras viables es de 0.295%. Las métricas de clasificación obtenidas por los modelos de clasificación y regresión son similares. Sin embargo, el mejor ajuste entre la predicción de viabilidad y el factor de utilización de la estructura jacket que presenta el modelo de regresión incrementa su utilidad.

Este modelo subrogado es incorporado a un proceso de optimización para evaluar la utilidad de usar modelos basados en RNAs para asistir en el proceso de diseño de las estructuras jacket. Se implementa un proceso de optimización basado en el descenso del gradiente que incorpora al modelo subrogado para evaluar la viabilidad de la estructura. En sucesivas iteraciones, se evalúan los diseños resultantes con el modelo estructural para reentrenar las RNAs y repetir el proceso. Comparando con el proceso de diseño previo sin un modelo subrogado específicamente desarrollado, se obtienen jackets viables con una reducción de la masa de un 10%. Además, se aprecia una significativa reducción en el número de evaluaciones del modelo estructural, requiriendo únicamente un 3% de las iniciales. Se concluye que las estrategias de optimización asistidas por modelos subrogados, como la implementada en esta Tesis Doctoral, incrementan el alcance de los estudios paramétricos que analicen la influencia de las propiedades del aerogenerador y del emplazamiento en las variables de diseño del jacket.



BIBLIOGRAPHY





- [1] DNVGL-RP-C203. Fatigue design of offshore steel structures. Recommended Practice. Det Norske Veritas and Germanischer Lloyd, April 2016.
- [2] DNVGL-RP-C205. Environmental Conditions and Environmental Loads. Recommended Practice. Det Norske Veritas and Germanischer Lloyd, August 2017.
- [3] L. Arany, S. Bhattacharya, J. Macdonald and S. Hogan. Design of monopiles for offshore wind turbines in 10 steps. *Soil Dynamics and Earthquake Engineering*, 92:126–152, 2017.
- [4] DNVGL-ST-0437. Loads and site conditions for wind turbines. Standard. Det Norske Veritas and Germanischer Lloyd, November 2016.
- [5] C. Bak, F. Zahle, R. Bitsche, T. Kim, A. Yde, L. Henriksen, A. Natarajan and M. Hansen. Description of the DTU 10 MW Reference Wind Turbine. DTU Wind Energy, July 2013.
- [6] L. Wang, A. Kolios, X. Liu, D. Venetsanos and R. Cai. Reliability of offshore wind turbine support structures: A state-of-the-art review. *Renewable and Sustainable Energy Reviews*, 161:112250, 2022.
- [7] W. Musial, P. Spitsen, P. Beiter, P. Duffy, M. Marquis, A. Cooperman, R. Hammond and M. Shields. Offshore Wind Market Report: 2021 Edition. Office of Energy Efficiency & Renewable energy, 2021.
- [8] O. Maeso, J. J. Aznárez and J. Domínguez. Effects of space distribution of excitation on seismic response of arch dams. *Journal of Engineering Mechanics*, 128(7):759–768, 2002.
- [9] L. A. Padrón, J. J. Aznárez and O. Maeso. BEM–FEM coupling model for the dynamic analysis of piles and pile groups. *Engineering Analysis with Boundary Elements*, 31(6):473–484, 2007.
- [10] G. M. Álamo, A. E. Martínez-Castro, L. A. Padrón, J. J. Aznárez, R. Gallego and O. Maeso. Efficient numerical model for the computation of impedance functions of inclined pile groups in layered soils. *Engineering Structures*, 126:379–390, 2016.
- [11] A. Santana, J. J. Aznárez, L. A. Padrón and O. Maeso. A criterion to assess the relevance of structural flexibility on the seismic response of large buried structures. *Soil Dynamics and Earthquake Engineering*, 106:243–253, 2018.
- [12] J. D. R. Bordón, C. Van hoorickx, J. J. Aznárez, M. Schevenels, O. Maeso and G. Lombaert. Shape optimized inclined single and double wall wave barriers for ground vibration mitigation. *Soil Dynamics and Earthquake Engineering*, 112:215–231, 2018.
- [13] O. Maeso, J. J. Aznárez and F. García. Dynamic impedances of piles and groups of piles in saturated soils. *Computers & Structures*, 83(10):769–782, 2005.



BIBLIOGRAPHY

- [14] J. D. R. Bordón, J. J. Aznárez and O. Maeso. Two-dimensional numerical approach for the vibration isolation analysis of thin walled wave barriers in poroelastic soils. *Computers and Geotechnics*, 71:168–179, 2016.
- [15] R. Toledo, J. J. Aznárez, D. Greiner and O. Maeso. A methodology for the multi-objective shape optimization of thin noise barriers. *Applied Mathematical Modelling*, 50:656–675, 2017.
- [16] C. Medina, G. M. Álamo and R. Quevedo-Reina. Evolution of the seismic response of monopile-supported offshore wind turbines of increasing size from 5 to 15 MW including dynamic soil-structure interaction. *Journal of Marine Science and Engineering*, 9(11), 2021.
- [17] R. Quevedo-Reina, G. M. Álamo, L. A. Padrón and J. J. Aznárez. Surrogate model based on ANN for the evaluation of the fundamental frequency of offshore wind turbines supported on jackets. *Computers & Structures*, 274:106917, 2023.
- [18] R. Quevedo-Reina, G. M. Álamo, S. François, G. Lombaert and J. J. Aznárez. Importance of the soil–structure interaction in the optimisation of the jacket designs of offshore wind turbines. *Ocean Engineering*, 303:117802, 2024.
- [19] R. Quevedo-Reina, G. M. Álamo and J. J. Aznárez. Estimation of pile stiffness in non-homogeneous soils through artificial neural networks. *Engineering Structures*, 308:117999, 2024.
- [20] B. Benítez-Suárez, R. Quevedo-Reina, G. M. Álamo and L. A. Padrón. PSO-based design and optimization of jacket substructures for offshore wind turbines. *Marine Structures*, (under review), 2024.
- [21] R. Quevedo-Reina, G. M. Álamo, L. A. Padrón and J. J. Aznárez. Dynamic characterization of offshore wind turbines supported on a jacket using artificial neural networks. *World Congress in Computational Mechanics and ECCOMAS Congress*, Oslo, Norway, 5–9 June 2022.
- [22] R. Quevedo-Reina, G. M. Alamo, L. A. Padrón, J. J. Aznárez and O. Maeso. Characterization of pile stiffness using artificial neural networks. *Congress on Numerical Methods in Engineering*, Las Palmas de Gran Canaria, Spain, 12–14 September 2022.
- [23] R. Quevedo-Reina, G. M. Alamo, L. A. Padrón, J. J. Aznárez and O. Maeso. Structural evaluation of offshore wind turbines supported on a jacket using artificial neural networks. *Congress on Numerical Methods in Engineering*, Las Palmas de Gran Canaria, Spain, 12–14 September 2022.
- [24] C. Medina, G. M. Alamo and R. Quevedo-Reina. Respuesta sísmica de aerogeneradores marinos monopilotados de gran tamaño considerando la interacción dinámica suelo-estructura. *Congress on Numerical Methods in Engineering*, Las Palmas de Gran Canaria, Spain, 12–14 September 2022.



- [25] IEC-61400-1. Wind energy generation systems - Part 1: Design requirements. International Electrotechnical Commission, 2005.
- [26] DNVGL-RP-C202. Buckling Strength of Shells. Recommended Practice. Det Norske Veritas and Germanischer Lloyd, July 2017.
- [27] API RP 2A-WSD. Recommended Practice for Planning , Designing and Constructing Fixed Offshore Platforms-Working Stress Design. American Petroleum Institute, 2007.
- [28] J. C. Kaimal, J. C. Wyngaard, Y. Izumi and O. R. Coté. Spectral characteristics of surface-layer turbulence. *Quarterly Journal of the Royal Meteorological Society*, 98(417):563–589, 1972.
- [29] Z. Friedman and J. B. Kosmatka. An improved two-node timoshenko beam finite element. *Computers and Structures*, 47(3):473–481, 1993.
- [30] G. M. Álamo, J. D. R. Bordón and J. J. Aznárez. On the application of the beam model for linear dynamic analysis of pile and suction caisson foundations for offshore wind turbines. *Computers and Geotechnics*, 134, 2021.
- [31] G. M. Álamo, L. A. Padrón, J. J. Aznárez and O. Maeso. Numerical model for the dynamic and seismic analysis of pile-supported structures with a meshless integral representation of the layered soil. *Bulletin of Earthquake Engineering*, 20(7):3215–3238, 2022.
- [32] DNVGL-ST-0126. Support structures for wind turbines. Standard. Det Norske Veritas and Germanischer Lloyd, April 2016.
- [33] M. F. Randolph. The response of flexible piles to lateral loading. *Géotechnique*, 31(2):247–259, 1981.
- [34] J. Oest, R. Sørensen, L. C. T. Overgaard and E. Lund. Structural optimization with fatigue and ultimate limit constraints of jacket structures for large offshore wind turbines. *Structural and Multidisciplinary Optimization*, 55(3):779–793, 2017.
- [35] K.-H. Chew, K. Tai, E. Ng and M. Muskulus. Analytical gradient-based optimization of offshore wind turbine substructures under fatigue and extreme loads. *Marine Structures*, 47:23–41, 2016.
- [36] M. Stolpe, W. Wandji, A. Natarajan, R. Shirzadeh, M. Kühn and D. Kaufer. Innovative design of a 10MW steel-type jacket. Deliverable D4.34. INNWIND.EU, June 2016.
- [37] I. Couceiro, J. París, F. Navarrina, R. Guizán and I. Colominas. Optimization of offshore steel jackets: Review and proposal of a new formulation for time-dependent constraints. *Archives of Computational Methods in Engineering*, 27(4):1049–1069, 2020.



BIBLIOGRAPHY

- [38] S. Ju and C. Hsieh. Optimal wind turbine jacket structural design under ultimate loads using Powell's method. *Ocean Engineering*, 262, 2022.
- [39] S. Jalbi and S. Bhattacharya. Concept design of jacket foundations for offshore wind turbines in 10 steps. *Soil Dynamics and Earthquake Engineering*, 139, 2020.
- [40] A. Abdullahi, Y. Wang and S. Bhattacharya. Comparative modal analysis of monopile and jacket supported offshore wind turbines including soil-structure interaction. *International Journal of Structural Stability and Dynamics*, 20(10):2042016, 2020.
- [41] F. Sharmin, M. I. T. Hussan, D. Kim and S. G. Cho. Influence of soil-structure interaction on seismic responses of offshore wind turbine considering earthquake incident angle. *Earthquakes and Structures*, 13:39–50, 2017.
- [42] W. Shi, H. C. Park, C. W. Chung, H. K. Shin, S. H. Kim, S. S. Lee and C. W. Kim. Soil-structure interaction on the response of jacket-type offshore wind turbine. *International Journal of Precision Engineering and Manufacturing - Green Technology*, 2(2):139–148, 2015.
- [43] C. Chen and P. Duffour. Modelling damping sources in monopile-supported offshore wind turbines. *Wind Energy*, 21(11):1121–1140, 2018.
- [44] I. Negrin, M. Kripka and V. Yepes. Metamodel-assisted design optimization in the field of structural engineering: A literature review. *Structures*, 52:609–631, 2023.
- [45] Matlab. Deep Learning Toolbox, Version 9.9.0.1592791 (R2020b) Update 5. The MathWorks Inc., 2020.
- [46] H. Salehi and R. Burgueño. Emerging artificial intelligence methods in structural engineering. *Engineering Structures*, 171:170–189, 2018.
- [47] P. G. Asteris, A. K. Tsaris, L. Cavaleri, C. C. Repapis, A. Papalou, F. Di Trapani and D. F. Karypidis. Prediction of the fundamental period of infilled rc frame structures using artificial neural networks. *Computational Intelligence and Neuroscience*, 2016:5104907, 2016.
- [48] D. Thaler, M. Stoffel, B. Markert and F. Bamer. Machine-learning-enhanced tail end prediction of structural response statistics in earthquake engineering. *Earthquake Engineering & Structural Dynamics*, 50(8):2098–2114, 2021.
- [49] X. Li and W. Zhang. Long-term fatigue damage assessment for a floating offshore wind turbine under realistic environmental conditions. *Renewable Energy*, 159:570–584, 2020.



- [50] A. Franza, M. Morici, S. Carbonari, F. Dezi and M. DeJong. Artificial neural networks for the evaluation of impedance functions of inclined pile groups. *Numerical Methods in Geotechnical Engineering IX: Proceedings of the 9th European Conference on Numerical Methods in Geotechnical Engineering (NUMGE 2018)*, 25–27 June 2018.
- [51] M. Kumar, V. Kumar, B. G. Rajagopal, P. Samui and A. Burman. State of art soft computing based simulation models for bearing capacity of pile foundation: a comparative study of hybrid anns and conventional models. *Modeling Earth Systems and Environment*, 9(2):2533–2551, 2023.
- [52] D. V. Kennedy, B. B. Guzina and J. F. Labuz. A machine learning framework for in situ sensing of pile length from seismic cone penetrometer data. *Computers and Geotechnics*, 159:105505, 2023.
- [53] C. M. Bishop. *Pattern recognition and machine learning*. Springer, 2006.
- [54] I. Goodfellow, Y. Bengio and A. Courville. *Deep Learning*. MIT Press, 2016.
- [55] G. Cybenko. Approximation by superpositions of a sigmoidal function. *Mathematics of Control, Signals and Systems*, 2:303–314, 1989.
- [56] K. Hornik, M. Stinchcombe and H. White. Multilayer feedforward networks are universal approximators. *Neural Networks*, 2(5):359–366, 1989.
- [57] E. N. Rovithis, H. Parashakis and G. E. Mylonakis. 1D harmonic response of layered inhomogeneous soil: Analytical investigation. *Soil Dynamics and Earthquake Engineering*, 31(7):879–890, 2011.
- [58] E. Buckingham. On physically similar systems; illustrations of the use of dimensional equations. *Phys. Rev.*, 4:345–376, Oct 1914.
- [59] J. L. Ba, J. R. Kiros and G. E. Hinton. Layer normalization. *arXiv*, 2016.
- [60] D. P. Kingma and J. Ba. Adam: A method for stochastic optimization, 2014.
- [61] G. Folino and P. Sabatino. Ensemble based collaborative and distributed intrusion detection systems: A survey. *Journal of Network and Computer Applications*, 66:1–16, 2016.
- [62] M. F. Randolph. The response of flexible piles to lateral loading. *Géotechnique*, 31(2):247–259, 1981.
- [63] T. G. Davies and M. Budhu. Non-linear analysis of laterally loaded piles in heavily overconsolidated clays. *Géotechnique*, 36(4):527–538, 1986.
- [64] M. Budhu and T. G. Davies. Analysis of laterally loaded piles in soft clays. *Journal of Geotechnical Engineering*, 114(1):21–39, 1988.



BIBLIOGRAPHY

- [65] G. Gazetas. Formulas and charts for impedances of surface and embedded foundations. *Journal of Geotechnical Engineering*, 117(9):1363–1381, 1991.
- [66] K. Syngros. Seismic response of piles and pile-supported bridge piers evaluated through case histories. Ph.D. Thesis, The City College of the City University of New York, 2004.
- [67] G. E. Mylonakis and J. J. Crispin. Simplified models for lateral static and dynamic analysis of pile foundations. CRC Press, 2021.
- [68] X. Karatzia and G. Mylonakis. Discussion of “Kinematic Bending of Fixed-Head Piles in Nonhomogeneous Soil” by Raffaele Di Laora and Emmanouil Rovithis. *Journal of Geotechnical and Geoenvironmental Engineering*, 142(2):07015042, 2016.
- [69] G. M. Álamo, A. E. Martínez-Castro, L. A. Padrón, J. J. Aznárez, R. Gallego and O. Maeso. A proposal for normalized impedance functions of inclined piles in non-homogeneous media. *Procedia Engineering*, 199:86–91, 2017. X International Conference on Structural Dynamics, EURODDYN 2017.
- [70] K. Miura, A. M. Kaynia, K. Masuda, E. Kitamura and Y. Seto. Dynamic behaviour of pile foundations in homogeneous and non-homogeneous media. *Earthquake Engineering & Structural Dynamics*, 23(2):183–192, 1994.
- [71] J. Jonkman, S. Butterfield, W. Musial and G. Scott. Definition of a 5MW reference wind turbine for offshore system development. National Renewable Energy Laboratory (NREL), February 2009.
- [72] C. Desmond, J. Murphy, L. Blonk and W. Haans. Description of an 8 MW reference wind turbine. *Journal of Physics: Conference Series*, 753(9), 2016.
- [73] E. Gaertner, J. Rinker, L. Sethuraman, F. Zahle, B. Anderson, G. Barter, N. Abbas, F. Meng, P. Bortolotti, W. Skrzypinski, G. Scott, R. Feil, H. Bredmose, K. Dykes, M. Shields, C. Allen and A. Viselli. Definition of the IEA 15-Megawatt Offshore Reference Wind Turbine. IEA Wind TCP Task 37. National Renewable Energy Laboratory, 2020.
- [74] F. Vorpahl, W. Popko and D. Kaufer. Description of a basic model of the “upwind reference jacket” for code comparison in the OC4 project under IEA wind annex 30. Fraunhofer Institute for Wind Energy and Energy System Technology (IWES), Germany, 450, 2011.
- [75] C. Akdag. Behavior of closely spaced double-pile-supported jacket foundations for offshore wind energy converters. *Applied Ocean Research*, 58:164–177, 2016.
- [76] K. Wei, S. R. Arwade, A. T. Myers and V. Valamanesh. Directional effects on the reliability of non-axisymmetric support structures for offshore wind turbines under extreme wind and wave loadings. *Engineering Structures*, 106:68–79, 2016.



- [77] K. Wen, X. Wu and B. Zhu. Numerical investigation on the lateral loading behaviour of tetrapod piled jacket foundations in medium dense sand. *Applied Ocean Research*, 100:102193, 2020.
- [78] D. Zwick and M. Muskulus. Simplified fatigue load assessment in offshore wind turbine structural analysis. *Wind Energy*, 19(2):265–278, 2016.
- [79] J. Häfele, R. R. Damiani, R. N. King, C. G. Gebhardt and R. Rolfes. A systematic approach to offshore wind turbine jacket predesign and optimization: Geometry, cost, and surrogate structural code check models. *Wind Energy Science*, 3(2):553–572, 2018.
- [80] N. Feng, G. Zhang and K. Khandelwal. Finite strain FE2 analysis with data-driven homogenization using deep neural networks. *Computers & Structures*, 263:106742, 2022.
- [81] R. Falcone, C. Lima and E. Martinelli. Soft computing techniques in structural and earthquake engineering: a literature review. *Engineering Structures*, 207, 2020.
- [82] C. Wang, L. han Song, Z. Yuan and J. sheng Fan. State-of-the-art ai-based computational analysis in civil engineering. *Journal of Industrial Information Integration*, 33:100470, 2023.
- [83] DNVGL-OS-B101. Metallic materials. Offshore Standard. Det Norske Veritas and Germanischer Lloyd, July 2015.
- [84] L. E. S. Stieng and M. Muskulus. Reliability-based design optimization of offshore wind turbine support structures using analytical sensitivities and factorized uncertainty modeling. *Wind Energy Science*, 5(1):171–198, 2020.
- [85] A. Mathern, V. Penadés-Plà, J. Armesto Barros and V. Yepes. Practical metamodel-assisted multi-objective design optimization for improved sustainability and buildability of wind turbine foundations. *Structural and Multidisciplinary Optimization*, 65(2):46, Jan 2022.
- [86] Q. Shen, F. Vahdatikhaki, H. Voordijk, J. van der Gucht and L. van der Meer. Metamodel-based generative design of wind turbine foundations. *Automation in Construction*, 138:104233, 2022.
- [87] National Renewable Energy Laboratory. OpenFAST Documentation. Available on: <https://openfast.readthedocs.io/en/main/index.html>, Release v3.4.1.
- [88] S. François, M. Schevenels, D. Dooms, M. Jansen, J. Wambacq, G. Lombaert, G. Degrande and G. De Roeck. Stabil: An educational matlab toolbox for static and dynamic structural analysis. *Computer Applications in Engineering Education*, 29(5):1372–1389, 2021.



NOMENCLATURE





Acronyms

Symbol	Description	Units
CCDF	Complementary cumulative distribution function	
CDF	Cumulative distribution function	
DAF	Dynamic amplification factor	
ELU	Exponential linear unit activation function	
EOG	Extreme operating gust	
ESS	Extreme sea estate	
ETM	Extreme turbulence model	
EWH	Extreme wave height	
FLS	Fatigue limit states	
FN	False negative	
FP	False positive	
MCC	Matthews Correlation Coefficient	
MSE	Mean square error	
NoHL	Number of hidden layers	
NoNpHL	Number of neurons per hidden layer	
NoP	Number of parameters	
NPV	Negative predictive value	
NTM	Normal turbulence model	
OWT	Offshore wind turbine	
PPV	Positive predictive value	
ReLU	Rectified linear unit activation function	
SLS	Serviceability limit states	
SSI	Soil–structure interaction	
TN	True negative	
TNR	True negative rate	



Nomenclature

TP	True positive
TPR	True positive rate
ULS	Ultimate limit states

Greek Symbols

Symbol	Description	Units
α_{br}	Angle of the bracing	$^{\circ}$
α_{ch}	Relative length of chord	–
α_{leg}	Angle of the jacket legs	$^{\circ}$
α_w	Angle between the wind direction and element axis	rad
$\beta_{br,AVB}$	Relative diameter of brace A or B	–
γ_{ch}	Diameter to thickness ratio of chord	–
γ_M	Material factor	–
Δ	Nondimensional roughness	–
δ	Pile cross-section inner and outer ratio	–
ε_r	Relative error	–
ξ_{ae}	Aeroelastic damping ratio	–
η	Requirement utilization factor	–
ζ_{br}	Relative gap between braces	–
$\theta_{br,AVB}$	Angle of brace A or B	$^{\circ}$
θ_H	Rotation of pile head	rad
λ_{wave}	Scale parameter of the Weibull distribution of waves	m
$\lambda_{f_r,max}$	Latent variable to generate rotor maximum rotation speed	s^{-1}
$\lambda_{f_r,min}$	Latent variable to generate rotor minimum rotation speed	$m s^{-2}$
Λ_1	Scalar parameter of longitudinal turbulence	m



λ_{wind}	Scale parameter of the Weibull distribution of wind	m s^{-1}
ν_{pile}	Poisson's ratio of the pile	–
ν_{s}	Poisson's ratio of the soil	–
$\xi_{\text{ae,SS}}$	Aeroelastic damping ratio in side-side direction	–
$\xi_{\text{ae,FA}}$	Aeroelastic damping ratio in fore-aft direction	–
ξ_{n}	Equivalent viscous damping	–
Q_{a}	Air density	kg m^{-3}
Q_{s}	Soil density	kg m^{-3}
Q_{w}	Water density	kg m^{-3}
$\sigma_{\text{a0,Sd}}$	Design axial compression stress	N m^{-2}
σ_{ETM}	Standard deviation of wind turbulence in ETM	m s^{-1}
$\sigma_{\text{ETM},f_{\text{KS}} \geq f_{\text{r,max}}}$	Standard deviation of wind turbulence above $f_{\text{r,max}}$ in ETM	m s^{-1}
$\sigma_{\text{mi,Sd}}$	Maximum design bending stress about given axis	N m^{-2}
σ_{NTM}	Standard deviation of wind turbulence in NTM	m s^{-1}
$\sigma_{\text{NTM},f_{\text{KS}} \geq f_{\text{r,max}}}$	Standard deviation of wind turbulence above $f_{\text{r,max}}$ in NTM	m s^{-1}
σ_{v}	Equivalent von-Mises stress	N m^{-2}
$\tau_{\text{br,A \vee B}}$	Relative thickness of brace A or B	–
φ_{s}	Soil's angle of internal friction	$^{\circ}$
ω	Angular frequency	rad s^{-1}

Roman Symbols

Symbol	Description	Units
A_{h}	Factor to account for cyclic or static loading condition	–
\tilde{a}_i^{ly}	Output of neuron i of layer ly , before activation function	–



Nomenclature

a_i^{ly}	Output of neuron i of layer ly	–
A_p	Gross end area of the pile	m^2
A_R	Wind turbine rotor area	m^2
A_s	Side surface area of the pile	m^2
B_i^{ly}	Bias of the neuron i of layer ly	–
h	Activation function	–
C^a	Punctual aeroelastic damper	$N s m^{-1}$
C_A	Added mass coefficient	–
C_D	Drag coefficient	–
C_M	Mass coefficient	–
c_s	Shear wave propagation velocity in the soil	$m s^{-1}$
C_T	Thrust coefficient of the wind turbine	–
CV	Coefficient of variation	–
D	Diameter	m
D_{bottom}	Wind turbine tower bottom diameter	m
D_{br}	Diameter of bracing tubular members	m
$D_{br,AVB}$	Diameter of brace A or B	m
D_{br_i}	Diameter of bracing tubular members of level i	m
$\overline{D_{leg_i}}$	Average value of leg diameters for each bracing level	m
D_{ch}	Diameter of chord	m
D_{leg}	Diameter of legs tubular members	m
D_{pile}	Pile diameter	m
D_{rotor}	Rotor diameter	m
D_{top}	Wind turbine tower top diameter	m
E_{pile}	Young's modulus of the pile	$N m^{-2}$
E_r	Relative Young's modulus of the pile	–



E_s	Young's modulus of the soil	N m^{-2}
E_s^0	Young's modulus of the soil at free surface	N m^{-2}
E_s^L	Young's modulus of the soil at the reference depth	N m^{-2}
\tilde{f}	Complex natural frequency	Hz
f_{akd}	Design local buckling strength	N m^{-2}
f_{Ei}	Euler buckling strength about given axis	N m^{-2}
\mathbf{F}_{ext}	External forces vector	N, N m
$F_{H,L}$	Lateral force on pile head	N
$F_{H,V}$	Vertical force on pile head	N
f_{kcd}	Design column buckling strength	N m^{-2}
f_{KS}	Wind turbulence frequency in Kaimal spectrum	Hz
f_n	Natural frequency	Hz
$f_{r,max}$	Rotor maximum rotation speed	Hz
$f_{r,min}$	Rotor minimum rotation speed	Hz
f_{RO}	Wind turbine operating excitation frequencies	Hz
f_s	Unit skin friction capacity	N m^{-2}
F_{TH}	Wind thrust force on the wind turbine rotor	N
f_{th}	Sectional thrust force owing to wind on elements above sea level	N m^{-1}
f_{wn}	Sectional normal force owing to sea on submerged elements	N m^{-1}
$f_{wn}^{current}$	Sectional normal force owing to current velocity	N m^{-1}
f_{wn}^{eq}	Sectional normal force owing to sea, including dynamic amplification	N m^{-1}
f_y	Elastic strength of the material	N m^{-2}
g	Acceleration of gravity	m s^{-2}
g_a	Air gap between the jacket platform and the maximum wave crest.	m



Nomenclature

g_{br}	Gap between braces	m
G_s	Shear modulus of the soil	$N m^{-2}$
$H_{ESS,1}$	1-y significant wave height	m
$H_{ESS,50}$	50-y significant wave height	m
$H_{EWH,1}$	1-y extreme wave height	m
$H_{EWH,50}$	50-y extreme wave height	m
H_{jck}	Height of the jacket structure	m
$H_{jck,min}$	Minimum jacket height according to Equation (2.26)	m
H_{tower}	Height of the wind turbine tower	m
H_w	Water depth	m
h_{wave}	Wave height	m
I_{pile}	Pile cross-section moment of inertia	m^4
I_{ref}	Expected value of turbulence intensity for 15 m/s	–
$I_{RNA,roll}$	Rotor-nacelle assembly moment of inertia about roll axis	$kg m^{-2}$
$I_{RNA,yaw}$	Rotor-nacelle assembly moment of inertia about yaw axis	$kg m^{-2}$
\mathbf{K}	Static stiffness matrix	$N m^{-1}, N, N m$
$\tilde{\mathbf{K}}$	Complex stiffness (and damping) matrix	$N m^{-1}, N, N m$
K^{eq}	Equivalent stiffness of the fundamental mode of the fixed-base wind turbine	$N m^{-1}$
$\mathbf{K}_{f,f}$	Stiffness sub-matrix of external forces on the foundation link due to foundation link displacements	$N m^{-1}, N, N m$
$\mathbf{K}_{f,j}$	Stiffness sub-matrix of external forces on the foundation link due to jacket structure displacements	$N m^{-1}, N, N m$
k_h	Initial modulus of soil's subgrade reaction	$N m^{-3}$
K_{hh}	Horizontal stiffness of single pile	$N m^{-1}$



\hat{K}_{hh}	Dimensionless horizontal stiffness of single pile	–
K_{hr}	Horizontal-rocking coupling stiffness of single pile	N m
\hat{K}_{hr}	Dimensionless horizontal-rocking coupling stiffness of single pile	–
$\mathbf{K}_{j,f}$	Stiffness sub-matrix of external forces on the jacket structure due to foundation link displacements	$\text{N m}^{-1}, \text{N}, \text{N m}$
$\mathbf{K}_{j,j}$	Stiffness sub-matrix of external forces on the jacket structure due to jacket structure displacements	$\text{N m}^{-1}, \text{N}, \text{N m}$
K_r	Rocking stiffness of single pile	N m
\hat{K}_{rr}	Dimensionless rocking stiffness of single pile	–
\mathbf{K}_{SSI}	Foundation impedance matrix	$\text{N m}^{-1}, \text{N}, \text{N m}$
K_v	Vertical stiffness of single pile	N m^{-1}
\hat{K}_v	Dimensionless vertical stiffness of single pile	–
k_{wave}	Shape parameter of the Weibull distribution of waves	m
k_{wave}	Wave number	m^{-1}
k_{wind}	Shape parameter of the Weibull distribution of wind	–
L_{ch}	Length of chord	m
L_{pile}	Pile length	m
$L_{pile,min}$	Minimum pile length considered to achieve active length.	m
L_r	Relative pile length	–
LR	Likelihood ratio of obtaining evidence knowing whether a prior condition occurs or not.	–
\mathbf{M}	Mass matrix	kg, kg m, kg m ²
M_H	Bending moment on pile head	N m
M_{jck}	Mass of the jacket foundation	kg
M_{pltf}	Mass of the jacket platform	kg



Nomenclature

M_{RNA}	Rotor-nacelle assembly mass	kg
m_w	Sectional added mass owing to water–structure interaction	kg m^{-1}
N_{ANN}	Number of ANNs in the ensemble model	–
n_{br}	Number of bracing levels of the jacket	–
N_{check}	Number of checks considered	–
n_{leg}	Number of legs of the jacket	–
N_s	Number of samples	–
n_s	Exponent of generalized power law function of the soil profile	–
N_{wave}	Number of waves during the duration where significant wave is measured	m
P_i	i th percentile of the distribution	–
\bar{P}_i	Mean of i th percentile of the distributions	–
p_s	Sectional reaction of soil	N m^{-1}
p_u	Sectional ultimate bearing capacity of soil	N m^{-1}
Q_p	Total end-bearing resistance	N
q_p	Unit end-bearing capacity	N m^2
Q_s	Skin friction resistance	N
Q_u	Ultimate axial bearing capacity	N
S_{base}	Legs spacing at the base of the jacket	m
S_{top}	Legs spacing at the top of the jacket	m
$S_{top,min}$	Minimum legs spacing at the top of the jacket according to circumscribe the wind turbine tower bottom diameter	m
T	Thickness	m
t	Time	s
T_{bottom}	Wind turbine tower bottom thickness	m
T_{br}	Thickness of bracing tubular members	m



$T_{br,AVB}$	Thickness of brace A or B	m
T_{br_i}	Thickness of bracing tubular members of level i	m
T_{ch}	Thickness of chord	m
T_{leg}	Thickness of legs tubular members	m
T_{pile}	Pile thickness	m
T_{pltf}	Platform thickness considered for dataset generation	m
T_R	Return period of waves	m
T_{top}	Wind turbine tower top thickness	m
T_{wave}	Wave period	s
\mathbf{u}	Nodal displacements vector	m, rad
U	Uniform distribution function	–
u_{avg}	Average annual wind speed at the hub	$m s^{-1}$
u_{e50}	Extreme wind speed with a 50-y recurrence period	$m s^{-1}$
$u_{H,L}$	Lateral displacement of pile head	m
$u_{H,V}$	Vertical displacement of pile head	m
u_m	Mean component of the wind speed at the hub	$m s^{-1}$
$u_{m,10}$	Mean velocity of the wind at 10m above sea surface	$m s^{-1}$
U_{out}	Cut-out wind speed of wind turbine	$m s^{-1}$
u_p	Lateral pile deflection	m
U_R	Rated wind speed of wind turbine	$m s^{-1}$
u_{tb}	Turbulent component of the wind speed at the hub	$m s^{-1}$
u_{wind}	Wind velocity	$m s^{-1}$
$v_{c,circ}$	Circulational current velocity	$m s^{-1}$
$v_{c,wind}$	Wind generated current velocity	$m s^{-1}$
v_n	Normal component of water particle velocity	$m s^{-1}$



Nomenclature

v_n	Normal component of water particle acceleration	m s^{-2}
w_i	Radial basis functions weights	–
$W_{i,j}^{ly}$	Weight of the output of neuron i of layer $(ly-1)$ in neuron j of layer ly	–
X	Jacket design variables included in the optimization process	–
x	Horizontal distance in the waves' propagation direction	m
X_{c_i}	Radial basis functions centres	–
Y_i	Target value for sample i	–
\hat{Y}_i	Prediction value for sample i	–
$\hat{Y}_{i,j}^k$	Prediction value of output j , given by the ANN k , for sample i	–
z	Vertical position measured above sea level	m
z_p	Depth measured from the mud line	m
z_{ref}	Vertical position (z) taken as reference	m

DOCTORAL
DISSERTATION



INSTITUTO UNIVERSITARIO
SIANI
INGENIERIA COMPUTACIONAL

Edificio Central del Parque Tecnológico
Campus Universitario de Tafira
35017 Las Palmas de Gran Canaria
e-mail: info@siani.es · www.siani.es



ULPGC
Universidad de
Las Palmas de
Gran Canaria